Detecting Geomagnetically Induced Currents in Electric Power Transmission Lines

by

Andrew Lackey

A thesis submitted to the Faculty of Graduate and Postdoctoral Affairs in partial fulfillment of the requirements for the degree of

Master of Applied Science

In

Electrical and Computer Engineering

Supervised by:

Professor Rafik Goubran and

Dr. Felix Kwamena

Carleton University

Ottawa, Ontario, Canada

Abstract

Modern electric power transmission systems are becoming increasingly complex due to smart grid development and the need for climate change adaptation, rendering transmission systems more vulnerable to impacts via GIC. A current challenge in the field of GIC detection and measurement is the focus on simulation tools and techniques not advancing towards real-world implementation due to the complexities of GIC events. This thesis addresses this engineering challenge through design and implementation of a GIC test bench and demonstration of a new approach for simple GIC detection and measurement. Furthermore, the work establishes capabilities of a robust GIC measurement platform designed and implemented to enable straightforward use and integration with modern grid infrastructure. This thesis has resulted in systems that bridge the gaps between simulation tools and real-world deployments of GIC detection and measurement systems, providing a solid foundation for further research and development.

Acknowledgements

I would like to thank my supervisors Prof. Rafik Goubran, Dr. Felix Kwamena for their unending support. I appreciate the guidance and always-helpful discussions with Dr. David Boteler. I thank my Parents and Sister for putting up with me, and encouraging me through all of my endeavours. Dedicated to my fiancé Amy, for helping me make it through the most difficult times. Thank you to all of you, without whom I would not have been able to complete this Thesis.

Table of Contents

List of Tables

List of Illustrations

Appendix

Glossary

Acronym	Meaning
GIC	Geomagnetically Induced Current
MNA	Modified Nodal Analysis
SQUID	Superconducting Quantum Interference Device
I2C	Inter-Integrated Circuit
VLAN	Virtual Local Area Network
CME	Coronal Mass Ejection
SOHO	Solar and Heliospheric Observatory
OTT	Natural Resources Canada, Ottawa Geomagnetic Observatory
EMP	Electro-Magnetic Pulse

Chapter 1. Introduction

1.1. Research Motivation

Geomagnetically induced currents are a constant threat to electric transmission systems. Potential impacts due to GIC can be severe as they are difficult to predict, measure, and mitigate. Damage from GIC can result in regional outages that take significant time and resources to repair. Alongside the growing dependence on electricity from all critical infrastructure sectors, GIC is a threat that can cascade into all aspects of a modern society as shown in [1].

Modern electric transmission systems are going through a transformation in order to deliver on the energy needs of the future. Traditional radial and loop designs do not provide the flexibility and adaptability in order to integrate distributed energy resources and deliver energy to a changing load. Smart grid infrastructure, as presented by [2], has emerged as the leading method to address issues in relation to flexibility of electric transmission systems, increasing the deployment of monitoring, remote control, and power electronics systems. Adopting new power electronics and switching mechanisms changes the dynamics of electric transmission systems in ways that are not fully accounted for by current GIC simulation models and measurement methods, leaving a technical gap in understanding that has not been addressed by previous work.

Anticipated requirements for electric transmission infrastructure is also changing due to the realities of climate change. Adapting to climate change through the electrification of existing technologies is expected to increase electricity generation capability between 100% and 200% estimate by [3], straining existing transmission

infrastructure to its limits. Electric vehicle charging stations change the load profile for remote and residential areas requiring non-traditional approaches and a renewed dependence on electricity infrastructure to deliver critical services for the transportation sector. Industrial facilities as outlined by [4] are moving towards electrification of heating processes requiring greater on-demand electricity and increased reliability in order to deliver a competitive product. Adapting to climate change results in further dependence on electricity infrastructure that is vulnerable to GIC, requiring new monitoring systems and strategies that leverage technologies of the future grid.

Considering the electric transmission system transformation and the integration of new technologies, the threats due to GIC have been amplified. However, the technology used to detect and measure GIC has significant limitations. Existing methods are cumbersome to install, require careful synchronization, are not able to provide a complete picture of GIC flow, or are too complex to be deployed by the majority of small to medium utilities. There is an apparent lack of industry knowledge and expertise required to mitigate the impacts of GIC. Utilities have identified the need for technical solutions that require minimal investment and training in order to operate. There is an opportunity to develop a system to address the present and future vulnerabilities of the electric transmission system to GIC through the development of a detection and monitoring system.

Since the effects of GIC on traditional power transmission systems are widespread and range from physical to operational, there is a need to develop a detection and monitoring system that can be deployed in a diverse set of environments. Half-cycle saturation caused by GIC leads to spot heating [5] and insulation failures of power

transformers. Grid instability issues traced to GIC penetration and influx lead to an increase in reactive power generation or load shedding requirements [6]. Furthermore, power system protection components have operated under abnormal conditions because of GIC generated system harmonics [7]. In addition, the disruption of wireless and wired communication methods compound the effects of a GIC event, potentially overloading protection systems and induce a drastic decrease in communication method signal to noise ratios [8]. Existing measurement methodologies can only be deployed in select circumstances and require supporting infrastructure.

Characteristics of space weather events mean that a significant space weather event will have a high impact but low frequency. The economic impacts of GIC range from a minor increase in preventative maintenance costs to extensive physical component damage. Examples of the potential damage due to GIC include the Carrington [9] and 1989 Québec [10] events. Examining the overall cost due to power loss requires a range of assumptions due to broad impacts to multiple sectors. One incident isolated to the province of Ontario in Canada shows the potential economic losses due to power failure can exceed $11.21 Billion CAD for a multi-hour outage as estimated by [11]. Significant investment in complex GIC detection and measurement systems is impractical, requiring solutions that are costly for all sizes of utilities.

Due to increases in computing power, simulation is now the first method considered when developing new technical solutions. GIC simulation tools, such as that developed by [12] have been extensively used to model power transmission networks and GIC. Yet, when developing systems for deployment in the field there is a need for test-benches that allow for the rapid prototyping, testing and verification of devices as

identified by Defence Research and Development Canada [13]. Developing innovative technologies for power system owners and operators to detect, measure, and predict GICs allows threats from space weather to be mitigated.

Combining the risks due to transformative infrastructure, integration of new technologies, changing load and generation dynamics, and a growing interdependence between all critical infrastructure sectors, electric power systems are increasingly vulnerable to the impacts of GIC. Advancing detection and measurement of GIC is necessary to mitigate the impacts of space weather on electric power systems.

1.2. Objective

The main objective of this research is to design and develop a non-contact simple GIC detection system that can determine GIC flow through a power transmission line. Through this work, we seek to address technical gaps in the field of GIC detection, specifically between GIC simulations and real-world conditions.

1.3. Research Contributions

The research contributions of this thesis centre on advancing the field of GIC detection and measurement. The current field of GIC research has focused on simulations and mathematical models to evaluate the impacts of GIC as shown by [14], [15], and [16]. The main contribution of this research is bridging the engineering gap between pure simulation and real-world deployments for GIC detection and measurement.

First, to speed the development of sensing systems a scaled GIC test bench was designed and implemented to consider the unique aspects of GIC in power transmission lines. This system integrates GIC signatures into a scaled bench-top system, with accurate

physical and electrical configurations. Second, to reduce the complexity of measurement systems a single magnetometer based sensing system was designed, implemented and tested. This system demonstrates the use of a single location system for non-contact magnetic measurements in order to determine GIC in a power transmission line. Third, to ensure accurate and reliable measurements from the sensing system and to enable easy deployment, a magnetometer platform was designed and implemented that demonstrated improved accuracy and precision over the single sensor system. In addition, the platform integrates security and data management features to ease deployment. Finally, to speed transition of the detection systems towards deployment in proximity to power transmission lines a simulation tool was developed of GIC field distributions near sensor installation locations. The result of the model is a simulation tool that can evaluate the suitability of field deployment locations.

The contributions of this thesis are demonstrated in the following IEEE international peer-reviewed publications that have been presented at their associated technical conferences.

A. Lackey and R. Goubran, "Low-Cost Magnetometer Sensing System for Detecting Geomagnetically Induced Currents in Transmission Lines," *in Proc. of IEEE Sensors Applications Symposium*, Glassboro NJ, 2017. [17]; and

A. Lackey, R. Goubran and F. Kwamena, "Geomagnetically Induced Current Measurement Using an Integrated Magnetometer Platform," *in Proc. of IEEE Sensors Applications Symposium*, Seoul, South Korea, 2018. [18].

1.4. Thesis Outline

This thesis is organized into eight chapters. Chapter 1 is an introduction, laying out an overview of the motivations and contributions of the research.

Chapter 2 provides a background on electromagnetic threats to power transmission lines, space weather, challenges associated with GIC measurement, GIC measurement principles, and methods of modelling GIC in a power system network. The chapter starts with a literature review to develop a strong basis for the research. Continuing with a review of the phenomena of space weather, its complexities and some significant challenges associated with GIC detection and designing systems for GIC detection. In addition, an overview of the impacts of space weather provides an indication of the severity of space weather and potential for disruption.

Chapter 3 provides a detailed overview of the current approach to GIC detection and measurement through modelling. Current mathematical models and methods are presented and their limitations in determining real-world GIC identified. One of the overall goals of the thesis is to bridge the gap between modelling and real-world measurements while leveraging the advantages of work already completed in the field.

Chapter 4 presents the design and implementation of a scaled GIC test bench to emulate real-world GIC in electric transmission lines. The design is configured to closely resemble real world power transmission lines with respect to GIC flows. The implementation of the test bench provides an environment for detection and sensing system development and verification.

Chapter 5 presents the design and implementation of a simplified GIC detection system. Included is the complete design process, data measurements obtained by the system during operation, and a summary of overall performance of the detection system in different configurations and test conditions.

Building on the system developed in the previous chapter, Chapter 6 outlines the design and implementation of a GIC measurement platform. Consideration and use of several different magnetic field sensors are configured and used in a single sensing system and a method developed to integrate simultaneous measurements from multiple sensors. Measurements obtained by the system are presented and the performance is discussed.

Chapter 7 presents the design and implementation of a GIC field simulation tool for the purpose of evaluating the predicted performance of GIC detection and measurement systems. The tool is used to evaluate the potential GIC encountered in a number of transmission line configurations.

Lastly, Chapter 8 provides conclusions on the work completed and outlines future work that can be undertaken to further advance the field of GIC detection and measurement.

Chapter 2. Background

This chapter provides required background on the electromagnetic threats to transmission lines including geomagnetically induced currents (GIC) and space weather. In addition, a review of GIC flow through power transmission lines provides context for the development of a GIC detection system. The impacts of GIC and its associated mitigation methods underline the need to develop GIC detection systems that are application specific and take into account the whole threat vector. The chapter concludes with a review of the state-of-the-art GIC detection methods and systems.

2.1. Electromagnetic Threats to Power Systems

Transmission systems are protected against a wide range of electromagnetic threats from different vectors. Electromagnetic threats can either be direct or indirect and have different protection mechanisms in place to mitigate their effects. Direct impacts are from devices and components that are connected to the power transmission and distribution systems, for example the surges associated with a welder being operated or a motor starting. These impacts to operations have been studied since the inception of power transmission networks, and can be addressed through correct power system protection implementation, such as relays, fuses, and circuit breakers [19]. Indirect impacts are from electromagnetic activity that is not directly wired to a transmission network. There are three types of indirect electromagnetic events that can cause damage to power transmission systems: lightning, GIC, and Electro Magnetic Pulse (EMP) each requiring unique mitigation measures. While EMP share many similarities with lightning and GIC its potential impacts are not fully understood on a wider scale and significant research is on-going [20].

The most common significant electromagnetic event is lightning. Direct strikes cause spikes in current and indirect strikes cause a propagating voltage spike along a transmission line. Lightning generates a strong electromagnetic field in proximity to its strike location, this field then directly couples with the phase conductors inducing a high frequency voltage component. Figure 2-1 shows a typical lightning strike in proximity to a transmission pylon. The phase conductors are protected from over voltage and direct strikes by the shield wire running along the top of the pylon. In addition, direct strikes are mitigated through the addition of lightning arrestors on critical components such as transformers.

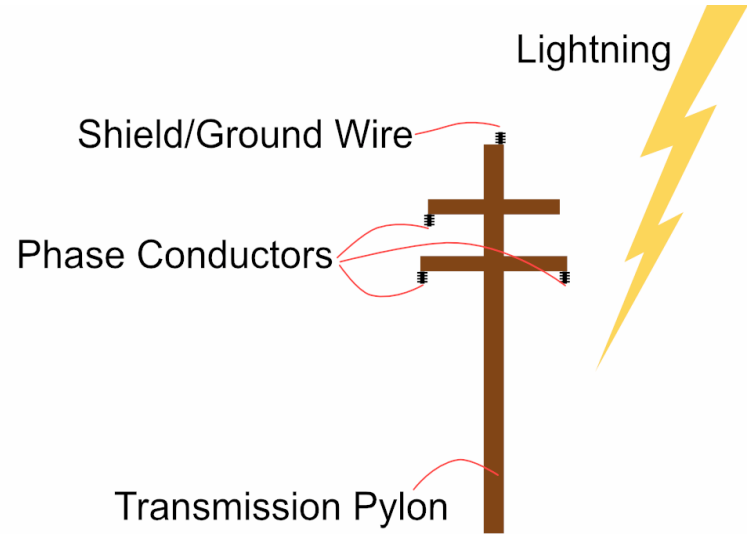

Figure 2-1. Electromagnetic Threats to Transmission Lines

The primary difference between lightning and GIC is frequency, with the high frequency pulse induced by lightning methods have been developed to reduce their impacts however low frequency GIC will bypass lightning protection mechanisms. The second difference is their coupling mechanism, lightning must either strike or directly couple with the phase conductors to influence the normal system operation but GIC can

enter through any grounding point in a power system, resulting in different approaches to mitigation.

2.2. Introduction to Space Weather

Space weather is a natural hazard that has the capability to disrupt electric power supply and communication networks. Generation of space weather is a complex process that originates through the fusion of hydrogen atoms in the Sun. The physics underlying the Sun's energy production result in dynamic concentrations of electromagnetic fields that unpredictably direct the flow of plasma and particles within its core.

Plasma within the core is trapped by magnetic fields and transported away from the surface of the Sun in long arcs. Deterioration of the stability of the arcs results in the ejection of particles from the Sun's gravitational pull. This process is known as Coronal Mass Ejections (CME) as shown by the artistic rendition in Figure 2-2. Particles that escape the Sun via CME propagate toward the Earth with speeds between 300km/s and 2000km/s taking between 20 and 135 hours to reach the Earth estimated by [21] through the analysis of Solar and Heliospheric Observatory (SOHO) satellite data. The generation of space weather amplifies challenges related to predicting the flow of GIC, analogous to predicting weather on Earth as a combination of pattern recognition and estimations.

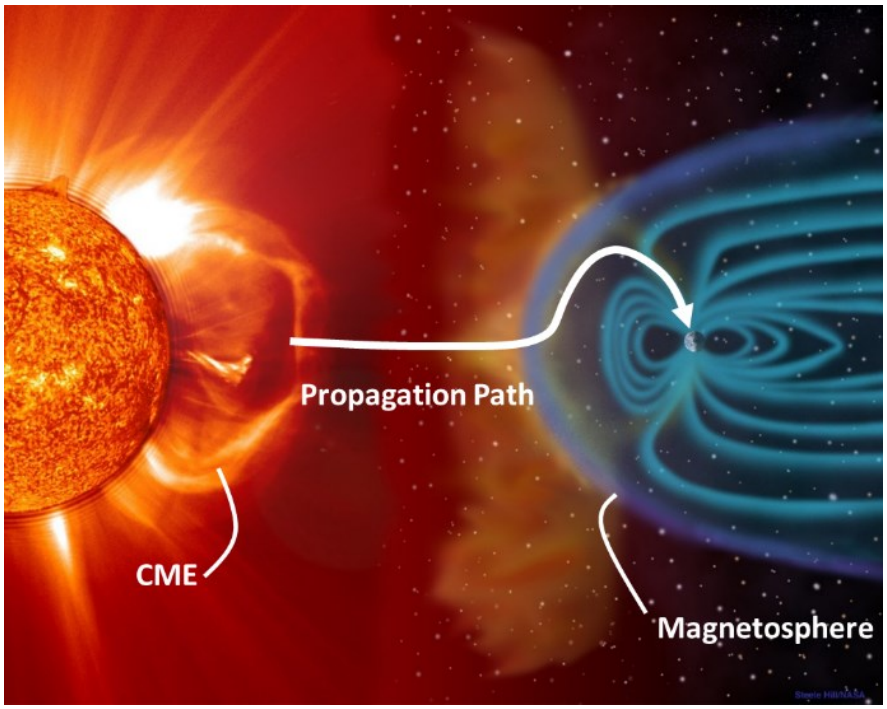

Figure 2-2. Space Weather Propagation Towards the Earth [22]

2.2.1 Predicting Space Weather

The Sun follows an approximate 11 year cycle of activity, as shown in Figure 2-3. The number of sunspots on the surface follow a periodic pattern that correlates with activity levels. The number of sunspots provides a rough indication of overall solar activity in turn providing a rough indicator of potential geomagnetic activity on Earth. However, the probability of a major geomagnetic event is not solely dependent on average solar activity and can occur with little warning. The general indication of solar activity does not provide an absolute measure of the probability of a major geomagnetic event occurring [23].

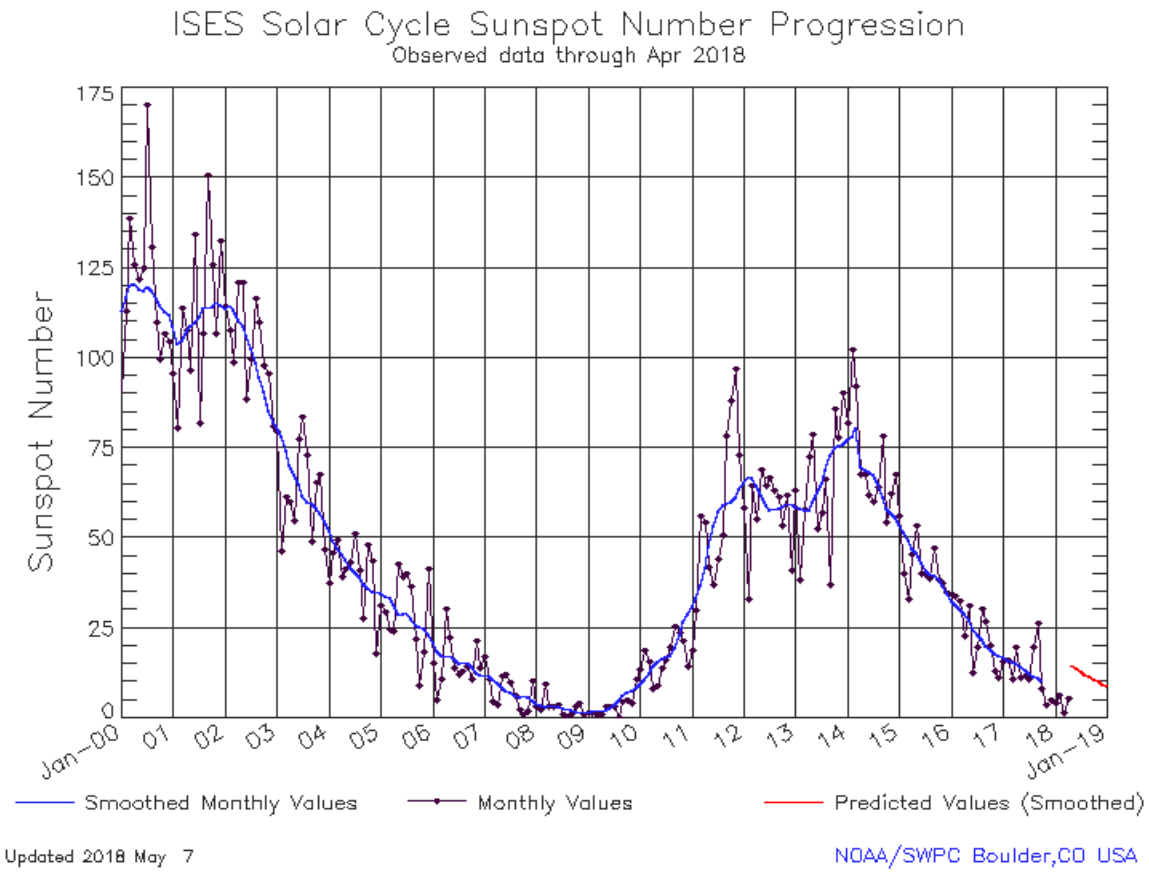

Figure 2-3. 11-Year Solar Cycle [24]

The multitude of unknowns in predicting space weather phenomena requires the design and construction of robust detection, measurement and monitoring systems that provide granular information on power system operations.

2.2.2 Atmospheric Electro-jet

Space weather is the primary driver of GICs. Particles ejected towards the Earth first interact with the magnetosphere, the outer most protective layer. The magnetosphere redirects most of the incoming particles away from the Earth, however a portion flows towards the poles. Particles that pass through the magnetosphere then interact with the ionosphere. The ionosphere is positioned between 400km and 70km from the Earth's

surface and is constantly changing. Particles passing through this protective layer are ionized resulting in charged sections of atmosphere. Non-uniform distribution of charges leads to potential voltage differences being developed between regions, the outcome being the flow of current. Collectively the currents flowing through the ionosphere are known as Electro-jets.

Electro-jets are generally located between 150km and 100km from the Earth's surface, due to the collection and flow of charge. Auroral electro-jets, located north of 40° latitude, have significantly higher current flows than equatorial electro-jets due to their relatively higher concentration of incoming particles. Currents flowing in electro-jets are non-uniform ranging from hundreds to thousands of amperes. The end result of electro-jets are the generation of a broad range of magnetic fields that impact all electrical systems on the surface of the Earth such as electricity transmission lines, communication infrastructure, navigation sources, and pipelines.

2.2.3 Damage of Space Weather Events to Energy Infrastructure

There is a constant threat of a major space weather event occurring. Previously, there have been numerous examples of GIC influencing critical infrastructure systems.

In March 1989, a space weather event caused transformers to saturate in the province of Québec and protection system to fail. The resulting outage affected millions and caused complete blackouts for over 9 hours with full restoration taking over 3 weeks. Estimation of the total economic impact by [10] places damage upwards of $4.2 Billion CAD.

The Carrington event of 1859 occurred prior to the construction of most modern infrastructure and monitoring systems. However, it is widely regarded as one of the most significant space weather events in modern history [25]. Failures and sparking of telegraph systems, auroras observed as far south as Mexico and off the chart measurements only provide a rough indication of its potential impacts today. As recently as September 2017, there have been space weather events impacting critical infrastructure [26]. The next event may arrive with minimal warning and little time for preparation.

2.3. GIC and Electric Power Transmission Systems

Electromagnetic fields generated via the atmospheric electro-jet propagate to the Earth's surface and through potential voltage differences, generate currents in long conductors. Conductors include pipelines, transmission lines, and communication networks and electric power transmission lines. GIC have been known to exist since the 1800's [1] and their effects have been studied around the globe [27].

When a significant voltage difference is created, a current will begin to flow through the soil. This current will interact with any long conductors, such as electric power transmission lines and pipelines that is in contact with the Earth. GIC enters into transmission lines through grounding points and flows from one geographic location to another. The characteristics of GIC are fundamentally quasi-DC in nature with observed frequencies below 1Hz, adding to mitigation challenges. GIC are generated through space weather but their magnitudes are influenced by power systems configurations and components in addition to geophysical conditions of a power network. Figure 2-4 illustrates the electro-jet and how GIC enter into a power system through a transformer neutral wire.

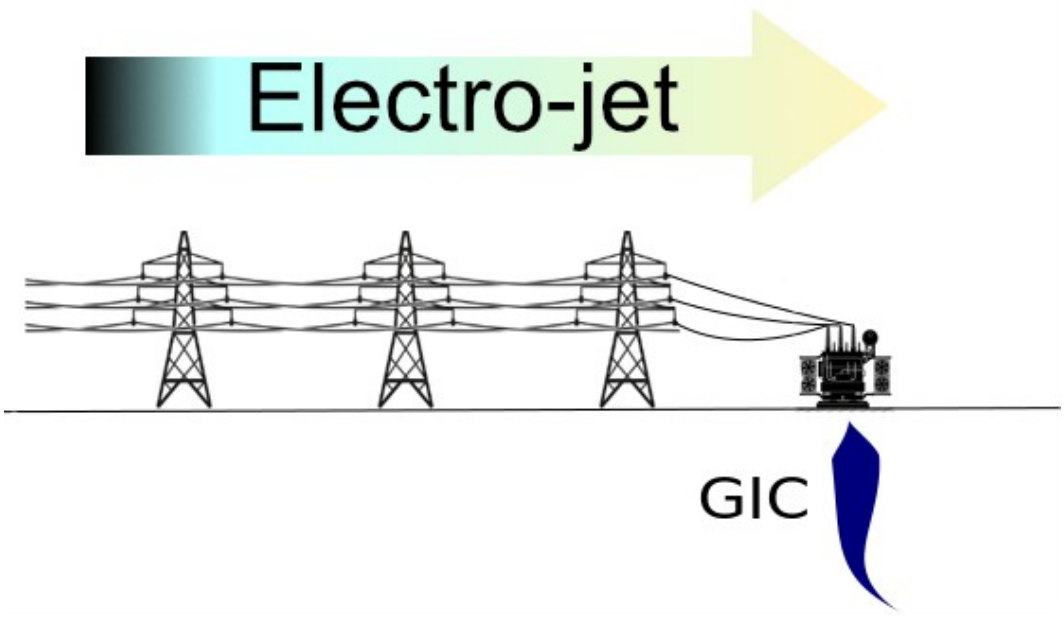

Figure 2-4. GICs Generated Through the Electro-jet Enter Into Conductors Along the Earth's Surface

2.3.1 Factors Influencing GIC Flow

GIC flow is greatly influenced by both physical and electrical characteristics of each power transmission system. The first factor is directional sensitivity of lines entering a substation, as analyzed by [28], shown to change the direction and magnitude of flows. Secondly, transmission line and substation conductivity improvements and changes have resulted in an increased potential for higher observed GIC magnitudes, demonstrated by [29]. The overall length of a complete transmission network is a third factor that can impact GIC flows, with penetration from external networks requiring further consideration. Since GIC mitigation has not been a primary concern during the design and construction of power systems, other solutions must be implemented to protect system operations. Geophysical effects are a fourth influencing factor towards the magnitude of GIC found in a power system.

Geophysical effects on GIC flow can be system wide or have isolated effects on particular subsystems. Latitude of a system is a primary geophysical influencing factor inferred from observed GIC magnitudes. Under higher latitudes the Auroral electro-jet generates larger GIC as shown in [30] thereby increasing the risk of damage due to GIC. Soil conductivity properties and changes in soil conductivity between regions influences the probability of larger induced voltage potentials and can regionally impact transmission lines. Additionally, abrupt changes in ground conductivity, such as a body of water can severely influence calculations and estimation of GIC flow. GIC mitigation measures must take into account all factors that influence the flow of GIC to be effective. Previous research has focused on modelling and mathematically calculating the flows of GIC to develop mitigation solutions and reduce its impacts.

2.4. Impacts of GIC on Electric Grid Operations

Primary impacts of GIC on power systems includes transformer damage, and network instability. The range of impacts are tightly coupled and are likely to cascade and effect multiple systems over large geographic regions, if precautions are not taken.

Power transformers are fundamental components of all AC transmission systems. Utilities invest significant resources in both their procurement and maintenance to ensure system reliability. Regulations require that transformers be operated within a certain percentage of nameplate capacities and have correct grounding capabilities. All electric grids are vulnerable to the impacts of GIC through grounding points in power transformer neutral-to-ground connections. Neutral-to-ground connections are required by design when a three-phase transformer feeds an unbalanced load. Quasi-DC GIC flowing through transformer coils results in a DC shift of its operating point, by introducing

additional magnetic flux. Under the shifted operating point, the ferromagnetic core is unable to accommodate or sustain the required flux according to nameplate specifications. After a DC shift, AC waveforms can saturate the flux in the core resulting in half-cycle saturation. Half-cycle saturation appears as a "clipping" of the peaks of the AC signal.

Half-cycle saturation in transformer cores induces a variety of secondary effects. Thermal spot heating in the coils is amplified [31] . Excessive heating leads to the degradation of insulation materials and can cause complete breakdown as shown in Figure 2-5. Unmonitored GIC influx and saturation can increase maintenance costs by reducing the expected lifetime of transformer insulation.

Figure 2-5. GIC Causing Damage to Power Transformers [32]

Electrical impacts of GIC on transformers can have far-reaching system wide effects. Transformer core saturation leads to requirements for increased reactive power generation [33], straining existing generation resources. In addition, distortion of the AC signal can lead to the generation and propagation of harmonics. Stability of the electricity

supply can quickly deteriorate resulting in blackouts and brownouts. Tertiary impacts of GIC are its influence on protection and control mechanisms. Simple electro-mechanical relays, used in all aspects of power system protection, have mis-operated leading to cascading failure of the electric grid. Power electronics fundamental to smart grids are vulnerable both by the generation of higher order harmonics and the presence of DC signal components [34]. Finally, to compound resilience and response efforts, communication networks have been observed to fail during GIC events with little indication or warnings [35].

2.5. GIC Mitigation Methods

GIC can be mitigated via two different methodologies. The first method is through power system design, physical component configurations, and system planning. The second method is through electric grid operations in reaction to changes in system behaviour.

Previous work has informed system designs through extensive use of modelling methods. Modelling GIC in power system networks requires a complete investigation into power system components at DC frequencies to determine the network configurations as equivalent resistances. Figure 2-6 shows an exemplary model of a power transmission system with lines 1, 2, and 3 indicating transmission lines connected at a common node. R_{gnd} is representative of the transformer neutral to ground resistance. The resistive network has been demonstrated to adequately model GIC flow by [14]. The flow of GIC can be bi-directional and can change depending on dominant space weather conditions.

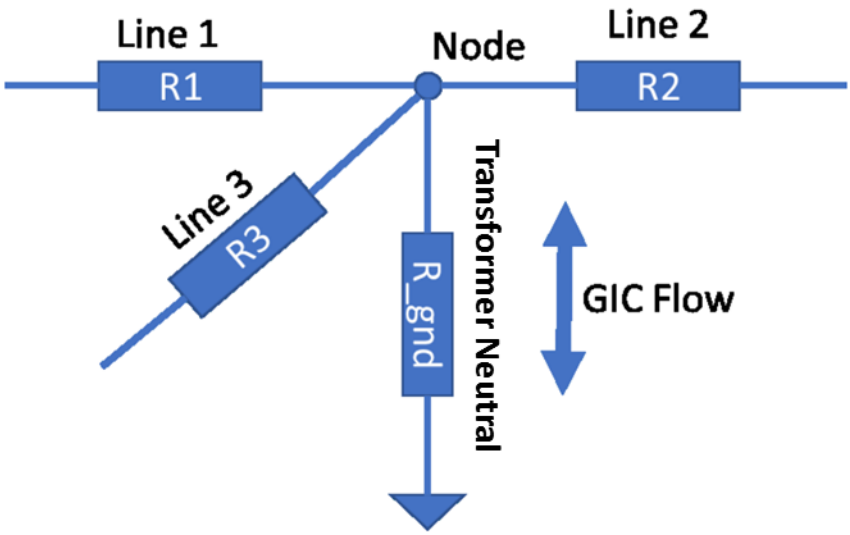

Figure 2-6. Resistive GIC Power System Model

Additional simulation of GIC through transformers and other components can be used to supplement flow modelling and design system components to reduce the impacts of GIC. Capacitive blocking devices can be installed inline with the transformer neutral-to-ground connections allowing AC fault conditions to correctly flow to ground while blocking the influx of GIC into the system. Drawbacks of this method can include the required installation times, expense and maintenance costs. In addition, the installation of capacitive blocking devices can shift the GIC flow problem to other nodes in the electrical grid, potentially having a severe impact on transformers that have previously been identified as low risk as shown by [36]. Modified system operations can be used to mitigate GIC if it is detected in a timely manner. Switching loads or changing to alternate power delivery routes to protect vital equipment has been demonstrated to effectively reduce the risk of damage due to GIC. Smart grid infrastructures allow the use of reactive power compensation to reduce frequency and voltage instabilities induced by GIC [37].

Both categories of mitigation methods benefit from new sensing technologies. The deployment of GIC detection and measurement systems allow electric utility owners and operators to both plan and respond in real time to dynamic changes in space weather. The characteristics of GIC signatures provides an additional challenge due to typical monitoring systems being unable to detect and measure DC or quasi-DC signals rendering them unable to provide useful data on GIC flows. Dedicated measurement systems are required to mitigate against GIC in electric power grids.

2.6. State of the Art of GIC Detection and Measurement

The field of GIC detection and measurement has had limited recent developments due to a range of social and economic influences. Deployment environments are challenging due to complex technical and physical requirements and limitations on potential prototype systems. Existing GIC measurement systems are inflexible and do not take advantage of modern sensor developments.

Two principle direct measurement methods have been previously developed. The first method is to deploy a hall-effect sensor mounted on a transformer neutral-to-ground wire, which requires specialized training and provides limited visibility of GIC flow, as described in [38]. The second method is to deploy a differential magnetometer technique, that requires external synchronization and complex sensors as described in [39].

Existing GIC measurement methodologies offer limited deployment flexibility, or external support systems to function correctly. Deployment restrictions limit the amount of information that can be obtained about GIC flow in a power grid. An indirect method using phasor measurement measures the total harmonic distortion generated by

transformers as described by [40] can be used to infer GIC levels. Review of existing technologies offers insights into the gaps in technical knowledge and skills in the field of GIC detection and measurement.

2.6.1 Hall Effect Measurement of GIC

A widely accepted measurement method for GIC has been to use hall-effect sensors to measure the DC component of current flowing through a transformer's neutral-to-ground wire. Figure 2-7 shows the location of the sensor installation from an electrical perspective. Precise measurements can be obtained with this method, providing a direct indication of the GIC flow through a specific transformer. A major drawback of this method is an inability to measure GIC when blocking capacitors, protection devices, or reactive power compensation devices are installed on the system [41]. In addition, the installation of the measurement devices requires direct contact with power systems, requiring additional specialized training and safety considerations prior to deployment. Sensing platforms that use this method are restricted by the required placement of the device on the transformer ground-to-neutral wire reducing overall flexibility.

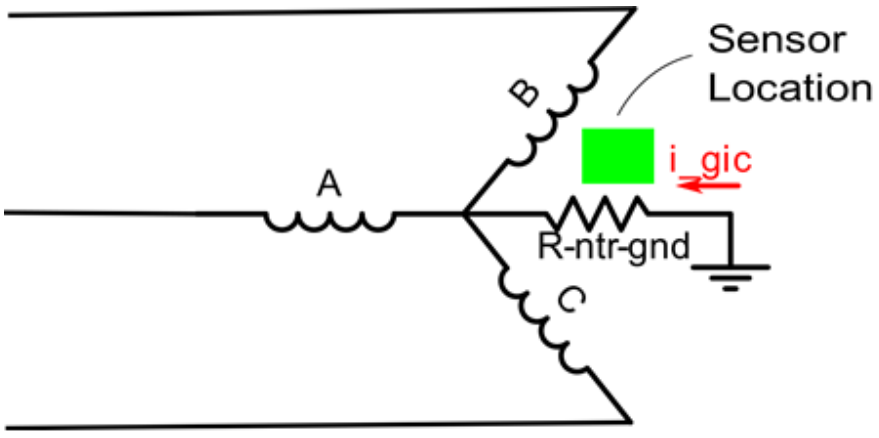

Figure 2-7. Hall Effect Method for Measuring GIC

Technical challenges of the system are in its inability to measure current flows in connected substations, leading to limited information on the flow of GIC through a power system as a whole. Installation is partial to large power transformers due to costs and accessibility of components reducing the uptake of the technology from small to medium sized utilities. The challenges with this method spur the need for easily deployable sensing platforms that can be quickly integrated into existing and future power system operations of all sizes.

2.6.2 Differential Magnetometer Measurement of GIC

Differential magnetic field measurement is a non-contact method that has been used to measure the GIC in power transmission lines. The concept was initially proposed by [15] and was further developed for testing in lower latitude regions by [42]. This system relies on two distinct GIC measurements from under the transmission line and a separate magnetometer to measure and evaluate background fields. Specifically the method employed by these measurement systems is to use differential magnetic field readings to eliminate background biases caused by parasitic fields; this includes both naturally occurring magnetic fields and the magnetic field induced by electro-jets and man-made sources. The system requires sensors that can detect very low magnetic field strengths and implements a fluxgate type sensor to achieve the required sensitivity and precision. An example of the required position of the sensors is shown in Figure 2-8.

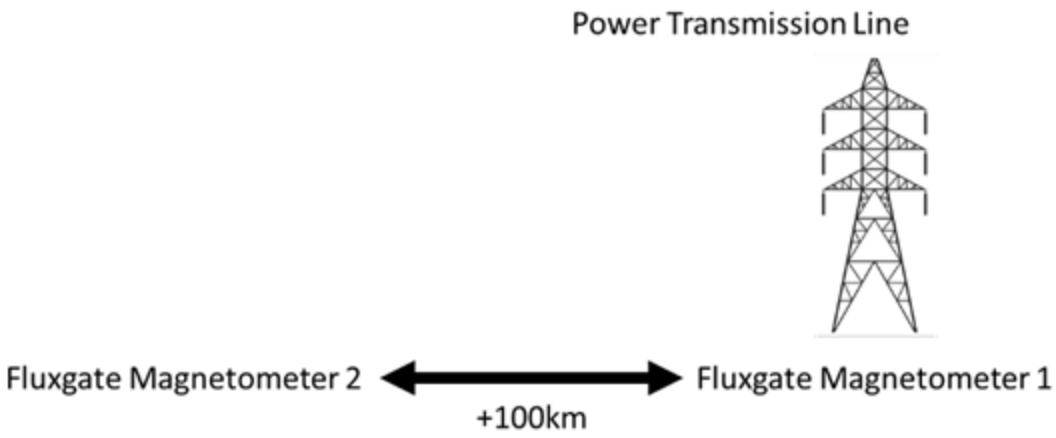

Figure 2-8. Differential Magnetometer Method of Measuring GIC

There are several drawbacks to using this method including synchronization of signals, interference from unknown fields, and requirement of complex magnetometers. Distances required to obtain satisfactory measurements between the sensors requires a synchronization method between data measurement sites. Large distances increase the need for a reliable communication infrastructure that adds to system complexity and installations requirements. Ground conductivity changes as described in [43], can also have an effect on the image current and background fields. Finally, the differential technique has limited potential for real-time functionality and required the operator to have specific knowledge of GIC in order to operate the system correctly.

2.6.3 General GIC Measurement Challenges

Electric power systems are expected to operate through extreme weather, space weather, earthquakes, cyber attacks, and other threats to critical infrastructure. The challenge of operating electricity infrastructure is amplified by the vulnerabilities of aboveground conductors, large monitoring areas, and aging infrastructure itself. Availability of technology, tight regulations, and physical and technical application

environments limit utility owners and operator's ability to detect, measure, and mitigate the impacts of GIC.

Field-testing measurement platforms requires consideration of temperature ranges and moisture ingress for equipment deployed over extended periods. Geophysical properties of the earth's surface have a profound impact on the magnitude of GIC flow. Improving the simplicity of systems allows for a decrease in maintenance costs and improvements in resilience, increasing the potential for industry adoption of new technologies. Integrating new sensors into smart grid environments requires compatible technologies and methodologies that account for present day physical and cyber security challenges.

In addition to the technical and implementation challenges of measuring GIC there are problems with obtaining verification data for detection and measurement deployments. Due to the frequency and magnitude of space weather events being difficult to predict deployments can obtain data for extended periods of time without recording a significant event for investigation. The research and design that has been performed addresses both the technical limitations of existing methods in addition to deployment and adoption issues from an industry perspective.

Chapter 3. GIC Modelling

GIC modelling and simulation techniques are the primary tools available for determining the flow of currents in a power system network. There are two steps to modelling GIC flow, the first is to develop an electrical circuit model, second is to develop a model of geophysical properties [12]. These two steps are required to enable accurate modelling of GIC flows and are often undertaken by people with different skillsets. Simulation tools leverage the development of GIC models to calculate the practical values of GIC expected in a particular power system network. GIC models are generalized in order to be applied under a wide range of conditions while simulation tools examine specific conditions and parameters of interest. In order to generate relevant and applicable results a combination of modelling and simulation tools are often employed [44]. Simulation is defined as "…the imitative representation of the functioning of a system…" and modelling is defined as "…a system presented as a mathematical description of an entity or state…" by [45], this provides a basis to differentiate between different research on GIC simulation and modelling. This chapter will review the current approach to GIC modelling and highlight the gap between modelling and real-world GIC detection and measurement systems.

3.1. Circuit Model Properties

Circuit and power system models are used throughout the electricity industry to model scenarios and their impacts on systems operation. Future smart grids require significant modelling and simulation to understand vulnerabilities and challenges as shown by [46]. Fundamentally, the information gathered on power system parameters are focused around the frequency of interest at either 60Hz or 50Hz. System parameters that

are recorded include inductance, resistance, and capacitance for select transmission lines. The grounding resistance is regulated to a threshold for safety implications. The difference in frequencies leads to a significant change in the circuit model used for transmission lines.

Initially the circuit can be represented by the power transmission single line diagram represented shown in Figure 3-1 where R, L, and C are the transmission line's resistance, inductance, and capacitance respectively. R_S and L_S are the equivalent substation resistance and inductance representing both the transformer coils and the grounding wire characteristics. Nodes 1, 2, and 3 indicate individual bus bars at each substation. The figure shows a starting point for developing a GIC circuit model.

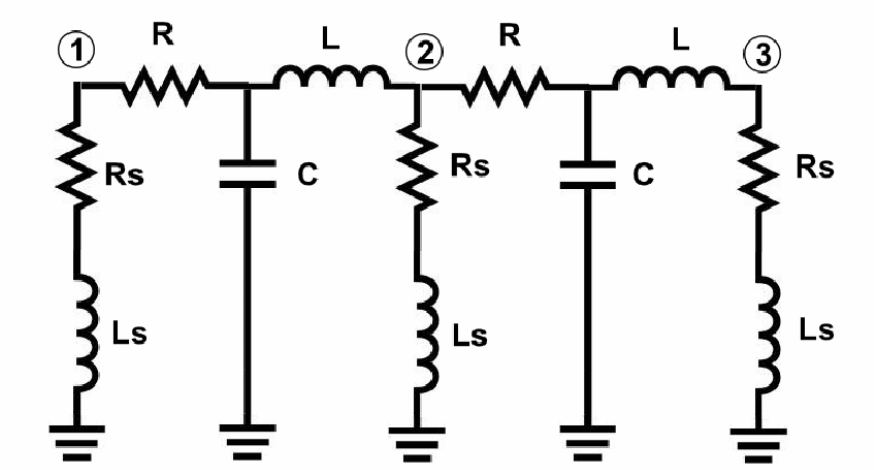

Figure 3-1. Transmission Line Single Line Diagram for a Test Network

Fundamental electromagnetics as determined by Faraday-Maxwell demonstrate that the properties of inductance and capacitance are frequency dependent. The impedance of each component can be calculated using $Z_L = j2\pi fL$ for inductors and $Z_c = \frac{-j}{2\pi fC}$ for capacitors respectively. As $f \to 0, Z_L \to 0 \; and \; Z_c \to \infty$, leading to the simplification of

Figure 3-1 into the circuit shown in Figure 3-2. This can be assumed to the quasi-DC nature of geomagnetically induced currents.

The resistance of any conductor at DC frequencies can be calculated using $R_{DC} = \frac{\rho l}{A_{CX}}$ where ρ is the resistivity in ohm-meters, l is the conductor length in meters, and A_{CX} is the conductor cross-sectional area. However, since power systems operate in a wide range of temperatures the resistivity must be modified according to equation (1).

$$\rho(T) = \rho(T = 20°)(1 + \alpha(T - 20°)) \quad (1)$$

The α parameter is dependent on the conductor material and the resistivity at temperature $T = 20°$ is found via experimentation for different conductor materials. In addition, the stranding of a conductor can change the DC resistance of the line by 1-2% [47], but will be ignored in this case to simplify the final equations.

R_S in Figure 3-2 represents a combination of resistances found in a substation (bus-ground connection), primarily the transformer coil resistance (R_{TC}) and the grounding resistance (R_G). The ground resistance for a typical substation can be calculated using equation (2).

$$R_g = \rho_g \left(\frac{1}{L_g} + \frac{1}{\sqrt{20 A_g}} \left(1 + \frac{1}{1 + d_g \sqrt{\frac{20}{A_g}}} \right) \right) \quad (2)$$

In equation (2), ρ_g is the ground conductivity, L_g is the total buried length of conductors, and A_g is the area occupied by the grounding grid, and d_g is the depth of the grounding grid [48]. The transformer coil resistance is closely linked to the type of transformer type installed at the substation, and the wiring of the primary and/or secondary coils. Calculating the resistance of transformer coils is often used to determine the expected

power dissipation and integrated into efficiency calculations for typical grid operations at 60Hz. For each unique transformer a test apparatus can be used to apply a known voltage and inject a known current into an isolated transformer winding to determine R_{TC}. In addition this value can change based on the deterioration of insulation and temperature changes [49].

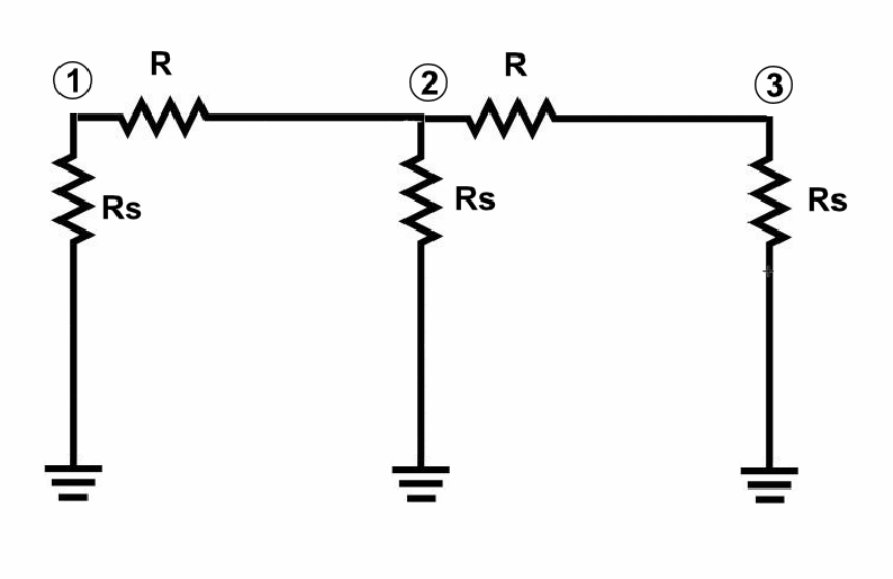

Figure 3-2. DC Transmission Line Circuit

The final step in developing the electrical circuit is to model the induced geoelectric potentials as their equivalent voltage sources. Inserting a voltage source along the length of each transmission line segment, as shown on the left side of Figure 3-3, has been found to accurately represent real-world conditions. The voltage sources can be easily converted to its equivalent current sources using Thevenin-Norton equivalent circuit theory as shown in the right side of Figure 3-3, this is done to simplify the circuit model and to assist in solving for unknown values. Further details on how the voltage sources are modelled are provided in Section 3.2.

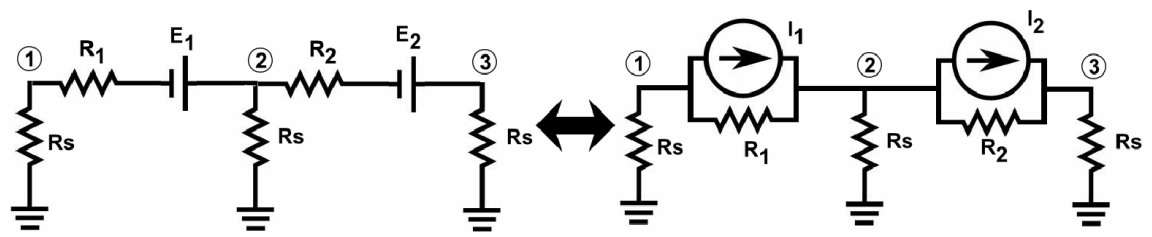

Figure 3-3. GIC Circuit Model with Induced Voltage Sources and Thevenin (Left) -Norton (Right) Equivalents

In Figure 3-3 the three nodes are shown as an illustration of a very small power transmission line network. In reality, the networks are vast interconnected infrastructures that span thousands of kilometres. Previous work has indicated the inaccuracies introduced by ignoring neighbouring networks can account for errors from 5% to 7% [14]. Thus to have an accurate network model, further information is required by utilities in order to simulate the interconnects between their network and neighbouring networks.

Modified Nodal Analysis (MNA) can then be applied to the circuit shown in Figure 3-3, each resistance (R) is converted to its equivalent conductance (G) to simplify calculations. MNA results in a matrix representation of the form $[\mathrm{G}][\mathrm{V}] = [\mathrm{I}]$, where V and I are the voltage and current matrices of each node of the circuit. Performing MNA on the example circuit results in a matrix representation of the circuit, shown by equation (3).

$$\begin{bmatrix} G_s + G_1 & -G_1 & 0 \\ -G_1 & G_s + G_1 + G_2 & -G_2 \\ 0 & -G_2 & G_s + G_2 \end{bmatrix} \begin{bmatrix} V_1 \\ V_2 \\ V_3 \end{bmatrix} = \begin{bmatrix} I_1 \\ -I_1 + I_2 \\ -I_2 \end{bmatrix} \tag{3}$$

Equation (3) can then be solved via inversion, sparse matrices operations, or iterative methods (e.g. forward-backward Euler) depending on the size of the circuit under analysis. This provides a complete mathematical representation of the GIC in a

transmission line circuit. However, the currents, $I_1 and\ I_2$ for this example, are dependent on complex geophysical modelling.

3.2. Geophysical Model Properties

The geophysical models of the transmission line environment vary widely from system to system. Latitude, soil conductivity, system orientation, length, and other factors all influence the magnitude of GIC. The induced voltages can be calculated as the integral of the geoelectric field along the length of the transmission line, between grounding points, as shown in equation (4).

$$E_n = \int_A^B \overrightarrow{E_{field}} \cdot \vec{dl} \qquad (4)$$

Since the fields are conservative; equation (4) can be rewritten as equation (5) using Cartesian coordinates.

$$E_n = L_{AB}(E_{fieldX} sin\theta + E_{fieldY} cos\theta) \qquad (5)$$

Due to the length of the transmission lines involved strict Cartesian coordinates in a 2D plane do not fully represent the length of the transmission lines due to the curvature of the Earth and can be modified accordingly.

The geoelectric fields $E_{fieldx}\ and\ E_{fieldy}$ are an additional step in the geophysical modelling that required a further understanding of space weather phenomena. The geoelectric fields are most commonly calculated using the method proposed by [49] that employs a 1D-earth model and plane wave method. The process results in the electric field at the Earth's surface calculated using equation (6). Where E_n is the electric field at the desired calculation point *(n)*, ω is the frequency of the electro-jet, I_{jet} is the current

flowing through the electro-jet, μ_0 is the permeability of free-space, and *d* and *h* are the lateral and vertical distance of the calculation point from the electro-jet.

$$E_n = -\frac{i\omega\mu_0 I_{jet}}{4\pi}\frac{\sqrt{d^2+h^2}-h}{d} \quad (6)$$

In addition, the complex image is accounted for by emulating a conductor at the complex image depth as calculated by $p(\omega) = Z(\omega)/(\, i\omega\mu_0)$, where $Z(\omega)$ represents the 1D approximation of the Earth's impedance in the region. While 1D models are common, adding 2D or 3D details to the conductivity model have been demonstrated to improve accuracy but require additional data and computing capabilities. This method has resulted in improvements from 20% geoelectric voltage accuracy using a plane wave method compared to 15% using the more complex (3D) geometries [51]. Detailed information on specific regions requires geophysical surveys for accurate data representation, which are not always available for all utilities, considering the expertise required for interpretation.

The geoelectric fields induced via electro-jet vary in terms of frequency, magnitude, direction, position, distance, orientation, configuration, and other factors as described by the field of heliophysics. Predicting the occurrence of space weather events and modelling the electro-jet itself is outside the scope of this thesis.

3.3. Combining Circuit and Geophysical Models

Combining the geophysical modelling techniques with the circuit modelling techniques provides a complete picture of the GIC model. Using the overall MNA matrix developed in equation (3) we can now substitute the values for resistance, and the geophysical model for the induced voltages using equation (6). Expanding the matrix

shown in equation (3) and taking the first equation in the matrix as an example as follows the result is shown by equation (7).

$$V_1(G_s + G_1) - G_1 V_1 = I_1 \qquad (7)$$

Which relies on information expanded through equations (8), (9) and (10).

$$G_s = \frac{1}{\rho_g\left(\frac{1}{L_g}+\frac{1}{\sqrt{20A_g}}\left(1+\frac{1}{1+d_g\sqrt{\frac{20}{A_g}}}\right)\right)+R_{TF}} \qquad (8)$$

$$G_1 = \frac{A_{CX}}{\rho(T=20°)(1+\alpha(T-20°))\,l} \qquad (9)$$

$$I_1 = \left(\int_A^B \left(-\frac{i\omega\mu_0 I_{jet}}{4\pi}\frac{\sqrt{d^2+h^2-h}}{d}\right)\cdot\overrightarrow{dl}\right) G_1 \qquad (10)$$

Overall, the equation (7) depends on a large number, 13 at a minimum, of variable elements in order to solve the GIC flow through a specified power system. The summary of the variable details and their dependencies are shown in Table 1. The combination of separate areas of study from power system modelling and geophysical modelling is required to fully understand the flow of GIC in a power system.

Table 1. Summary of GIC Model Parameters

Parameter	Details	Dependence
ρ_g	Ground conductivity	Moisture, temperature, soil composition
L_g	Total length of the grounding conductors	Substation voltage level, fault currents, soil composition
A_g	Area of the grounding plane	Substation voltage level, fault currents, soil composition
d_g	Depth of grounding conductors	Substation voltage level, fault currents, soil composition
R_{TF}	Transformer coil resistance, typically obtained via specific testing.	Transformer type, size, insulation status
A_{CX}	Transmission line cross sectional area	Voltage, power system currents.
$\rho(T = 20°)$	Conductor resistivity at 20°C	Obtained through experimentation or specific testing of materials
α	Material property of the conductor	Tables are available for typical conductors
l	Total installed length of the transmission line from terminal to terminal	Approximates can be made based on simple distance; however this does not include sag and tension details.
$\int_A^B$	Integral from grounding point A to grounding point B	Can use Cartesian coordinates but the curvature of the Earth will have an impact on magnetic field declinations.
ω and I_{jet}	Frequency and current of the space weather induced electro-jet.	Time, space weather conditions.
d and h	Radial and horizontal distance of the surface of the Earth from the electro-jet.	Time, space weather conditions, Earth's impedance.
$\overrightarrow{dl}$	The integral of the component of the geoelectric field along the path of the transmission line.	Position of the transmission line in relation to the geoelectric field, can be simplified into x and y components.

Overall, the accuracy of the GIC models combined with simulation techniques have ranged from a maximum error of $\pm 20\%$ [52], to underestimation of GIC by an average of 49% [53].

3.4. Discussion

GIC modelling is a powerful tool that can be used to estimate different conditions of space weather and the expected flow of GIC in a network. Drawbacks of GIC models are the large number of physical parameters of the transmission line itself and geophysical parameters of the transmission line environment that must be gathered in order to obtain accurate results. To advance GIC detection and measurement a system must be developed that fills the gap between pure models, practical simulations and real-world deployments.

Chapter 4 will present the design and implementation of a scaled GIC test bench as a mechanism to bridge the gap between modelling and real-world conditions for GIC detection in transmission lines.

Chapter 4. Design and Implementation of a GIC Test Bench

GICs have various properties that contribute to a complex measurement environment. Unpredictable and inconsistent space weather is a key driver of this complexity. Long periods of inactivity followed by intense storms can result in data measurements that have limited usable results. In addition to the nature of GIC signals, the operating environment of power transmission lines requires robust environmental protection that would inhibit construction and slow prototyping speeds. Temperatures can range from ±40℃ over the course of a year. In addition, rain, snow, salt, and vegetation can cause significantly deteriorate the functionality of a deployed sensing system. A noisy magnetic environment contributes to difficulties in developing measurement solutions. Overcoming these challenges required a carefully designed system that could achieve the primary goals of a GIC detection and measurement system.

Test benches for power systems can range from field-deployed models with multiple life-sized poles and full sized transformers to real-time digital simulators with no physical hardware integration. Identifying and tailoring the application of a test bench towards GIC mitigation designs allowed for a unique system that reduces overall costs and provides a platform for further specialized development of technical solutions.

Technical challenges related to GIC measurement are amplified by an inability to demonstrate sensing effectiveness in relation to real world recorded data signatures. Additional technical challenges are imposed by the requirement of a test bench to deploy both AC and DC circuits along the same transmission path. Existing GIC testing systems are limited by their ability to effectively model a realistic magnetic field environment.

Addressing these challenges requires a new approach for simulating GIC generated fields in proximity to electric power transmission lines.

This chapter will provide an overview of the design and implementation of a test bench specifically tailored for duplicating quasi-DC magnetic fields produced by GIC in proximity to electric power transmission lines to design, test, and construct GIC detection and measurement systems.

Design and development of a test bench was considered to be the optimal method of developing and evaluating the performance of GIC measurement systems. The end target improvements of the GIC test bench over existing systems and methodologies includes:

- Developing a methodology to counter the introduction of transient magnetic field sources;
- Accelerating acquisition of real-world GIC signals to promote rapid sensing system development; and
- Minimizing environmental effects on preliminary sensing characterization.

The test bench herein described was implemented and validated via the design and implementation of GIC detection and measurement systems outlined in Chapter 5 and Chapter 6 of this thesis. Testing, validation, and configuration of measurement systems are facilitated through the implementation and use of the test bench. The design of the test bench started with a determination of requirements and key features.

4.1. Test Bench Design

Duplication of the real world-sensing environment was required to overcome challenges with infrequent high impact GIC events, impairing the testing and development new GIC measurement systems. Acceleration of the prototyping phase was required to enable rapid design revisions, testing, and validation to occur without waiting on natural phenomena. GIC testing and development required a test bench system that emulated real world infrastructure in a controlled environment. The requirements for a test bench were identified through examination of typical power system configurations to identify common system parameters. In addition, the test bench was required to be capable of use beyond the development of GIC measurement systems and include provisions for alternate GIC mitigation measures such as protection, control, and design based solutions. The test bench was designed and implemented to accurately duplicate real-world conditions for GIC measurement systems and associated power system infrastructure.

Initial design phases required consideration of power transmission line heights, span lengths, system components, and associated electrical configurations to develop a common baseline system configuration similar to the majority of electric grids. There are several requirements for the test bench that were identified to enable accurate representation of real-world electric power transmission systems. The magnetic field sources are a key part of the duplication of real world GIC.

4.1.1 Principle of Test Bench Magnetic Field Sources

Design of a test system that jointly produced both AC and DC magnetic fields was the first challenge identified in designing the test bench. Power supplies that are capable

of producing AC and DC do not typically have the capability to produce the desired current magnitudes and variations to emulate real world GIC. Independent current sources were critical in ensuring the test bench capabilities could recreate a range of GIC signatures that could be used for GIC detection and measurement systems as well as prototyping purposes. Lacking adequate power supplies required leveraging the linear superposition of magnetic fields from independent magnetic field sources.

Figure 4-1 shows the observed transmission line current and associated magnetic field decomposed into two distinct field components, AC and DC respectively. The DC component can be extracted from the overall signal as a constant shift in the average value from AC components. This is possible due to the regulatory and system requirements on frequency. Once the DC component has been extracted the AC components of the original signal remains. The result of this breakdown is a division of the observed magnetic field into its two separate components.

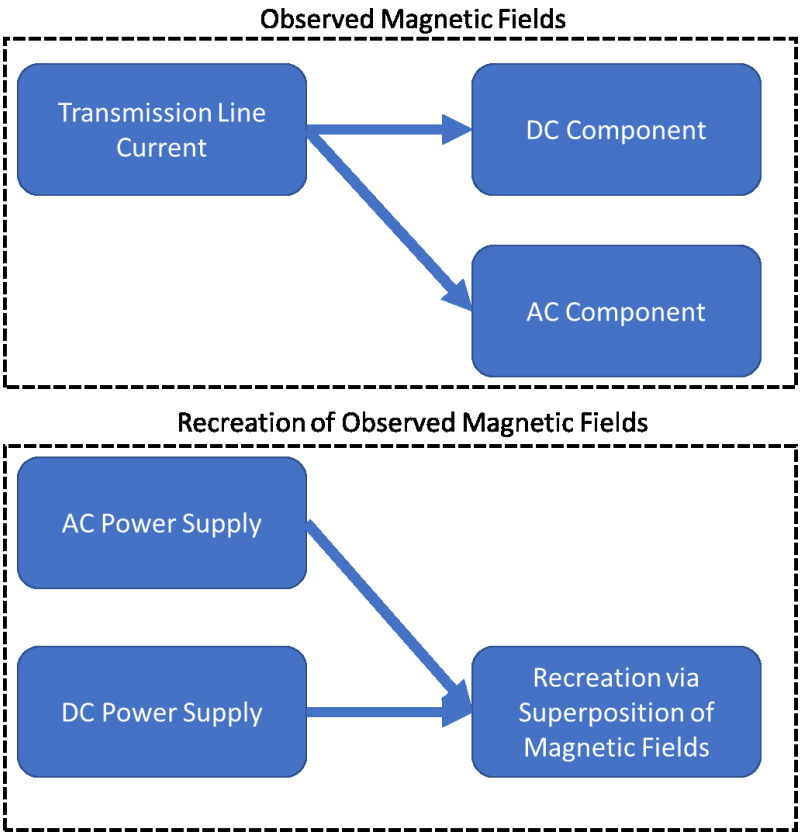

Figure 4-1. Superposition of Magnetic Fields from AC and DC Sources

Working backwards from independent magnetic field sources, the linearity properties of magnetic fields are used. Generation of fields using DC and AC power supplies results in two distinct magnetic field as represented by equations (11) and (12). The field generated by the DC power supply is shown in equation (11) where B_{DC} is the magnetic field, I_{DC} is the current produced by the power supply, d_{DC} is the radial distance from the transmission wire and μ_0 is the magnetic permeability of freespace. Similarly equation (12) shows the magnetic field ($B_{AC}(t)$), current ($I_{AC(t)}$) and distance (d_{AC}) for the AC power supply. The magnetic field and current in equation (12) are time dependant at low frequency, due to the frequency range of GIC signals equation (11) does not change with respect to time. Both equations are derived from modelling the transmission wires after

infinitely long conductors due to the relative proximity of the measurement device and the curvature/sag of the transmission line between towers, resulting in the approximation for Biot-Savart law.

$$B_{DC} = \frac{\mu_0 I_{DC}}{2\pi d_{DC}} \qquad (11)$$

$$B_{AC}(t) = \frac{\mu_0 I_{AC(t)}}{2\pi d_{AC}} \qquad (12)$$

The superposition of magnetic fields, according to Maxwell, results in their linear addition. Performing this operation with equations (11) and (12) and re-arranging for I_{DC} and $I_{AC}(t)$ results in equation (13).

$$I_{DC} + I_{AC}(t) = \frac{2\pi}{\mu_0}(B_{DC} d_{DC} + B_{AC}(t) d_{AC}) \qquad (13)$$

Configuring the conductors to follow the same path such that $d_{AC} = d_{DC}$ and equation (13) simplifies into equation (14). The constant terms of d_{AC}, d_{DC}, and $\frac{2\pi}{\mu_0}$ can be combined into a single term, *C* then represents a linear scaling according to a fixed measurement distance.

$$I_{DC} + I_{AC}(t) = C(B_{DC} + B_{AC}(t)) \qquad (14)$$

Referring back to Figure 4-1 the generation of currents via the left hand side of equation (14) results in the same magnetic fields as observed in practice. The benefit of this determination is that two separate power supplies can be confidently used in constructing the test bench to generate magnetic fields that closely resemble the magnetic fields produced by GIC in power transmission lines. Realistic generation of magnetic fields observed in proximity to power transmission systems is a critical first step in establishing the design feasibility of the GIC test bench. In addition, the use of two separate power supplies greatly simplifies wiring the test bench along with associated

power electronics components thereby facilitating the integration of new components for multiple test cases. After establishing the methodology of generating realistic magnetic fields the next step was to calculate the magnitudes of GIC required by the test bench that is capable of being scaled to the currents that damage transformers.

4.1.2 Positioning and Adjustment, and Scaling

The scaled model for a test bench was selected to accommodate all space and resources requirements for reproduction of the environment. Height adjustment of the model transmission lines over the measurement surface was also implemented. Physical spacing considerations of components was required to emulate the position and orientation of a traditional power transmission line. The physical geometry of the test bench transmission line were made adjustable to streamline the ability to perform a wide range of tests and experiments on different configurations.

4.1.3 Determination of GIC Potential Damages to Transformers

The test bench GIC source is a DC power supply. To determine the minimal capabilities of the supply an estimation of transformer operational parameters and degradation of insulation over time was performed. Design of the realistic testing environment was informed by calculation of GIC flow that could impact the operation of a power transformer.

Two aspects were considered to determine minimal GIC flow criteria. First, an overview of transformer designs, types and configurations seen at different voltage levels was performed. Second, asset utilization best practices that are used by utilities were considered. The combination of physical and operational considerations takes into account all potential impacts of GIC on transformers.

Power transformers have a multitude of designs, wiring configurations, operating voltages, and insulation properties. Due to the designs requirements a common feature of three-phase transformers is a neutral-ground wire, allowing GIC flow into the network. Spot heating in transformers due to GIC has been shown by [54] to develop temperatures over 115°C for long periods of time. Best practices for briefly overloading of transformers is ~125% for oil-filled transformers according to [55]. Considering power utilities advancements in energy efficiency asset utilization goals have increased towards 100% of nameplate rated VA, depending on available cooling mechanisms and ambient temperatures.

The GIC power source was selected based on the use of a 1.5kW, 120/240V step-up and step-down transformer driving a 1200VA AC load. Eighty percent asset utilization was used for the transformers to accommodate various test scenarios and leave room for potential expansion of the system. While evaluating specific impacts of GIC on transformers is outside the scope of this thesis, the power source was selected to enable a DC shift in the transformer operating point to 2.64kW or 176% of the nameplate capacity. The GIC generation capacity was a key consideration in designing the test bench. Implementation of previously observed GIC data was the next design factor.

4.1.4 Historic GIC Data

Due to the infrequency of GIC events, it was necessary for the test bench to emulate previously recorded GIC and geomagnetic information. Figure 4-2 shows the process that was used to import historical GIC and geomagnetic field data from web-based open source data repositories to the power supply. Firstly, data is imported into a data file using standard Python IO libraries and a Pandas [56] data structure. The data

structure is then checked for any missing data values. If missing data is encountered the average of the last three data points are used to fill in the missing data value. Consecutive missing data points were filled using this same method. The process was performed to enable the power supply to function throughout a data set and remove possible follow through of measurement errors. Outliers were not removed from the data set to ensure that any spurious extreme GIC variations could be modelled accurately without compromising the authenticity of the data set.

Next, the observed GIC currents are scaled to a subset of values between the maximum and minimum output capabilities of the power supply implemented to generate DC GIC for the test bench. The maximum and minimum values of current in the data set are found and used to map the data set to a scaled set of data that can be physically implemented. The mapped data set is then transferred to a programmable DC power supply.

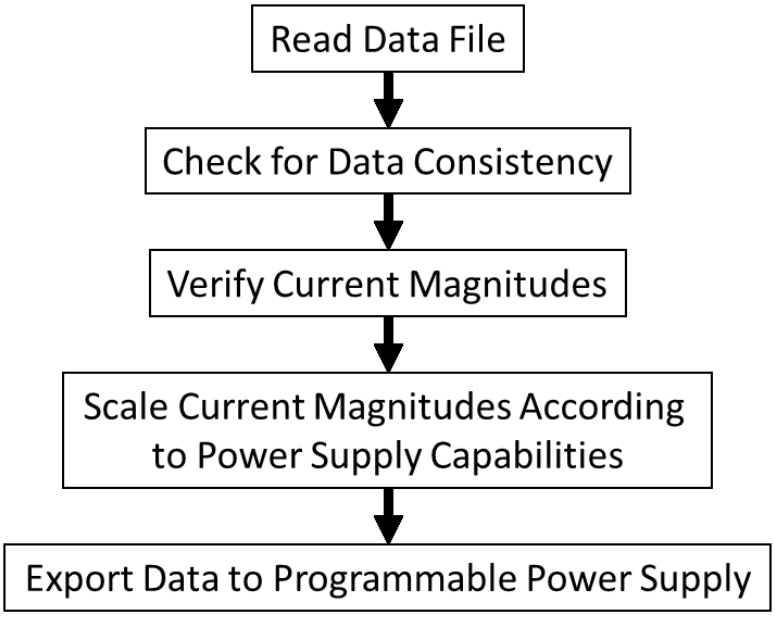

Figure 4-2. Power Supply Process for Emulating Historic GIC data

4.1.5 Electrical Component Configurations

A schematic of the design was first developed according to the desired outcomes for the test bench. Figure 4-3 and Figure 4-4 shows the designs for the AC and DC electrical circuits respectively.

The AC transmission line closely follows a simplified version of an electric power transmission line. The AC source acts as a generator supplying power to a step- up transformer. After conversion to a higher voltage level power is then transmitted across an adjustable value transmission line. A step-down transformer is used to reduce the operating voltage to usable levels and then feed an AC load. The load selected is an AC induction motor, completing the AC circuit.

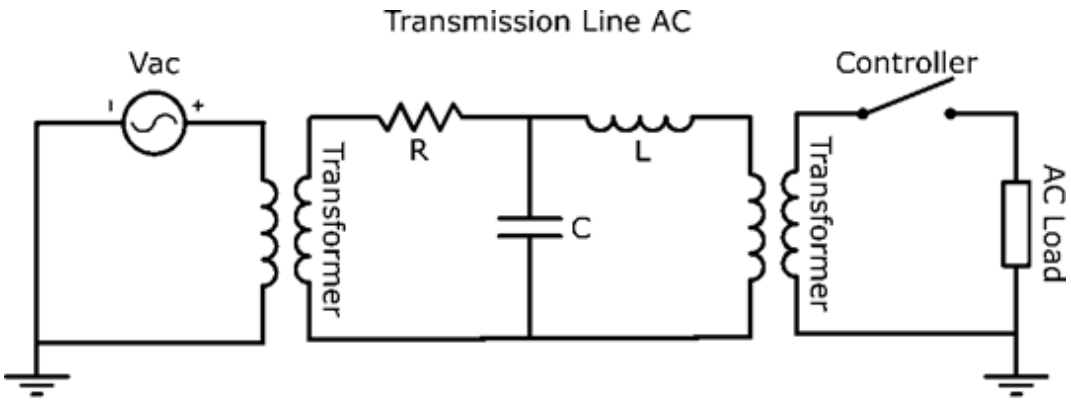

Figure 4-3. Schematic of AC Electrical Components of the GIC Test Bench

The DC components are comprised of four key pieces. The GIC source is a programmable DC supply connected to a transmission line with characteristic resistance. The GIC source feeds a load controller that has standard safety shutoff elements. The DC load is in the form of a high capacity power resistor. The components combine to emulate GIC flow through a transmission line.

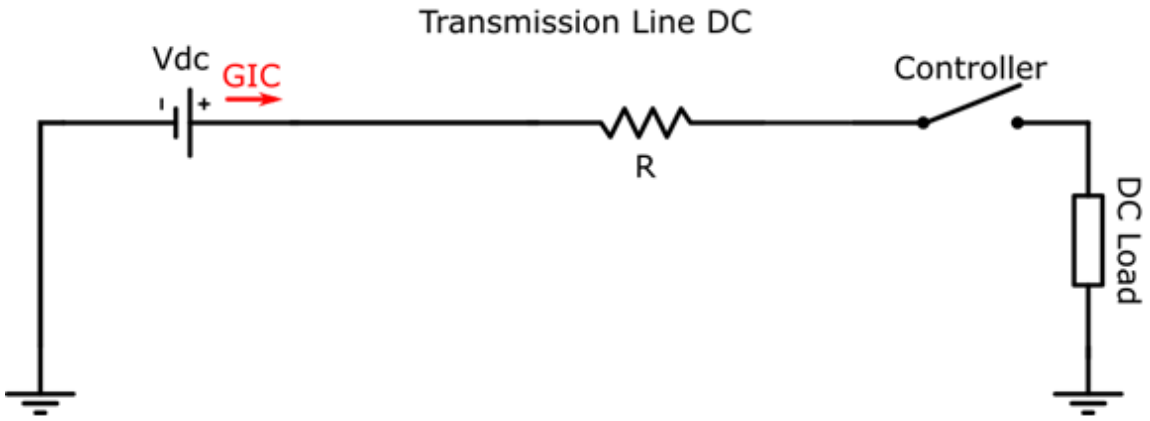

Figure 4-4. Schematic of DC Electrical Components of the GIC Test Bench

The physical components of the design were configured to allow full adjustability of test parameters. Figure 4-5 shows the physical configuration of the test bench. The AC and GIC circuits follow the same transmission line path to ensure that the resultant electromagnetic fields are correctly superimposed on one another. The sag of the transmission line can also be adjusted via cable tensioners located at the top of either transmission pole.

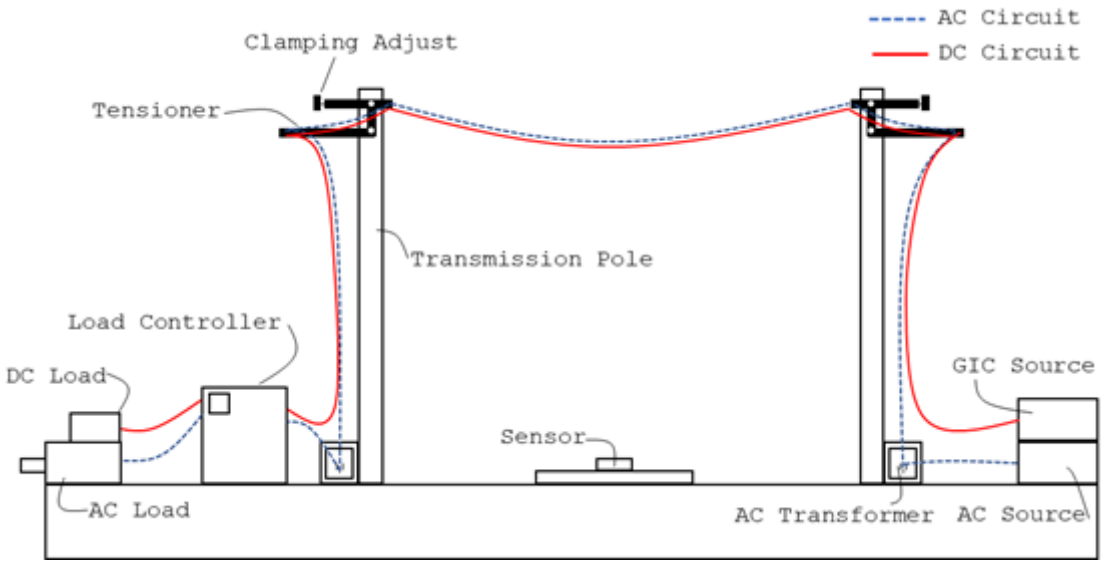

Figure 4-5. Schematic of the Physical Components of the GIC Test Bench

4.2. Test Bench Implementation

All test bench components were selected based on the identified requirements. Construction of the test bench used the items listed in Table 2.

Table 2. Test Bench Components

Component	Details	Description
DC Load	Keithley: 2380-120-60 [57]	120V, 60A, 250W
AC Load	Marathon: K235A [58]	1.5HP,120V, 60Hz
GIC Source	BK Precision: 9130B [59]	0-30V,-6 to 6A,<180us
AC Source	GW Instek: APS-7100E [60]	1000VA, 310VRms, 4.2A, 45-500Hz
AC Transformer	Todd Systems: SD-14-GTC [61]	240V,120V,1500W
Clamping Adjust/Tensioner	Custom	Sag/Line Height Adjustment
Load Controller	Custom	Thermal, OVP, Fused, Voltage, Switched
Sensor Platform	Custom	Basic EM Shielding

The components were configured according to the schematic designs. Figure 4-6 to Figure 4-8 shows the GIC test bench in operation with all components listed in Table 2. Partway through the construction of the test bench the wood transmission poles were exchanged with steel for a more accurate representation of real world systems. Initial implementation of the test bench used the wood poles, however the wires were re-hung

prior to the development of the detection and measurement system and all subsequent data measurements were obtained using the steel frame. In addition, this configuration improved the portability of the test bench when moving between laboratory locations.

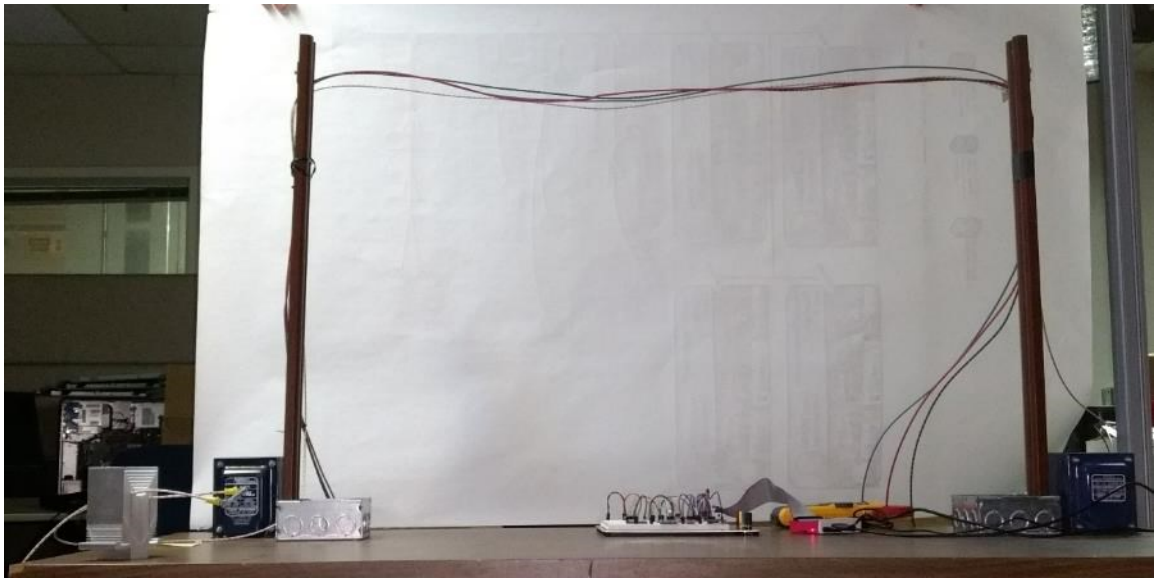

Figure 4-6. GIC Test Bench (V1) in Operation

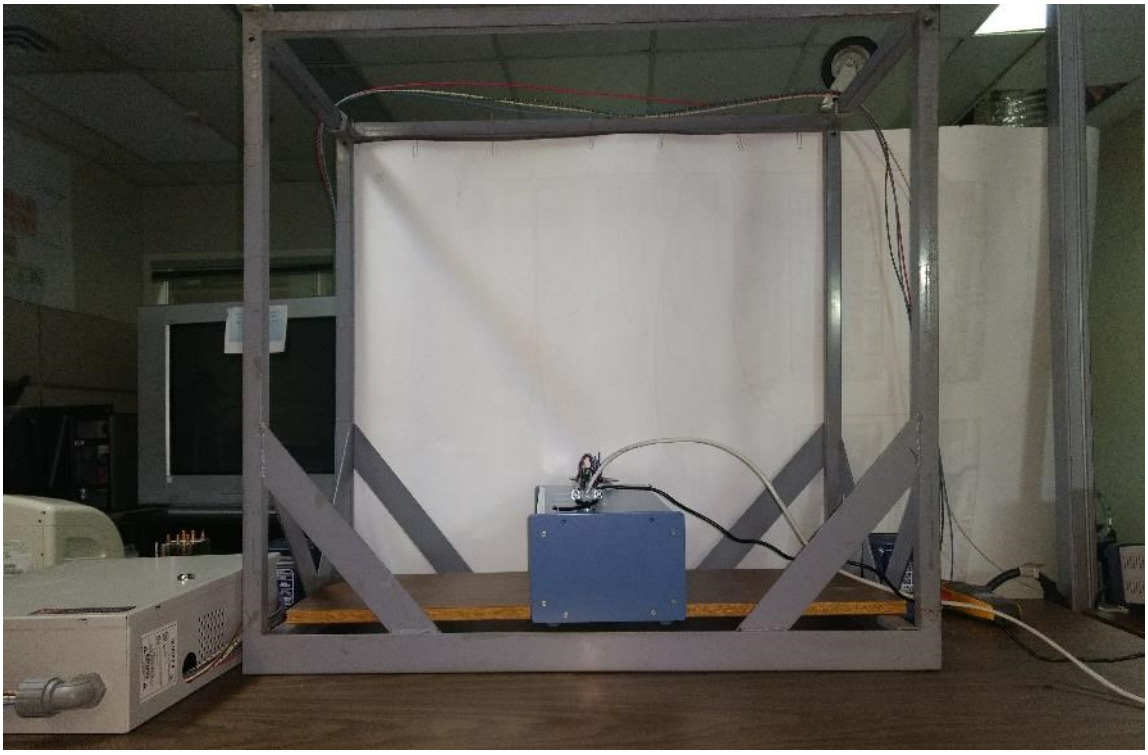

Figure 4-7. GIC Test Bench with Revised Transmission Towers and Sensor Platform

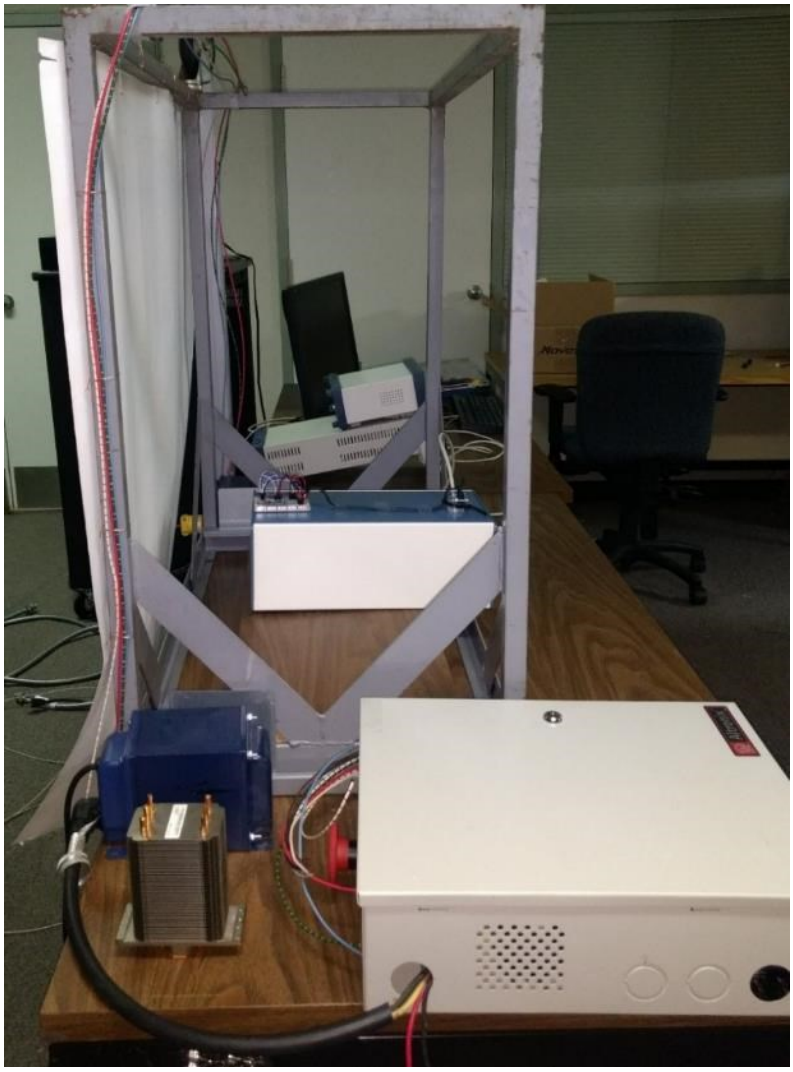

Figure 4-8. GIC Test Bench (V2) Side View

The GIC generator (DC supply) shown in Figure 4-9 is capable of delivering -12A to 12A over three channels. Providing an adequate scaling of observed GIC.

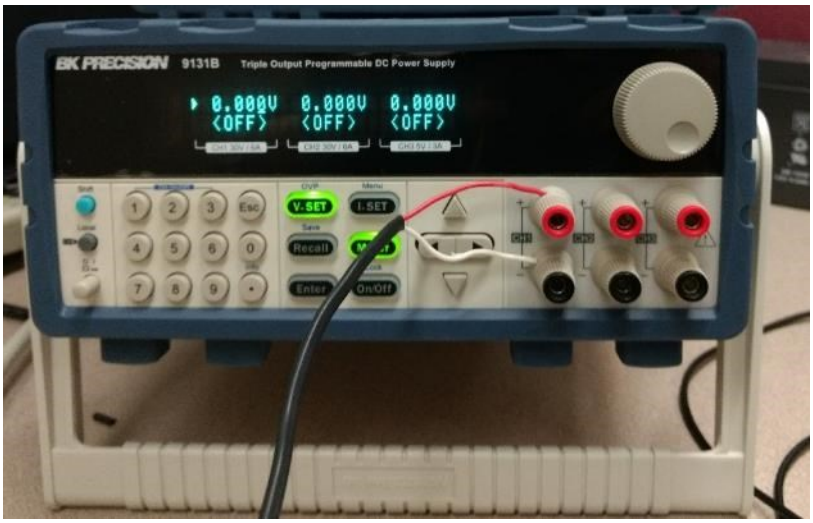

Figure 4-9. GIC Test Bench DC Power Supply

The load for the AC system required a 115v, 1.15kW supply. However, the AC supply shown in Figure 4-10 can deliver significantly more power, at high and low frequencies if higher levels of power transmission across the test bench is required.

Figure 4-10. GIC Test Bench AC Power Supply

The electrical loads used in the test bench are shown in Figure 4-11 and Figure 4-12 for the DC and AC circuit respectively.

Figure 4-11. Test Bench DC Load

Figure 4-12. Test Bench AC Load

Figure 4-13. AC Circuit Transformer

The sensor test platform contained all sensors, microcontrollers, and power supplies to be used for each GIC mitigation solution being tested or verified. Placing the sensors on the outside of the platform was done to reduce potential electromagnetic interference via digital switching and therefore improve overall measurement accuracy. An example of a sensing system under test is shown in Figure 4-14.

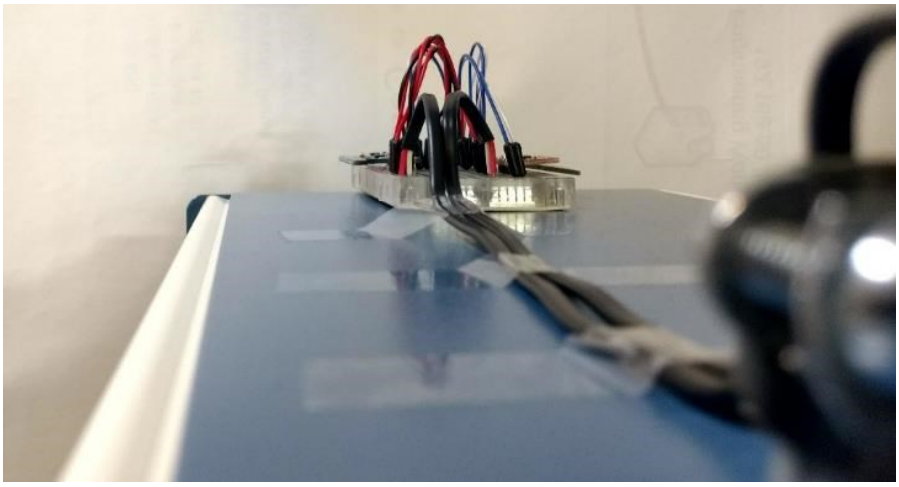

Figure 4-14. Test Bench Showing Sensor Under Test

The implementation of the test bench was verified by using field-measured data from the October 2003 geomagnetic storm, shown in Figure 4-15 for the Grand Rapids (Unit 1) transformer on the Manitoba Hydro system. The data includes a major GIC fluctuation and typical pre and post event measurements. Processing the data according to the process indicated in Section 3.1.4 results in the GIC signature shown in Figure 4-16, the time scale has been adjusted to ensure that tests can be run efficiently and the magnitude adjusted according to the capabilities of the DC power supply (±6A).

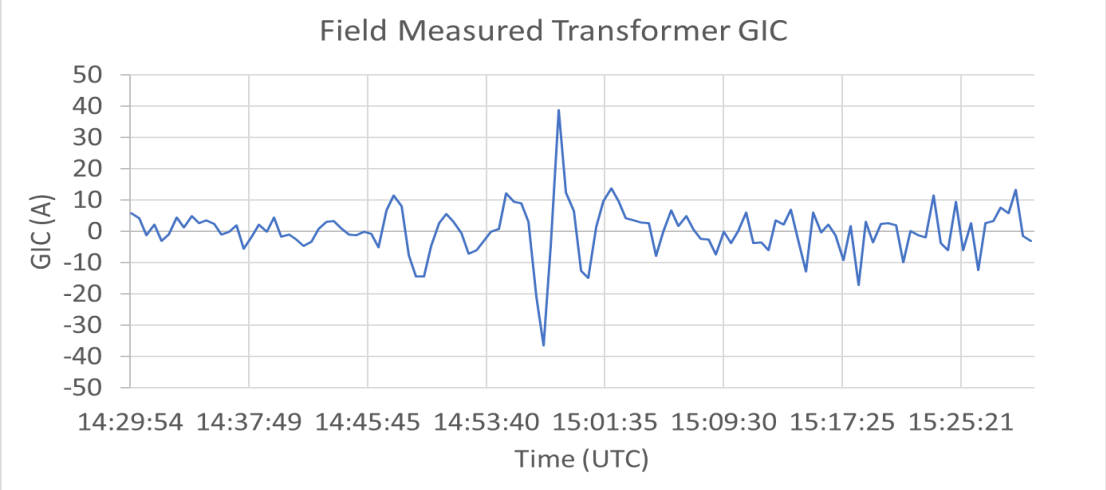

Figure 4-15. Manitoba Hydro GIC Measurements During 2003 Geomagnetic Storm [62]

Figure 4-16. Scaled Test Bench GIC

Matching data in Figure 4-15 and Figure 4-16 demonstrate that the GIC generation aspects of the test bench correlate those found from real-world measurements. The peak GIC event can still be clearly identified and a scaling factor for relative height of each particular transmission line can be selected. In this case scaling ratio between the real world GIC and the test bench GIC was calculated as 0.155 by taking the ratio of the maximum currents found for both sets of data. Meaning the physical configuration of the transmission line in the test bench should be 0.155 the size of the real world power system, for this case between 41cm and 43cm, from the ground.

4.3. Discussion

An inability to gather field data severely restricts the ability to develop technical solutions to address real-world challenges. Due to the nature of GIC, the magnitude and characteristics of its signal cannot be anticipated for the purposes of testing, development and implementation of sensing systems. This chapter showed the complete design and implementation of a technical methodology and framework to overcome these challenges.

The test bench provides a fundamental platform for GIC detection and measurement system design and construction. This research is the first to develop a test bench environment that is specifically targeted towards GIC sensing and measurement systems overcoming challenges in obtaining measurement data caused by infrequent real-world events. Demonstration of the scalability of a GIC test bench provides an opportunity for other researchers and industry stakeholders, with limited resources and knowledge, to continue to develop innovative GIC measurement solutions. In general, this research contributes to advancing the field of knowledge by demonstrating the design, scalability, and methodology for implementing an accurate emulation environment for GIC sensing and measurement studies. The test bench was used in all research described in Chapters 5, 6 and 7 of this thesis. Overall, the test bench overcomes several major obstacles encountered during the design and implementation of GIC detection and measurement systems.

Chapter 5. Simplified GIC Detection and Measurement System

In this chapter the design and implementation of a simplified GIC detection system is presented. Contributions made in this chapter resulted in the IEEE peer reviewed international conference paper [17]. The system demonstrates the effectiveness and capabilities of a simplified method and technology to detect and measure GIC in power transmission lines. The sensing environment, including models, hardware, and software components of the design are first presented. The design of the system and its operation in a test bench environment is then demonstrated. Sensor measurements and performance metrics are presented and compared with other GIC measurement methodologies. Results are followed by a discussion on the value and feasibility of deploying the designed system in the field as well as a summary of the contributions of the research presented in the chapter.

5.1. System Model

Understanding the sensing environment model is critical to measuring GIC in power transmission lines. Figure 5-1 shows an environmental model accounting for magnetic sources in the application of measuring GIC. Magnetic field sources are shown as blue circles or squares and the magnetometer position is indicated by a triangle. Sources shown include AC and GIC components of the transmission line, background magnetic field, image current, and transient temporary field. The magnetic field sources indicated are positioned with respect to the Earth's surface (not to scale).

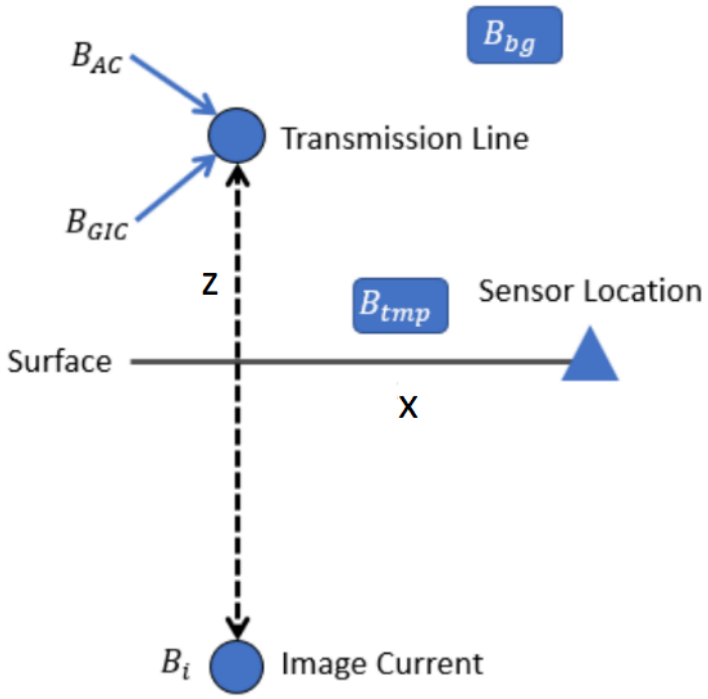

Figure 5-1. GIC Measurement Application, Distribution of Field Sources

Noisy magnetic environments are typical for GIC measurement applications. The total field measured at a sensor location ($B_{measured}(x, y, z, t)$) describes magnetic fields present in the application environment at any position in the measurement domain and is composed of the superposition of surrounding magnetic fields. Surrounding fields include; GIC ($B_{GIC}(x, y, z)$), AC power line ($B_{AC}(x, y, z, t)$), image current ($B_i(x, y, z)$), the Earth's background field ($B_{bg}(x, y, z, t)$) and any temporal field in proximity to the sensing location ($B_{tmp}(x, y, z, t)$). Ideally, direct measurement of the B_{GIC} term allows calculation of the magnitude and direction of GIC flow in a power transmission line.

First, $B_{AC}(x, y, z, t)$ is the time dependent field induced by a typical electric power system current. This magnetic field component can be filtered by using a digital notch filter centered at 60Hz, or alternatively a simple RLC low pass filter, for this application.

The advantage of using a notch filter is that the filter allows other high frequency components to be observed. The high frequency elements may be analysed for alternate purposes of a detection and measurement system.

Second, $B_i(x, y, z, t)$ is the magnetic field from the GIC image located within the Earth's surface. The GIC image location is a function of the skin depth characterized by equation (15) a function of frequency(ω), conductivity of the ground (σ), and the permeability of free space (μ_0) according to [43].

$$\epsilon = \sqrt{\frac{2}{\omega \mu_0 \sigma}} \qquad (15)$$

Simple calculation of the image current location using equation (15) and typical values for ω and σ, such as 0.1Hz and 6mS/m, shows that the depth of the image current is well beyond the potential detection range of the magnetometers deployed. The GIC image must still be taken into consideration for on-going modelling applications but will not impact performance of a deployed sensing system.

Third, $B_{bg}(x, y, z, t)$ is the background field due to the Earth's natural magnetic field and iron core composition. Previous work has been performed showing that the B_{bg} component can be eliminated through careful sensor positioning. The distance of the magnetometer sensing platform from the transmission line can vary from 5m to 25m depending on sensing performance.

Fourth, $B_{tmp}(x, y, z, t)$ represents any fields due to temporary disturbances such as vehicles driving by the measurement sites or alternate emission sources in proximity to the measurement system. This term will be considered zero for the initial test bench environment, but future field deployments will need to take this term into consideration.

Aspects of each magnetic source are used to reduce the overall complexity of the mathematical model. Techniques for reducing the complexity of the measurement environment are leveraged to simplify the initial field environment from the complex description of $B_{measured}(x, y, z, t)$ into the desired $B_{GIC}(x, y, z)$ as measured at the sensor location. The nature of GIC signals reveals further information to achieve accurate measurement results. The frequency range of GIC typically spans from 0Hz to 10Hz, thus considered to be quasi-DC. The independence from time indicates that the time component of $B_{measured}$ can be ignored.

In addition, the position of the sensor platform can be configured to eliminate additional measurement axis. If the transmission line is modeled as an infinitely long current carrying conductor the $B_{GIC}(y)$ components will cancel over the length of the line, thereby removing the 'Y' measurement axis.

Terms resulting from off axis positioning can be removed from the general field equation described in equation (16) by taking the limit as the x position approaches directly underneath the transmission line, simplifying the field equation into equation (17).

$$B_{GIC} = \lim_{x \to 0} \left(\frac{\mu_0 I}{2\pi} \left(\frac{z}{z^2 + x^2} \right) \right) \qquad (16)$$

$$B_{GIC} = \frac{\mu_0 I}{2\pi z} \qquad (17)$$

In summary, the complex field measured at the sensor location can be simplified into the desired B_{GIC} by leveraging the positioning and properties of surrounding fields in relation to the desired field has been simplified through careful interpretation into equation (17), also known as Ampere's law for a current carrying conductor. The

simplification of magnetic fields at the sensing location allows the design and implementation of a simple sensing system as described in the next section to directly measure GIC flowing through a transmission line.

5.2. Sensing System Design

Through the previous analysis of the system model a sensing system was designed to meet GIC detection and measurement requirements. The prototype GIC detection and measurement system was designed and implementation to overcome existing challenges with a simplified approach to GIC measurement.

5.2.1 Magnetic Field Sensor Selection

Magnetic field sensing technologies have a wide range of applications. Global manufacturing and supply chain development has increased the availability and reduced costs for sensitive magnetic field sensors, known as magnetometers. The simplified sensing system requires a sensing technology that was widely available, provides adequate sensitivity, had a simple design and modes of operation, with demonstrated economic feasibility for future deployment.

A summary of commercially available sensors is presented in Table 3 to evaluate the potential for each sensor type. The detectable field range was calculated based on the best available commercial sensors at either end of the spectrum. Complexity of the sensing system is a critical aspect for this application. Both the hall-effect and magneto-resistive sensors score low due to the use of a single active element in the sensing devices, the magneto-diode and transistor in addition to the fluxgate score medium on the complexity scale due to the use of active driver elements require a control system and/or

feedback loop. The highest complexity was given to SQUID type sensors due to the required cooling support systems. A score was given to each sensing technology based on the minimum detectable field (negative exponent is the score) and complexity (low=3, medium = 0, high = -3). Sensitivity shows the minimum detectable change in the magnetic field that each sensor category can detect. Based on this methodology as well as economic and availability considerations a magneto-resistive sensor was selected for the system.

Table 3. Commercially Available Magnetic Field Sensors

Type	Detectable Field Range (G)	Sensitivity (nT)	Sensor Complexity	Suitability Score
Hall-Effect	$10^0\ to\ 10^6$	$10^4\ to\ 10^7$	Low	3
Magneto-resistive	$10^{-7}\ to\ 10^2$	$10^2\ to\ 10^3$	Low	10
Magneto-diode or Magneto-transistor	$10^{-1}\ to\ 10^4$	$10^2\ to\ 10^3$	Medium	1
Fluxgate	$10^{-6}\ to\ 10^{-2}$	$10^{-2}\ to\ 10^1$	Medium	6
SQUID	$10^{-10}\ to\ 10^{-4}$	$10^{-5}\ to\ 10^{-2}$	High	7

While a wide range of magneto-resistive sensors are available that fulfill the requirements the LSM303 [63] sensor was selected since it meets all the requirements for

cost and sensitivity for a simplified system, falling within the ideal region, and offers additional advantages such as integrated temperature sensors and low power modes.

5.2.2 Sensor Positioning

Sensor positioning is highly dependent on the sensitivity of the sensor itself. To determine the optimal positioning of the sensor a determination of the typical GIC currents flowing through various types of transmission lines was required. The baseline of 10A was used to calculate the optimal positioning of the sensing system for determining its feasibility and capabilities according to the potential damages described in Section 4.1.3. The sensor was placed midway between the test bench transmission poles (±2mm) and directly under the transmission line wire (±5mm). A major issue identified is the sensor's proximity to the transmission line, due to safety considerations. It was calculated that a simple post could be used to decrease the distance between magnetometer and transmission line to obtain the desired results, with minimal deployment complexities.

5.2.3 Filter Design and Implementation

To reduce the overall impacts of the prevalent 60Hz background AC magnetic field due to regular power system operation a digital notch filter was designed and implemented to improve the signal to noise ratio during measurement. Several filters were evaluated based on the desired field to be recorded by the measurement system. A simple passive low pass filter was selected to filter all frequencies above 40Hz. This functioned to improve measurement accuracy of low frequency components but also eliminated all high frequency signals that can be used to determine inductive coupling

into pipeline, transients, and other harmonic information. Figure 5-2 shows the process for obtaining GIC measurements from the simplified sensing system.

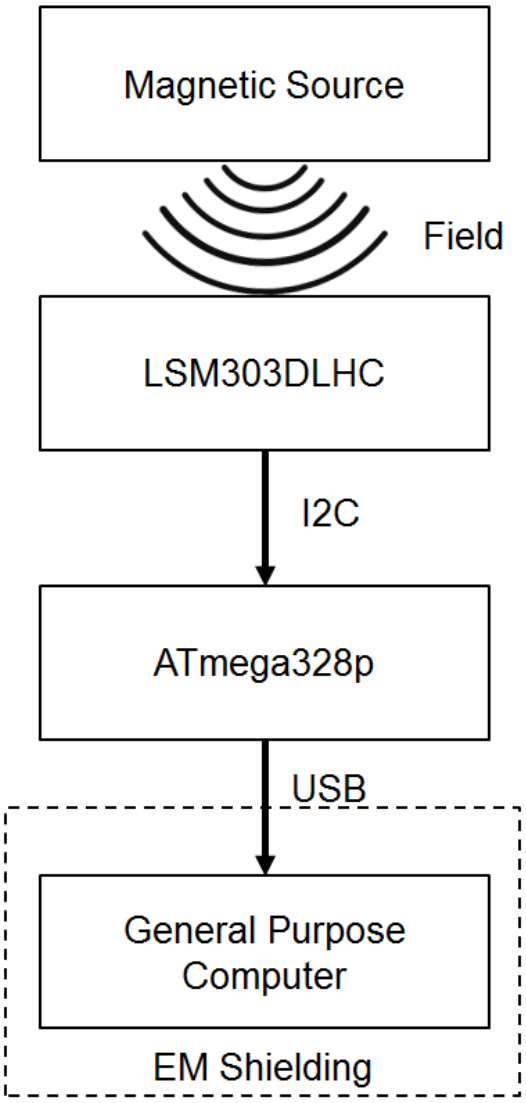

Figure 5-2. Process for GIC Detection and Measurement

5.2.4 Microcontroller and Other Hardware

Types of magnetic field sensors were analyzed and selected based on cost, availability, simplicity, technology, and capabilities. Selection of easily available simple hardware was a key aspect of the hardware design. In addition, the future requirements for a low power design were taken into consideration. The initial prototype leveraged the

popularity of the Arduino platform on an ATmega328p chipset as the primary microcontroller and analog-to-digital (ADC) converter.

Figure 5-3 shows the initial simplified system design and construction with the Arduino platform on the left and the magnetic sensor selected (LSM303) on the right. The Arduino was placed in a metal box for a small degree of electromagnetic shielding along with a general purpose computer for data storage.

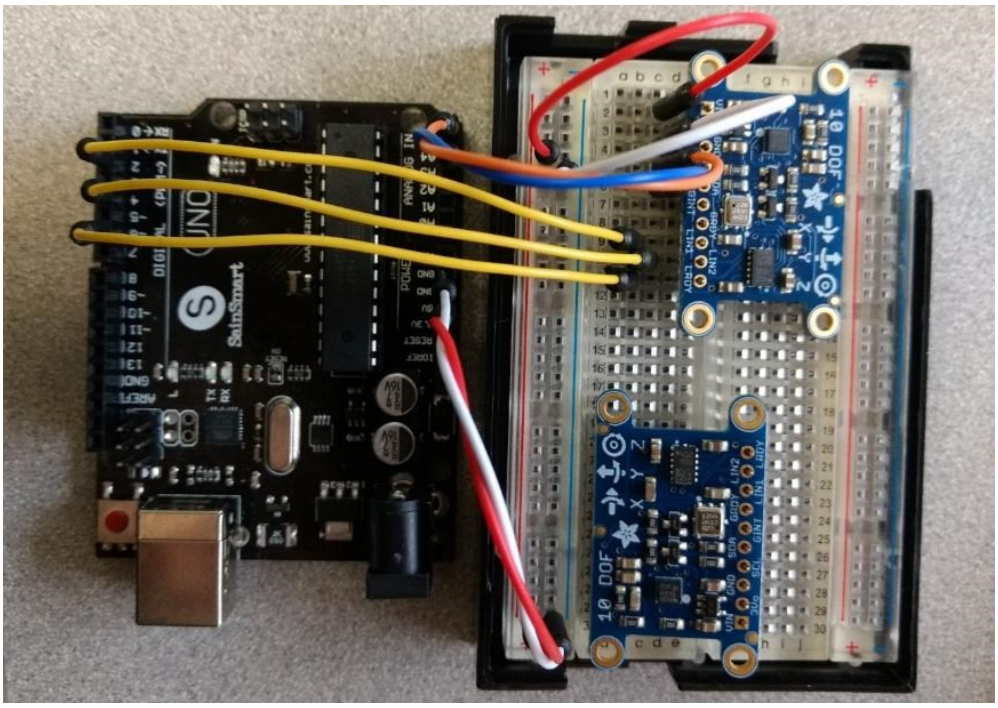

Figure 5-3. Simple GIC Detection and Measurement System

5.2.5 Sensor Calibration

Magnetic sensors that are based on magneto resistive materials are highly sensitive to a variety of environmental changes. Temperature variation were accounted for by using the built in temperature sensor of the LSM303. Temperature readings were taken every 10 minutes and used through a datasheet lookup table to calibrate measurements during that timeframe. Saturation of sensors was avoided by dynamically adjusting the

measurement range of the observed data approached a predefined minimum or maximum value for that particular sensor.

5.3. Detection and Measurement System Results

Data was first collected while the AC power system was shutoff to develop baseline for sensor performance and test sensing system functionality. Measurements were then taken while a GIC current was swept over the sensor test bench operating range. The sensing system magnetometers were selected to correctly detect both very low GIC in the transmission line and very high GIC without saturation. Figure 5-4 shows the baseline sensor readings over a period of ten seconds. The instantaneous readings provide minimal useful information on the true value of the reading. Further processing was required to obtain useful measurements. The measurements without a filter implemented provide an indication of the noise present in the raw data measurements in the GIC environment.

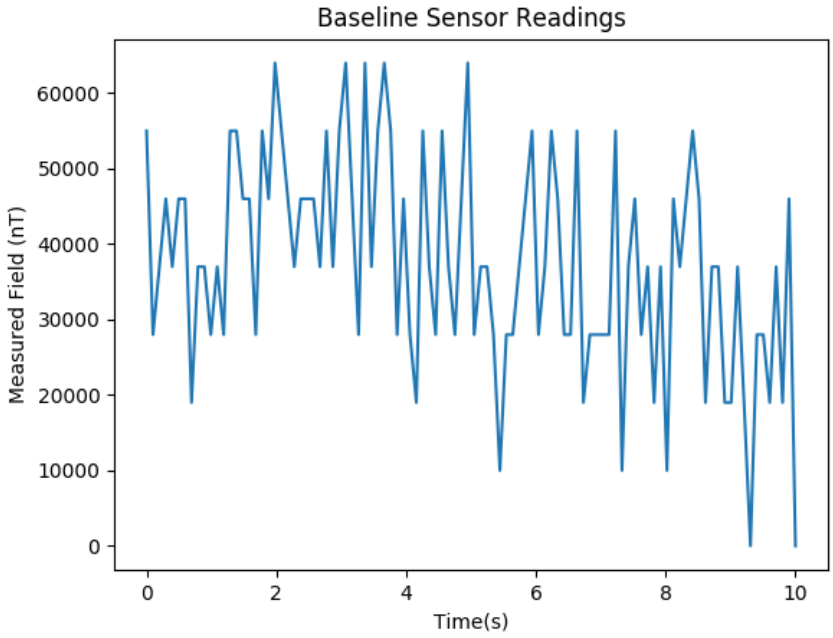

Figure 5-4. Sensing System Baseline Measurements of Background Magnetic Fields

Implementing a smoothing function to eliminate sensor noise was accomplished by using a post data capture processing technique. A Hanning window of length 11, taken from the standard Python Scipy libraries, was used to smooth the measured data. Figure 5-5 shows the application of the Hanning smoothing window on the data measurements.

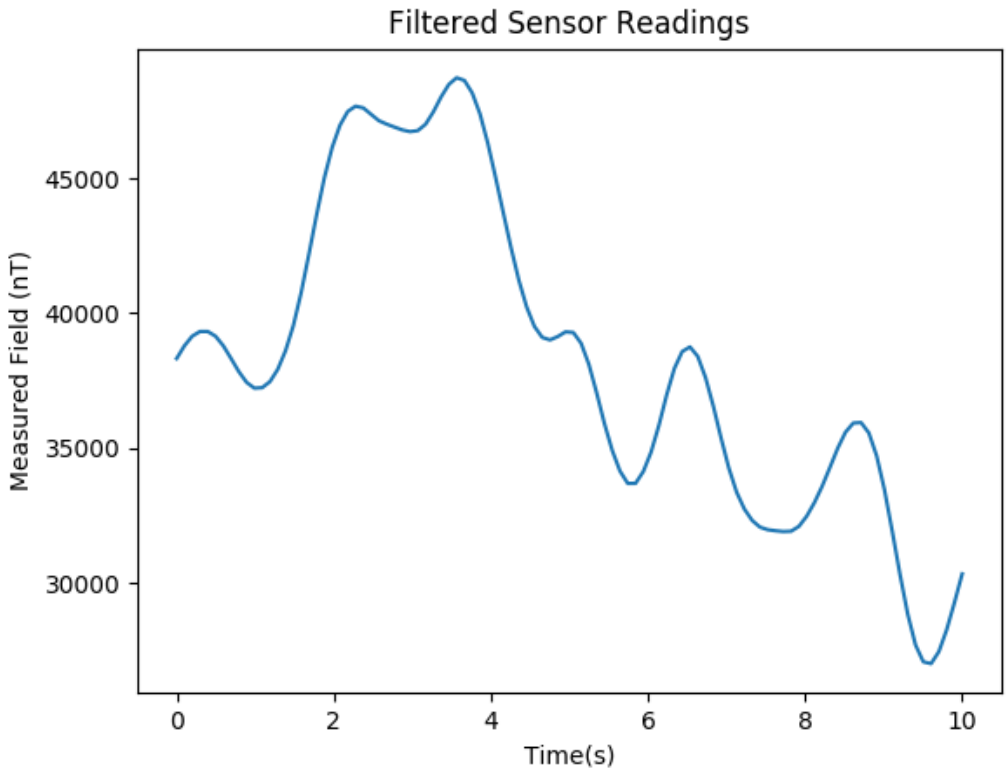

Figure 5-5. Smoothed Baseline Sensor Readings

Comparing the baseline measurement data to professionally measured data was accomplished by capture data and then downloading open source measurements for the same time frame. Evaluating the sensing system performance to obtain measurements in the presence of both an AC and GIC fields required testing using the GIC test bench. Figure 5-6 shows raw measurements with both AC and GIC fields applied in the test environment. The geomagnetic data has been obtained from the Natural Resources

Canada, Ottawa geomagnetic observatory (OTT) for the September 8th 2015 to September 9th, 2015 time period [64]. Figure 5-7 shows the smoothed measurements and reference AC field. Lastly, Figure 5-8 shows the smoothed and filtered GIC measurements for the sample specified.

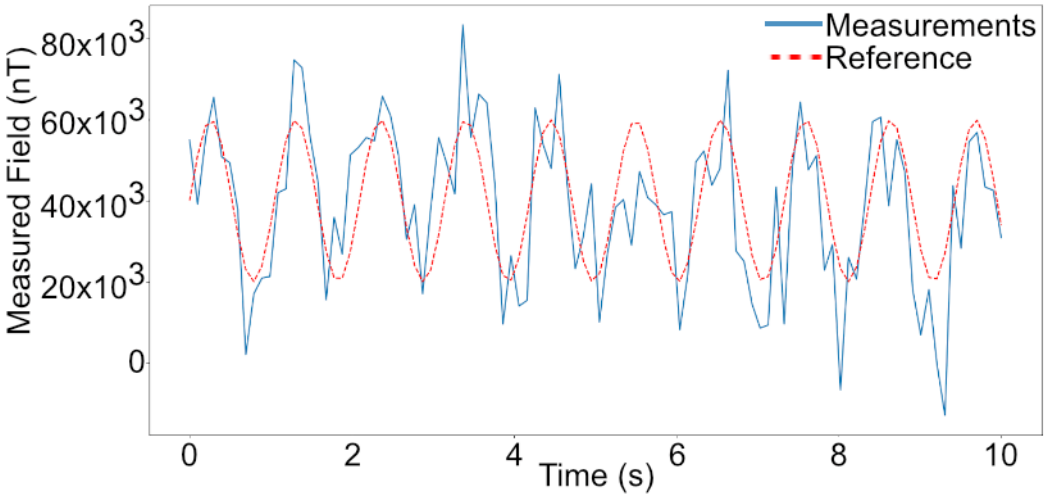

Figure 5-6. Raw Sensor Measurements with DC and AC Fields Present

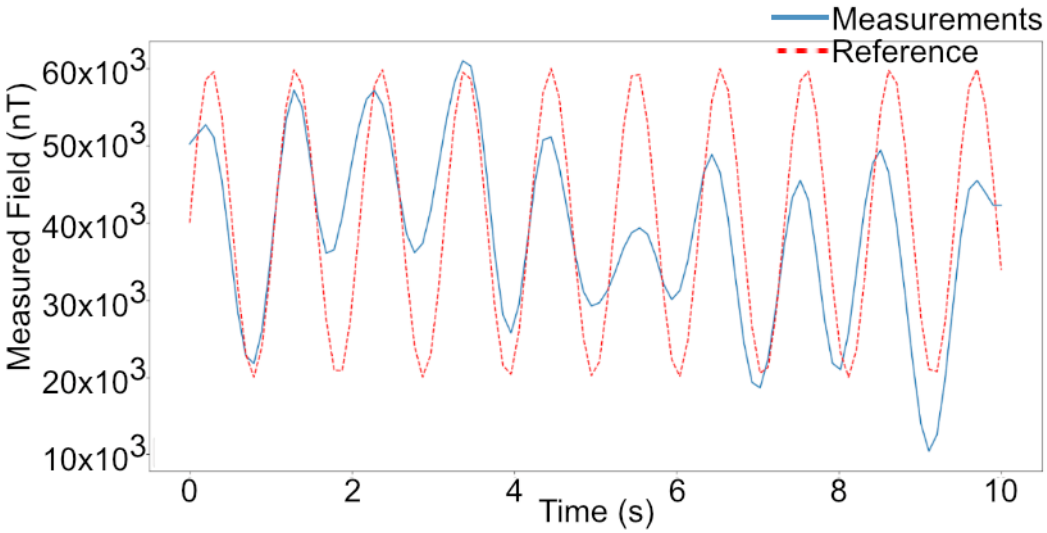

Figure 5-7. Smoothed Sensor Measurements with DC and AC Fields Present

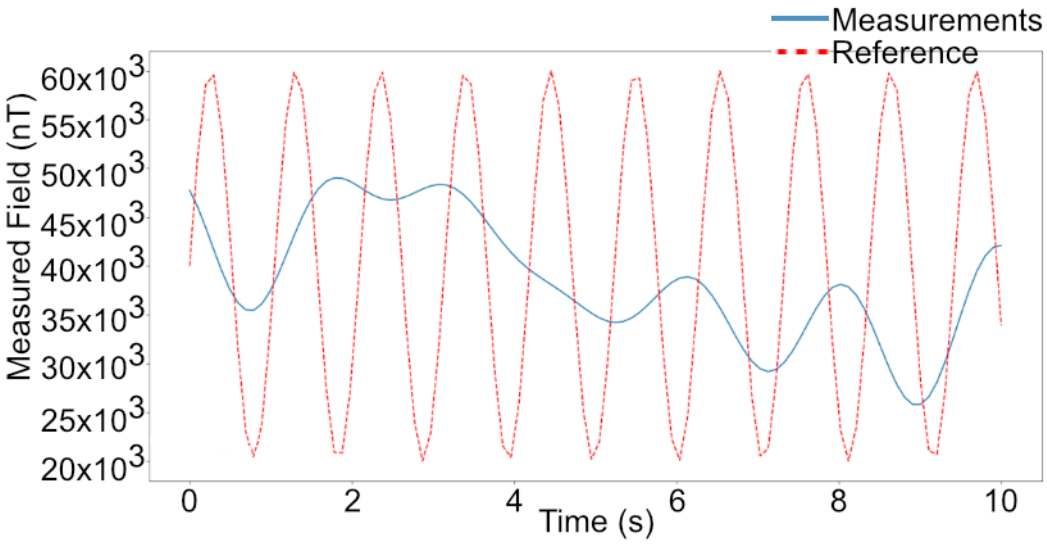

Figure 5-8. Smoothed and Filtered Sensor Measurements with DC and AC Fields

Figure 5-9 shows typical magnetometer readings from OTT. Magnetic field values are for a typical calm day for this solar cycle. Figure 5-10 shows the recorded sensor values during the same day in approximately the same geographic location. Values for X, and Y directions are included in both figures. The deployed system has significant noise but average values are approximately equal over the measurement time period. Daily variations in magnetic fields can be on the order of single to tens of nano-tesla while this is shown in Figure 5-9, comparison with measured values in Figure 5-10 required scaling the axis accordingly. Having an average measurement that compares well with professional measurement average values is of higher criticality for this application than matching minute field variations.

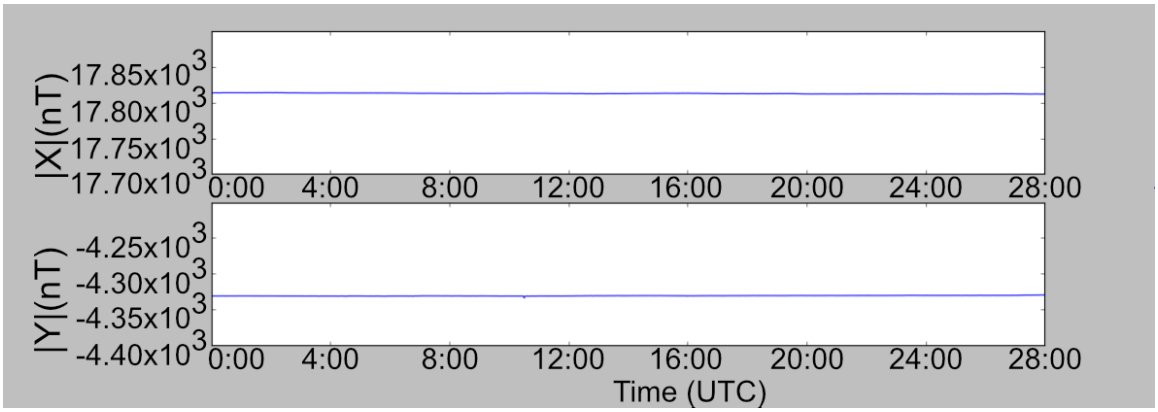

Figure 5-9. Geomagnetic Field Measurements from Geomagnetic Observatory

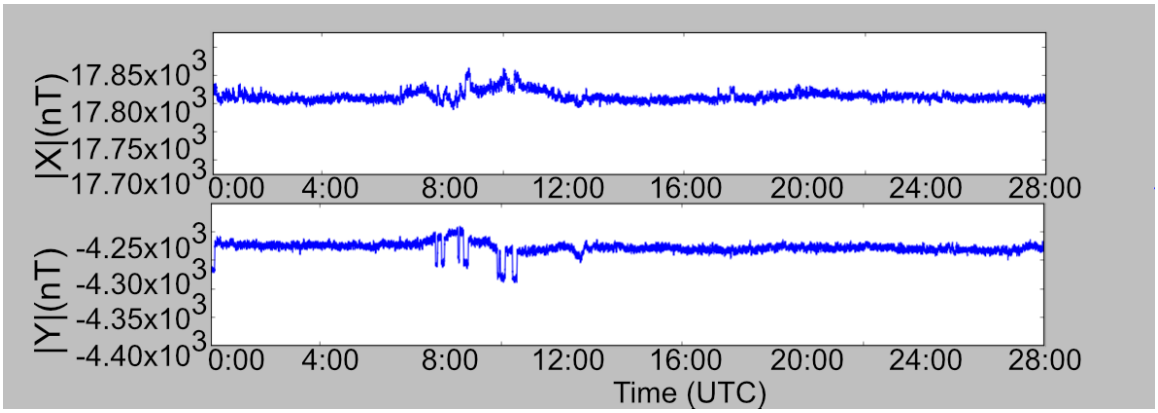

Figure 5-10. Geomagnetic Field Measurements from Designed Sensing System

Figure 5-11 shows that the designed filtering removes the majority of the 60Hz magnetic field frequency component as designed.

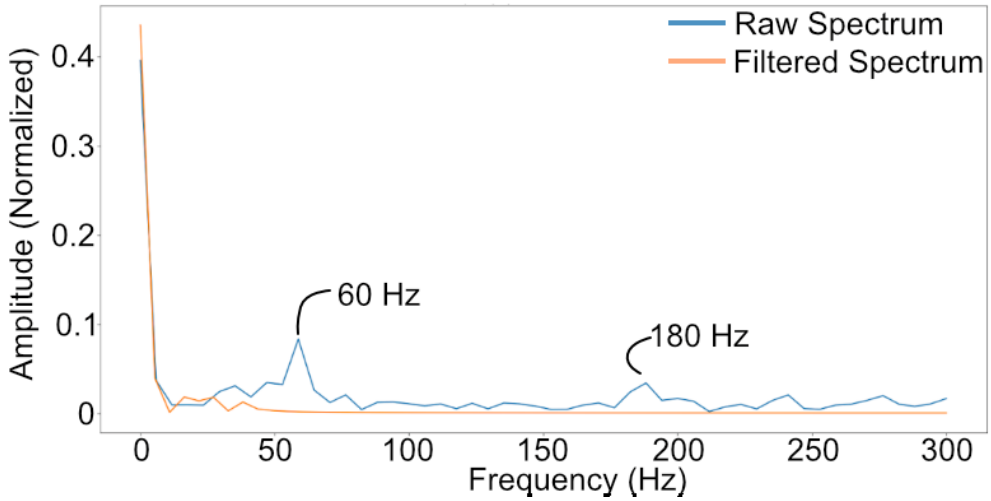

Figure 5-11. Frequency Spectrum Prior and Post Filtering

Transient performance of the sensing system was able to track instantaneous changes in GIC signals with minimal delay and overshoot. Delays were measured to be within ten samples from a step change in GIC. The first step change in GIC shown in Figure 5-12 seems to be anticipated by the system however in subsequent test the phenomena was not detectable or apparent. The settling time after each step change averaged to 60 seconds for all steps tested. Figure 5-12 shows the complete experiment reference and measured GIC field values in the test bench setup.

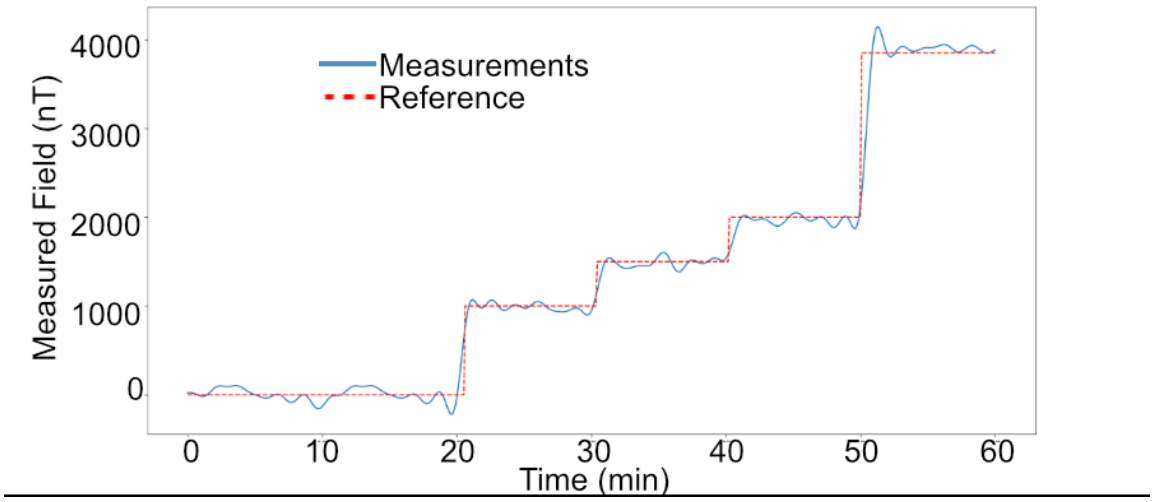

Figure 5-12. Transient Performance of Sensing System for Steps In GIC Magnitude

Overall accuracy of the simplified sensing system demonstrates its capabilities in detecting and measuring GIC. Mean measurements for 100 samples were obtained for GIC ranging from 0mA to 500mA in 100mA intervals. The results are presented in Figure 5-13. The ideal calculated field strength is compared to the real measurement date as an absolute standard, calculating the R-value as 0.99, a p-value of 2.76e-6 with a standard error of 0.0238.

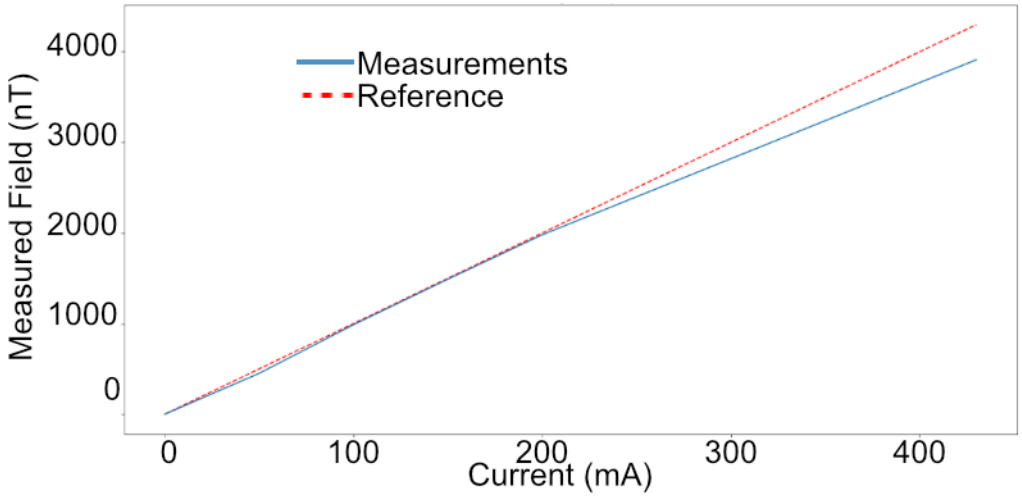

Figure 5-13. Steady State Sensing Accuracy of the Designed System

Comparing the simplified sensing system with results obtained by [39] results in an R-value improvement from between 0.5 and 0.8 to 0.99 (consideration of test bench vs real world). The simplified system was found to be 97.7% accurate compared with the ideal calculated values from the Biot-Savart law.

The sensor system offers several advantages over existing GIC measurement techniques. Simplification and ease of deployment was one of the primary goal of the system, compared to existing measurement techniques this goal was fulfilled. The prototype system demonstrated that the approach to measuring GIC through simplified sensing systems can function in real world environments. Research progressed from design through construction to enable a measurement system that can potentially be deployed in field environments.

5.4. Discussion

The simplified GIC detection and measurement system overcomes several existing technical problems that have been identified by academia, government, and industry. Sensing minute variations in magnetic field strengths in the noisy magnetic environment required a specific system model in addition to application specific methodologies to obtain reliable data.

The sensing system designed and implemented demonstrates that a non-contact simple method of detecting GIC in power transmission lines can be used effectively. The method offers improvements with respect to simplicity as there is only one sensor location involved. In addition, the solution removes difficulties with synchronization that can function incorrectly when communication systems are down. Operational

vulnerabilities caused by satellite communication malfunction during geomagnetic storms are thereby eliminated. This research also addresses the technical challenges of measuring a unique quasi-DC signal in a noisy magnetic environment.

Specifically, research presented in this chapter contributes to the field of GIC measurement and sensing by demonstrating the design and implementation of a sensing system using simple magnetic field sensors. Results of this work are the first to show how modern sensing capabilities can be leveraged to measure GIC with a simple design and minimal expertise required to deploy and use the described system. In depth analysis of the magnetic measurement environment in relation to sensor capabilities provides a solid foundational understanding of the challenges associated with GIC measurement. Analysis and implementation of the simple sensing system provides a new perspective on the capabilities of modern sensors in a field that has seen limited recent developments.

Data measured by the simple sensing system was obtained through the GIC test bench. The deployed system provides a very good approximation of the potential performance of field deployed systems. Scaling GIC values is an accurate method to model real transmission line environments. Availability of all components and a simple straightforward design and approach to deployment provides significant advantages over the state of the art of GIC measurement in terms of deploy-ability, dependability, and resilience.

Integration into existing grid monitoring systems is easily accomplished since the sensor system does not depend on system configurations to operate, thus improving the monitoring and modelling capability with respect to GIC. The microcontroller cost can be scaled since no control is being performed it may be replaced by an ADC and serial

interface during sensing operations in the field. Limitations of the simplified system such as data storage, limited accuracy, and data analytics capabilities have been addressed by subsequent research as described in Chapter 6 of this thesis. Existing methods are complicated and they required synchronization or direct physical contact with the power system themselves.

The system allows a resource restrained government to provide technical assistance to resource limited utilities enhancing the overall resilience of electricity infrastructure towards GIC and space weather events. The system also demonstrates the real-world conditions for the application of modern magnetic field sensors in measuring GIC.

Chapter 6. GIC Measurement Platform

While the simplified GIC detection and measurement system achieved its primary goals, there were several issues identified that needed addressing. Accuracy of field data also lags behind that of significantly more complex measurement methods. Lack of communications options restricts the amount of data that can be collected, stored and analyzed. To address the limitations of the simplified system further research, design and implementation of a sensing system was performed.

Progressing from the simplified GIC detection and measurement system a new GIC detection and measurement platform was designed and realized. The new platform uses multiple magnetic field sensors, integrates a communications and data storage system, and leverages data analytics. Research in this chapter is informed through the use of the GIC test bench described in Chapter 3. The contributions of the new platform are highlighted by the publications of the Author in [18].

The proposed approach for a magnetometer based power transmission line GIC measurement platform considers future deployment scenarios in all aspects of its design. Incorporating elements that synchronize with existing smart grids and systems improves the potential for real world integration. Ensuring the technology is ready for a feasible field deployment is critical to further verification and validation of results presented as well as leading to future deployment in the field. The proposed approach first considers the integration of four magnetometers into a single sensing platform capable of measuring GIC along a power transmission line.

6.1. Platform Design

6.1.1 Magnetometer Analysis and Selection

Design of the GIC measurement platform requires a selection of magnetometers to be integrated into a single system configuration. Commercially available simple magnetometers were selected to ensure potential resources constraint and deployment environments are accounted for from a power system perspective on accuracy and the need for an easily deployable platform. Table 4 shows the selected magnetometers including parameters for resolution, maximum range, and field measurement technology. The most sensitive sensor selected was the MAG3110 with a sensitivity of 0.10uT/LSB however during testing the sensor did not perform according to expectations. While more expensive but accurate technologies such as SQUID, fiber-optic, and coils were taken into consideration, they were deemed inappropriate for this application due to costs, availability and complexity.

Several sensor packages offered additional capabilities such as gyroscopes and accelerometers that were not leveraged in this application. The resolution and range parameters shown in Table 4 are configurable settings for each magnetometer allowing for a wide range of detection and measurement settings to be tested under the same physical setup.

Table 4. Magnetometer Parameters

Sensor	Resolution	Range	Technology
LSM303 [63]	0.20uT/LSB	±3.24mT	MAGNETO-RESISTIVE
MLX90393 [65]	0.161uT/LSB	±4.8mT	HALL-EFFECT
MAG3110 [66]	0.10uT/LSB	±8.0mT	MAGNETO-RESISTIVE
LSM9DS1 [67]	0.14uT/LSB	±12.8mT	MEMS

6.1.2 System Configuration

The select magnetometers were integrated into a single sensing platform. The overall system configuration is shown in Figure 6-1. The configuration shows both physical and digital connections between platform components. The platform was designed such that each sensor can be replaced or exchanged with minimal physical modifications to the platform setup. Each sensor takes simultaneous measurement of the magnetic field and then stores data for every sample. Methods of communication, storage, and security are taken into consideration during the design phase of the platform.

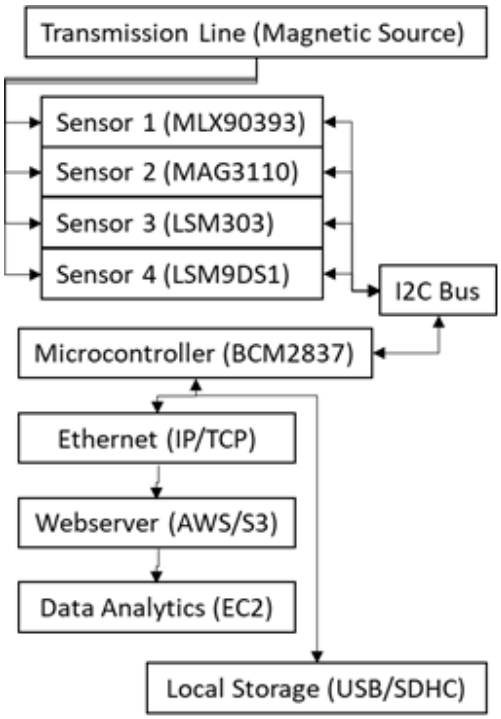

Figure 6-1. Magnetometer Platform System Components

6.1.3 Communications and Data Transfer

Communication over Inter-Integrated Circuit (I2C) was selected based on its availability, simplicity of physical wiring, and data transfer speeds. Considering the capabilities of each sensor, data was obtained at 400Hz allowing for harmonics, transient signals, and other potentially useful data to be detected, measured and either stored or filtered. In addition, optional low power modes that are made available through I2C will facilitate platform deployments in remote locations without a dependable power source.

Data storage was accomplished using a two-tiered system. Real-time, first-tier, measurement data was stored by the local microcontroller on an in-system USB drive. Two conditions were used to determine when data transmission to the second-tier storage occurred. First, a time limit was enforced on the age of data, the second was a maximum memory allocation. After either of the conditions were met data was then transferred

from USB over TCP/IP to a webserver. Scalability is a primary factor for implementing the two-tiered storage system. Consolidation of data in a single location enabled in-depth data analytics to be performed without compromising measurement capabilities.

6.1.4 Standardized Data Formatting

Geomagnetic observatories have measured fluctuations in the Earth's magnetic field for over 200 years. INTERMAGNET is an international group of magnetic observatories that have developed standardized methods of measurements, data reporting, and data storage. International Association of Geomagnetism and Aeronomy (IAGA) is the association responsible for maintaining data formatting standards for geomagnetic measurements. Integrating standard measurement data into the test bench allowed access to a wider variety of conditions to be tested and the performance of the measurement system evaluated.

Earth magnetic field measurements are available from geomagnetic observatories across the world. Data sets can be selected in various formats, for the purpose of the sensor system the IAG2002 format was used for both the magnetic observatory data sets and the measured field data sets. Uniform data formatting facilitated data processing and analysis and ensure consistency to compare results with previous work.

6.1.5 Security

Physical security, resilience, and cyber security are important aspects to all smart grid enabled systems. Mitigation of potential cyber risks was accomplished by using a Virtual Local Area Network (VLAN) gateway for data transferred from the local platform to a webserver. As a best practice in the age of Internet-of-Things and ease of deploying connected systems engineers must be aware of the risks and anticipate future

security vulnerabilities prior to deploying a system in any capacity weather on a university network or commercially. The security considerations were required due to the potentially sensitive nature of data measurements and the attractiveness of intellectual property theft in the field of technical development. Securing individual measurements is beneficial, but integrating multiple magnetometer measurements was used to improve accuracy over individual sensor readings.

6.2. Combining Sensor Measurements

Enhancing the overall measurement accuracy leveraged the strengths of individual sensors while reducing the negative impacts of sensor weaknesses. In addition, the methodology was implemented to ensure that any magnetic field sensor can be integrated into the platform with minimal modifications.

Measurement accuracy was improved using a two-phase process as shown in Figure 6-2. The first phase was to characterize the magnetometers present in the platform by recording measurements of both predetermined steady state GIC magnitudes and a typical GIC time varying signatures. The weighting of each measured data point (B_{GIC}) was calculated using equation (18). Where R1, R2, R3, and R4 are the raw field measurements for each magnetometer.

$$B_{GIC}(platform) = \left(\frac{(1+2\alpha)B_{GIC}(R1)+(1+\alpha)B_{GIC}(R2)+(1-\alpha)B_{GIC}(R3)+(1-2\alpha)B_{GIC}(R4)}{4}\right) \quad (18)$$

Where $0 < \alpha < 1$, determined through a single stage weighting process. The second phase was to use the calculated magnetometer weighting to improve GIC

measurement. The methodology as described was integrated into the GIC measurement platform.

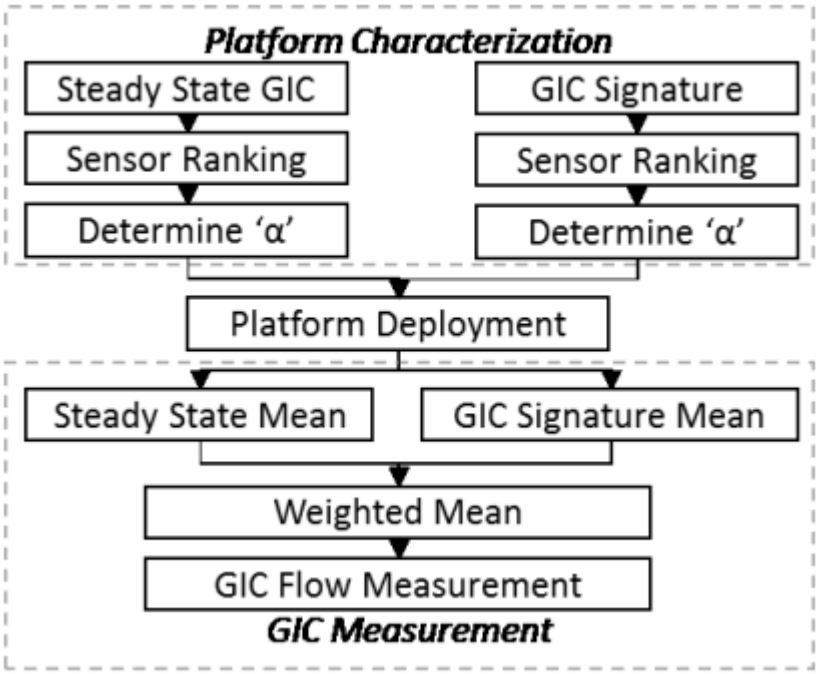

Figure 6-2. Combined Platform Measurements and Characterization Process

Initial deployment of the proposed system was accomplished using the GIC test bench environment that emulates a scaled power transmission system. Features of the test bench include the ability to generate both AC and DC magnetic fields with current sources ranging from -12A to 12A to emulate GIC signatures. The scaled test bench allowed GIC signatures to be verified and validated by the magnetometer sensing platform. In addition, the scaled test bench allows the magnetometer system to be placed in a simulated target location, on the ground between two transmission towers, directly underneath the transmission line. Chapter 4 describes the GIC test bench in more detail.

6.3. GIC Measurement Platform Results

Obtaining accuracy measurement results first required characterization of each individual magnetometer. This process was performed using steady state, GIC signature detection, and real-world scaled data. Temperature calibration was performed using temperature measurements obtained from the LSM303 and MLX90393 sensors and a lookup table of datasheet values using a simplified verification via [68]. The performance of each magnetometer is presented and the improvement in performance using an enhanced method is then demonstrated.

Figure 6-3 shows an image of the designed and constructed sensing platform. The magnetometers were placed on the surface of a metal box in close proximity to one another to minimize temporal spacing changes.

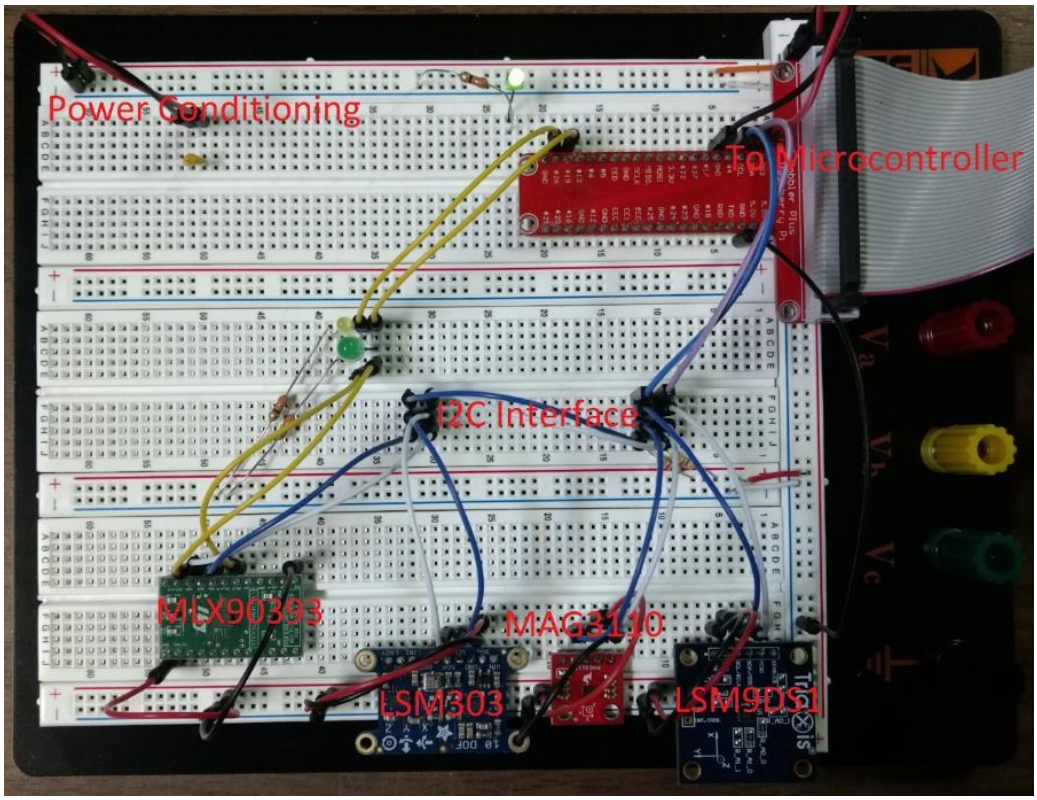

Figure 6-3. Implemented Sensing Platform

6.3.1 GIC Steady State Measurement Accuracy

The first characterization of the magnetometer sensing platform was performed using predefined steady state GIC values. The GIC value was set and measurements obtained over a period of one hour for values ranging from 0mA to 6000mA. Figure 6-4 shows the results of the first characterization step showing the measurement curve for each magnetometer in relation to the ideal calculated value. The figure shows the results for each individual sensor (LSM303-orange, LSM9DS1 – dark blue, MAG3110- grey, and MLX90393 – yellow) in relation to the ideal calculated values (light blue). At low current values the range of measured values is small (~3-4x10^3 nT), but as the measured current increases the range of measured values correspondingly increases (~40x10^3 nT). However, the error as a percentage of the total magnitude of the measured field stays relatively constant throughout the test currents. This fact led to the consideration of further data analytics techniques to leverage the capabilities of each magnetic field sensor.

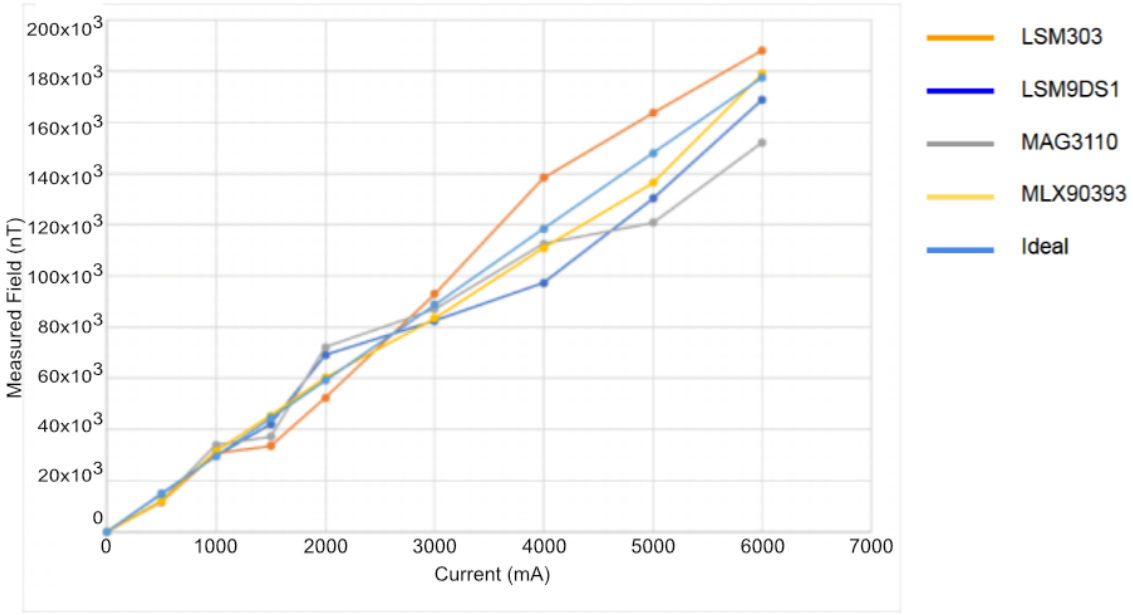

Figure 6-4. Average Steady State GIC Measurements for all Sensors

Post calibration none of the sensors adequately detected the GIC flow throughout the current ranges desired. The average percentage error for each magnetometer for all current settings is shown in Table 5, the error is taken as a difference from the ideal value. Critically, an error above 3% can result in GIC measurement errors above what can potentially damage power system equipment as discussed in Chapter 3. Subsequent characterization determined performance in measuring transient GIC signatures.

Table 5. Individual Magnetometer Error

Sensor	Error
LSM9DS1	3.18%±1.32%
LSM303	3.70%±1.45%
MAG3110	4.03%±0.97%
MLX90393	3.00%±1.42%

6.3.2 Transient GIC Signature Measurement Accuracy

The second characterization phase involved measuring the variations in GIC typical of a period of increased space weather and GIC. It is reasonable that changes of ±400mA/s to occur during periods of extreme space weather, as seen by [69]. Peak GIC detection is required to mitigate the potential of cascading impacts due to space weather. The current step selected was 0mA to 6000mA to 2000mA to stress the detection capabilities of each magnetometer and ensure that any potential change in GIC during a storm can be detected and measured.

The performance of each magnetometer for transient variations is shown in Figure 6-5,Figure 6-6, Figure 6-7, and Figure 6-8 . The ideal curve is shown in red and the measured values are shown in black. The MLX90393 (7.41% error ±2.3%) and LSM303 (3.27% error ±2.4%) performed the best on an individual basis and the LSM9DS1 (8.63%

error ±2.8%) and MAG3110 (8.59% error ± 1.7%) performed the worst in this application. In addition, the 'spikes' that can be seen during high field measurement are up to six times the ideal field strength. The differences in average error between steady state and signature measurements is due to the use of average error and number of points averaged over the sample period.

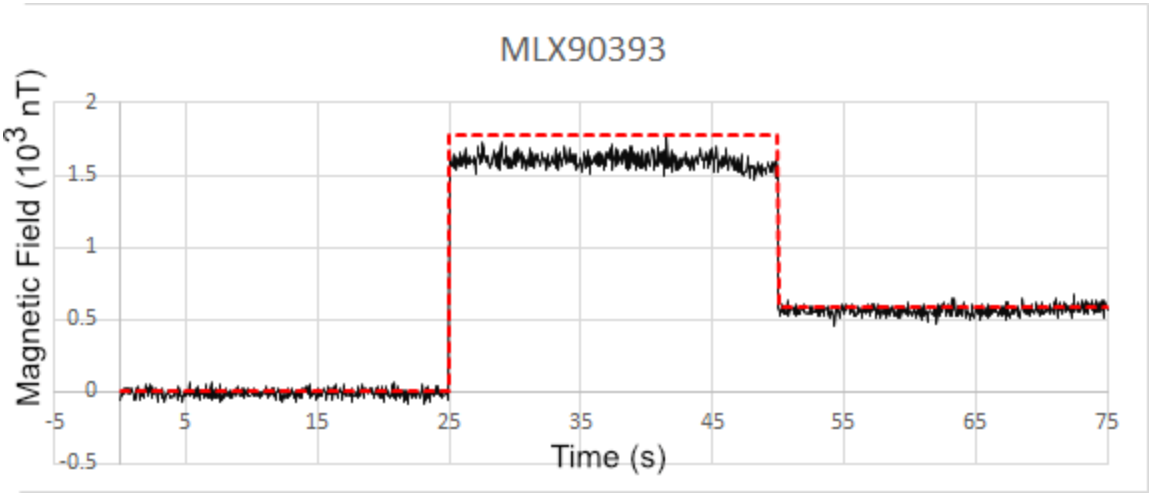

Figure 6-5. MLX90393, Transient GIC Measurement Performance

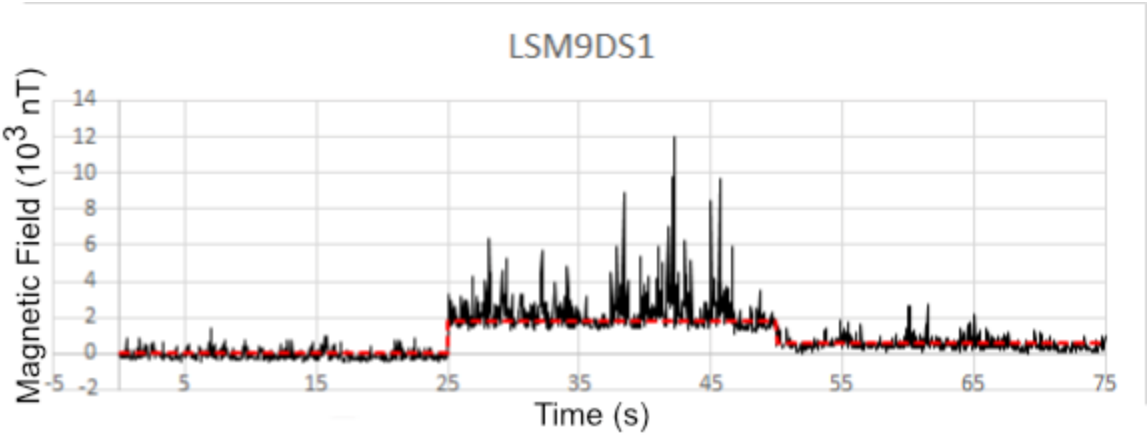

Figure 6-6. LSM9DS1, Transient GIC Measurement Performance

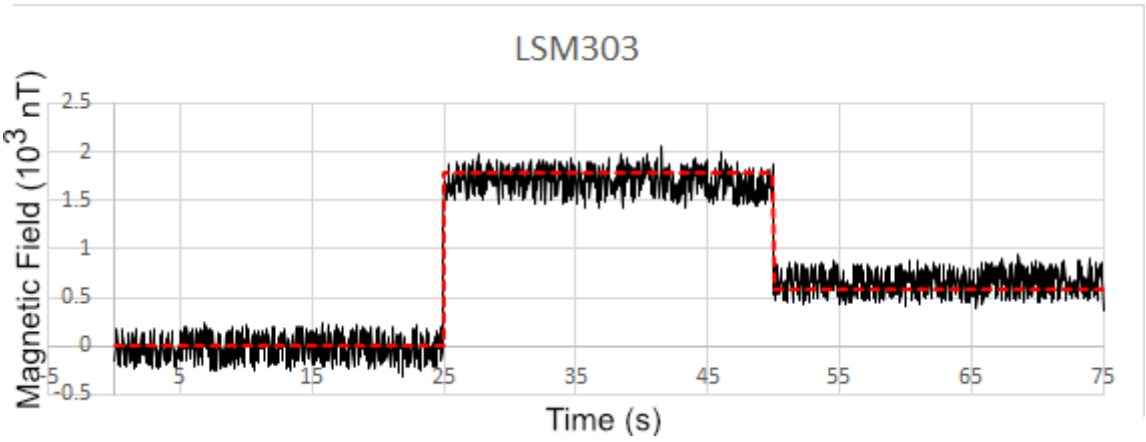

Figure 6-7. LSM303, Transient GIC Measurement Performance

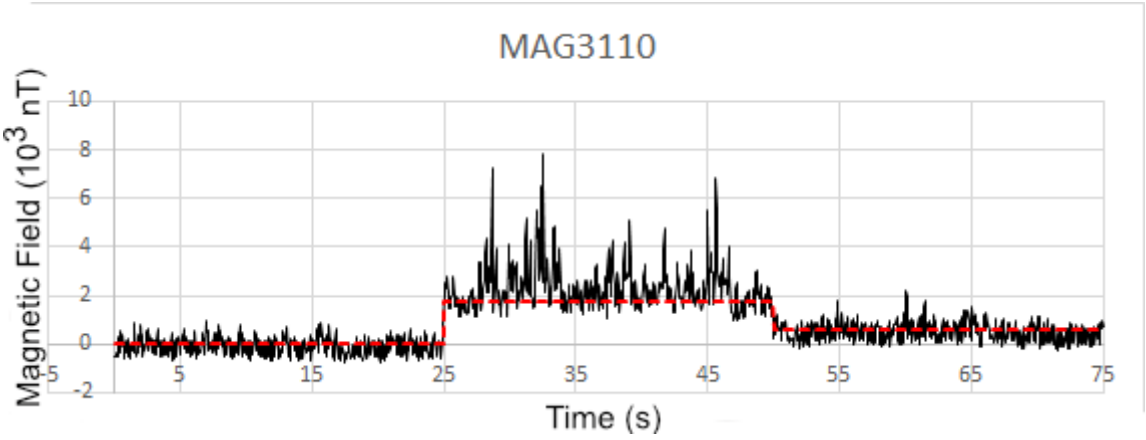

Figure 6-8. MAG3110, Transient GIC Measurement Performance

6.3.3 GIC Measurement in the Presence of an AC Field

Emulation of a real-world power system was performed by superimposing an AC field on top of the GIC field. An eleven-pole Butterworth digital notch filter centered at 60Hz removed the superimposed AC field component of the magnetometer measurements. The notch filtered allowed for additional information to be captured compared to the initial simplified system.

6.3.4 Combined Sensor Measurements

Integrating the described methodology to improve measurement accuracy resulted in an accuracy improvement to 99.47% for steady state measurement as shown in Figure 6-9. The overall platform achieved a steady state R-value of 0.99. In addition, the platform reduced standard error to 0.0161 from 0.0238 in the simple system an improvement of 6.7%. The system can detect the presence of harmful GIC at a distance within 20m of the transmission line, based on scaling measurement results.

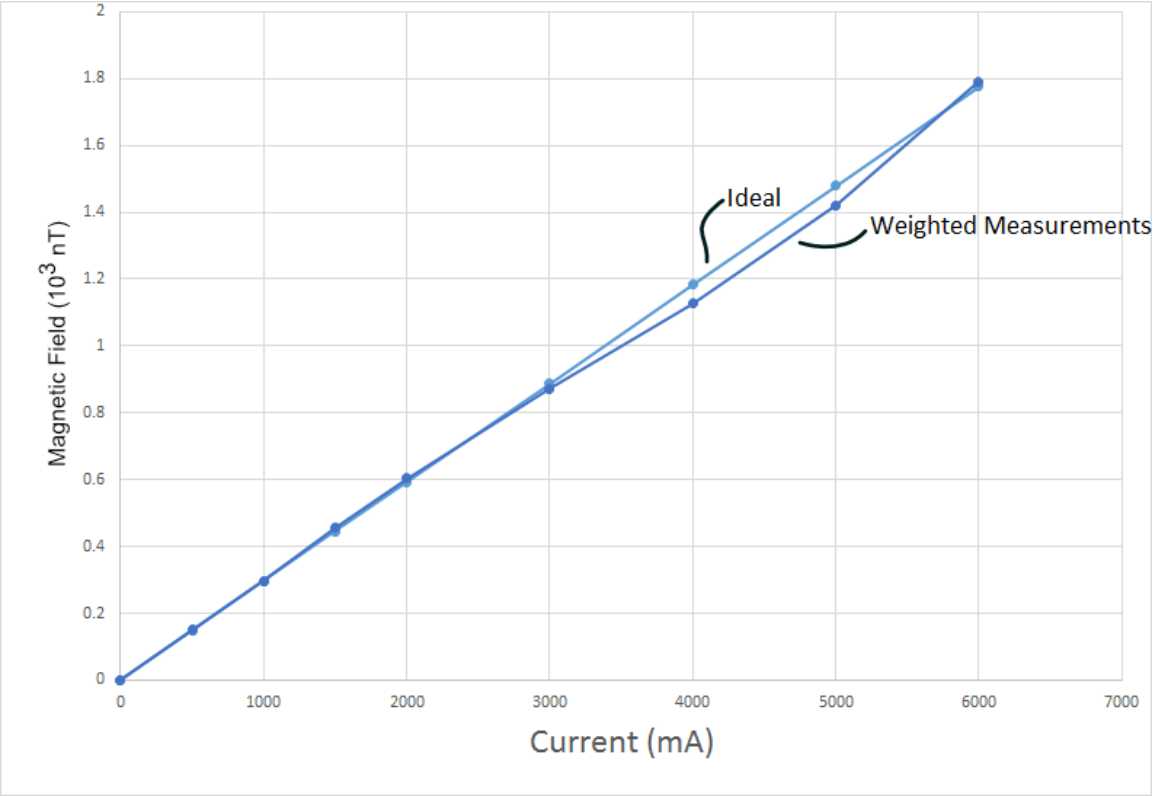

Figure 6-9. Steady State Measurement Accuracy for the GIC Measurement Platform

In addition, the measurement accuracy for GIC signature measurement improved to 97.7% from the maximum simple systems accuracy of 95.6% as shown in Figure 6-10.

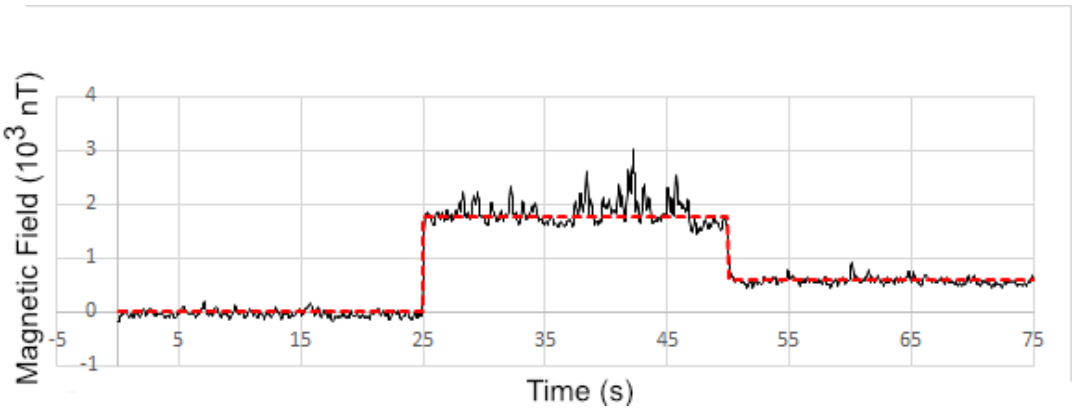

Figure 6-10. GIC Signature Measurements, Improved Method

Figure 6-11 shows the scaled test bench GIC currents and the measurements made by the magnetometer platform for the GIC signature introduced in Chapter 4, Section 4.2, obtained during the October 2003 geomagnetic storm. The figure shows that the platform closely follows the GIC signature with a maximum magnitude error of 0.86A with a standard error of ±0.24A. Scaling the error according to the scaling factor of 0.155, as previously discussed, results in an anticipated maximum error for the select transmission line configuration of 5.53A with a standard error of ±1.56A.

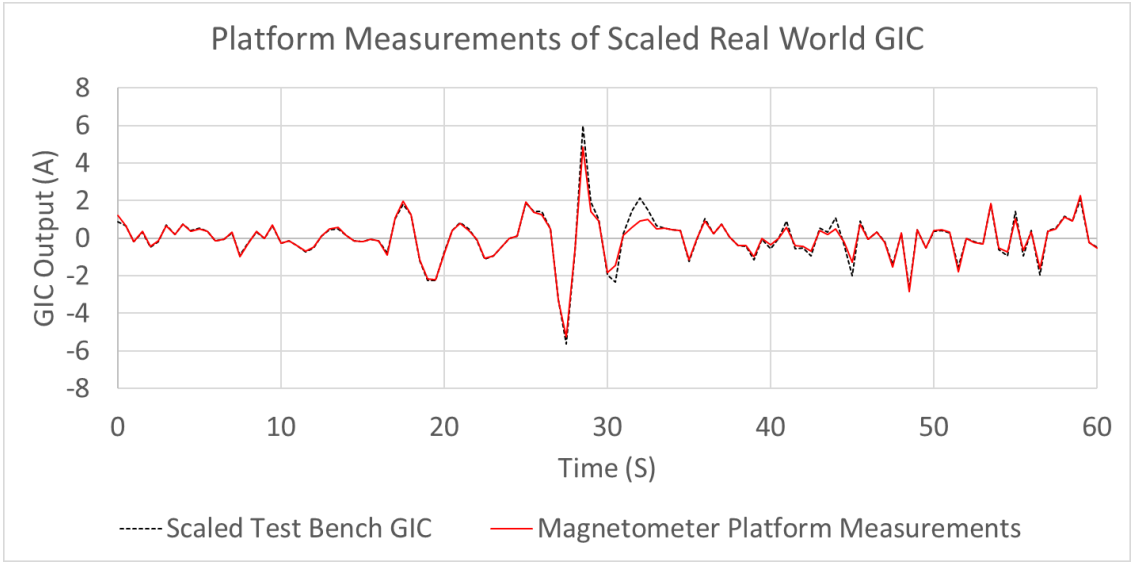

Figure 6-11. Comparison of Real-World GIC with Measurement Platform

6.4. Discussion

There are a multitude of practical technical challenges for the remote sensing and data measurement. Industry requires good data to be able to make the correct decision in an emergency situation, making good decisions on bad data results in bad outcomes. In addition, challenges related to data recovery, security, and data accessibility from a wide range of users has been addressed. Fundamental field deployment challenges related to the use of AC equipment to measure DC signals has been circumvented by an easily deployable and configured system.

Overall, the design of the sensing platform offers many advantages over the state of the art including simplicity, comparable accuracy, and reliable measurements. The designed platform succeeded in demonstrating the performance and capabilities of an integrated magnetometer platform. Implementation of a multi-sensor systems enabled cross checking measurement values and ensured that reported data can be verified by a pseudo independent source.

The research presented in this Chapter advances the field of GIC measurement by demonstrating that the combination of simple sensors can be used to achieve highly accurate GIC measurements. Prior to this work being completed there had been limited attempts to measure GIC below power transmission lines. Providing a complete systematic framework that is ready for deployment has not been articulated in the state-of-the-art. Additional advancement can be accredited to the demonstration of the sensing system in relation to the framework. The contributing framework and platform provides a new mechanism to measure GIC in power transmission lines.

Chapter 7. Preparing GIC Detection Systems for Field Deployment

As GIC transmission models leverage the abundance of magnetic field measurement data, a simulation tool was developed to model the magnetic field distributions of multi-phase electric power transmission lines. Evaluating the potential performance of the system efficiently and provide a generalized research and development model. The program uses both real-world captured data and field disturbances generated from a mathematical model to calculate ideal magnetic field distributions for transmission lines.

Building on the GIC models presented in Chapter 3, this chapter employs the models in order to simulate different conditions of GIC in transmission lines and their related magnetic fields. Desired parameters for each simulation leverage the characteristic mathematical models to calculate both GIC magnitude and direction for a wide variety of simulations. Using this approach ensured that simulated GIC values corresponded with previous GIC simulation work [12].

Varying field distributions were used to evaluate the platform's performance in detecting and measuring real GIC in conjunction with the GIC test bench. Validation of the magnetometer measurement platform required consideration of both the platform itself in addition to its deployment environment. Collected data from the test bench, as discussed in Chapters 4, 5 and 6, provide baseline measurements on the accuracy and precision of the sensing platform. However, to evaluate the potential performance of the magnetometer platform under real-world conditions it was required to leverage the measurements collected on field strength to calculate GIC through a transmission line.

7.1. Field Model Design

7.1.1 AC Field Modelling and GIC (DC) Field Modelling

There are fundamental differences between the behaviour of AC and DC magnetic fields of transmission lines. AC causes the magnetic field orientation in each conductor to reverse during each cycle meaning that a combination of time and frequency domain analysis must be used. DC fields have a fixed orientation. Furthermore, the modelling of AC fields is dependent on the operating conditions of a power transmission system and are well known. GIC field modelling requires an understanding of the complete geophysical process in order to develop relevant results. Overall the differences between AC modelling and GIC field modelling are the frequency of the generated currents and the method of determining the magnitudes of each current.

7.1.2 GIC Magnetic Field Simulation

Developing the simulation tool required careful inspection of the fundamental principles behind both generalized magnetic field modelling and DC magnetic field models. The simulation tool was designed to receive data inputs accounting for both electromagnetic and physical parameters. Physical parameters included transmission line length, height, conductance, conductor spacing, and bundle configuration. Electromagnetic inputs included the geoelectric field strength and direction.

Simulation and modelling work performed to determine the distribution of GIC field strengths around a power transmission line provided detailed calculation on the real-world field strength for a full-sized transmission line. Multiple configurations of single and three-phase power system configurations provided data sources with voltage levels

between 35kV and 735kV. This work laid the foundation for predicting and evaluating the performance of the magnetometer platform.

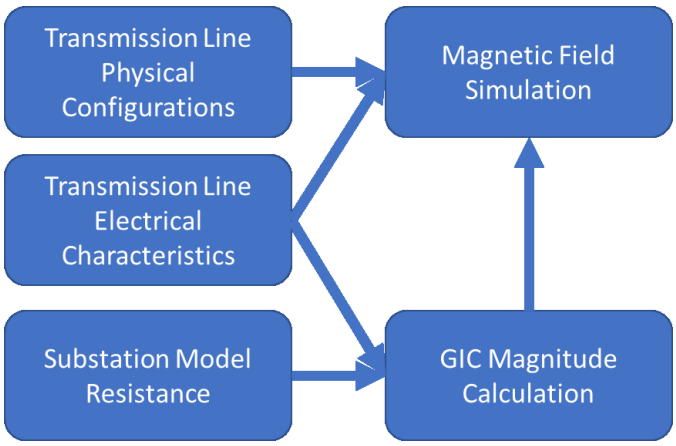

Figure 7-1. GIC Field Distribution Model Components

Figure 7-2 shows the process that was used in the simulation tool. First all parameters are initialized for the desired system. Next manual entry of line configurations or a database of technical configurations are presented. Third, the type of geomagnetic disturbance simulation is determined, and information taken from a live webserver if required using real world standardized data measurements. Fourth, the field due to the GIC in a transmission line is calculated and converted into polar coordinates for ease of use. Each line simulation is run in parallel to decrease processor runtime. The resulting fields can then be displayed and further analysis performed if required.

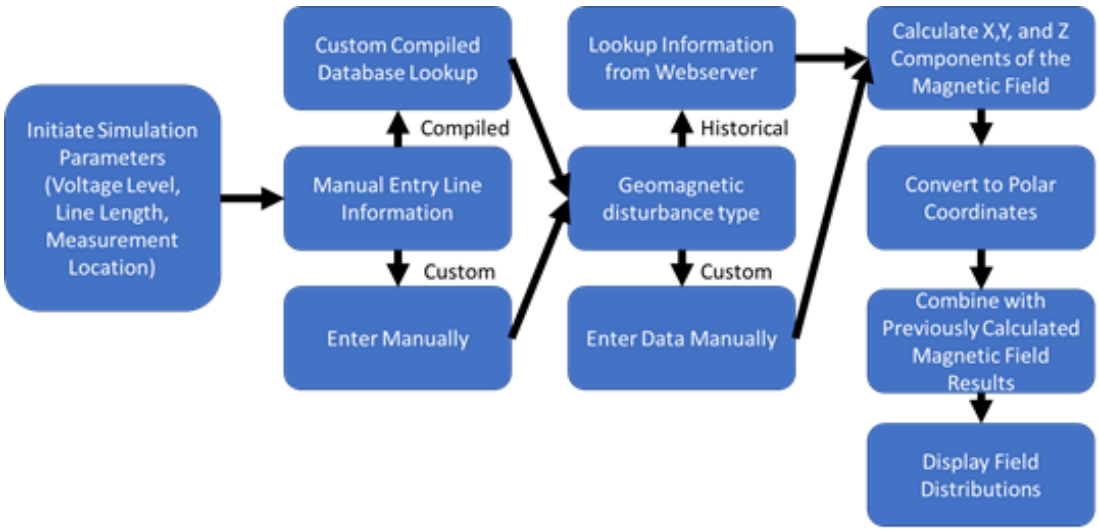

Figure 7-2. Simulation Flow for GIC Field Distributions

With respect to specific simulation operations, the simulator tool first sets out the simulation parameters and required data frameworks. Once the baseline parameters for a simulation have been selected according to user needs, the GIC flow through the selected configuration of transmission line is calculated based on the models presented in Chapter 3. The magnetic field due to the GIC is then calculated based on each specific transmission line geometry and the previously calculated GIC. The magnetic field strength is then plotted to provide the user with a graphic interface and the results saved. The complete simulation tool is contained within Appendix A.

7.1.3 Model Transmission Line Configurations

The designed system functions by specifying the desired physical parameters of a transmission line that the detection and measurement system will be installed on. Alternatively, there is a database of transmission lines as designated according to IEC 60826 [70] for various voltage levels. Table 6 shows test cases of transmission line specifications at different voltage levels.

Table 6. Transmission Line Test Cases

Case #	Voltage (kV)	Line Resistance (ohm/km)	Ground Clearance (m)	Phase Spacing (m)	Config.
1	230.0	0.064	20	2.2	Horizontal
2	230.0	0.064	20	2.2	Vertical
3	345.0	0.037	24.7	2.7	Horizontal
4	345.0	0.037	24.7	2.7	Vertical
5	500.0	0.013	34.2	3.7	Horizontal
6	500.0	0.013	34.2	3.7	Vertical
7	735.0	0.011	43.7	4.8	Horizontal
8	735.0	0.011	43.7	4.8	Vertical

Table 7 shows the transmission line modelling parameters that were used for all test cases. The electric field strength was taken as the minimum value taken from the 5-layer Earth conductivity model as shown in [43] . Calculation of the GIC in each line was accomplished using work completed by [12]. The reference level was calculated based on an average observed background field strength.

Table 7. Base Simulation Parameters

Parameter	**Test Value**
Electric Field	2.0 V/km
Line Length	300.0km
Substation Resistance	1.817 ohm
Reference Background Field	65.0uT

7.1.4 Simulation Validation

In order to validate the results of the simulation tool, baseline parameters were used from previous work completed in the area of GIC simulation including [12], [43], and

[71]. The simulator tool was then used to calculate GIC values based on the same inputs and the results from the simulator tool and previous work was found to be comparable. In addition, the validation of the magnetic field results was achieved by comparing the results found through the simulation tool with hand-calculated values. Further validation of the simulation tools was performed by simulating the parameters of the test bench presented in Chapter 4 and comparing the results with measured values obtained by the GIC measurement platform presented in Chapter 6. Overall, the results of each simulation system sub-component corresponds well with both previous simulation tools and observations demonstrating that the simulation results are in agreement with real-world values.

7.2. Simulation Results

Each test case in Table 6 was processed using the simulation tool. Various test cases were used to highlight the applicability of the system described in Chapter 6 to a wide range of power transmission lines. Figure 7-3 is the first simulation case for the field distributions of a 25.00m tall transmission tower with 4.37m phase spacing. The first graph shows the horizontal field distributions for each phase of the power transmission line shown in blue, yellow, and green according to each phase. Since the configuration of the transmission line phases is horizontal, the peak magnitude of each horizontal field component is the same but the location of the peak is offset from the centre of the transmission line. The second graph shows the vertical magnetic field component for the same transmission line configuration. The configuration of the line shifts the inflection point for the vertical field according to the centre of each conductor shown in blue, yellow, and green. The third graph is the total magnitude of the magnetic

field shown in blue, with a reference constant of 65nT shown in red. The fourth graph shows the resultant angle of the total magnetic field due to the indicated GIC in each conductor. The intersection of the reference field and the total field shows where the field due to the GIC flowing through the transmission line overcomes the background fields of the Earth. In each of the graphs, the magnetic field distributions are separated according to the phase spacing of the physical transmission line.

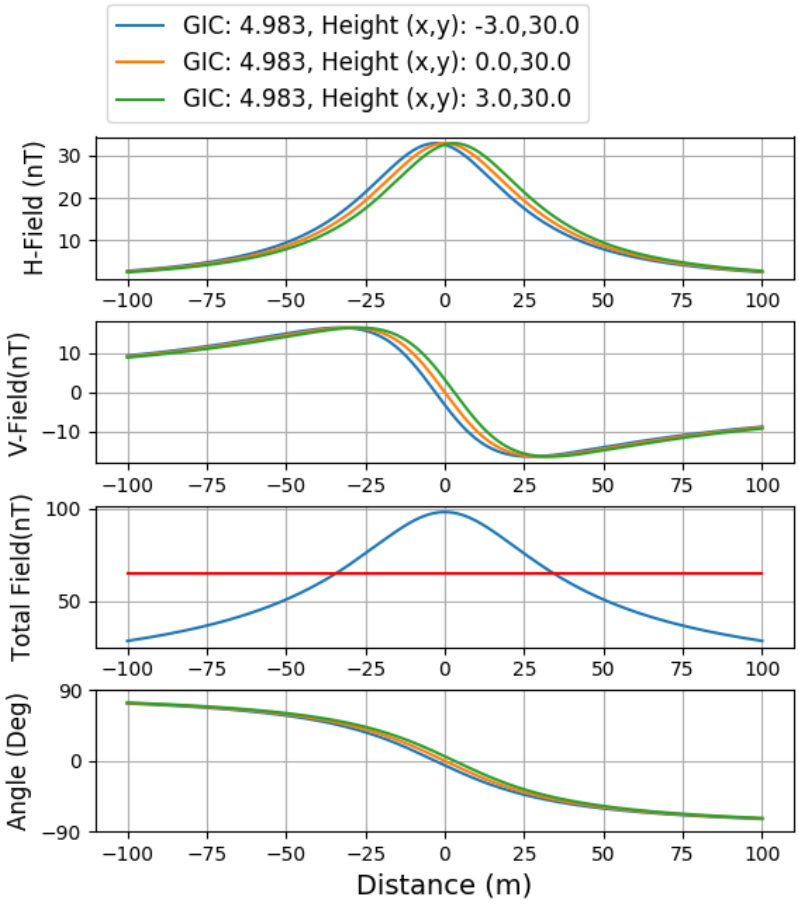

Figure 7-3. Model Test Case 1, 230kV, 300km, Horizontal

Figure 7-4 shows the resulting simulation for Test Case 2, a vertical configuration with the same voltage as Figure 7-3. Comparing the simulation results of Test Case 1 and Test Case 2 provides new insight into the distribution of magnetic fields due to GIC in

transmission lines. The total field graph shows that the total field intersects the reference field at further distances from the centre of the transmission line from ±33.4m to ±84.6m indicating that the vertical and horizontal configuration of transmission lines can have a significant impact on the observed magnetic fields from a detection and measurement system. In addition, the peak value of the field has increased by a factor of 1.9 showing that the measurement system requires further consideration of the physical configuration of the transmission line. The third element that changes between the horizontal and vertical configurations is the angle of the resultant magnetic field. The horizontal spacing results in a simulated observed measurement with a larger margin of error directly underneath the transmission line centre, while the vertical spacing has a low margin of error at 0m distance increasing as the distance from the transmission line increases. In both cases, the angle approaches ±90˚ as the distance increases beyond the indicated values.

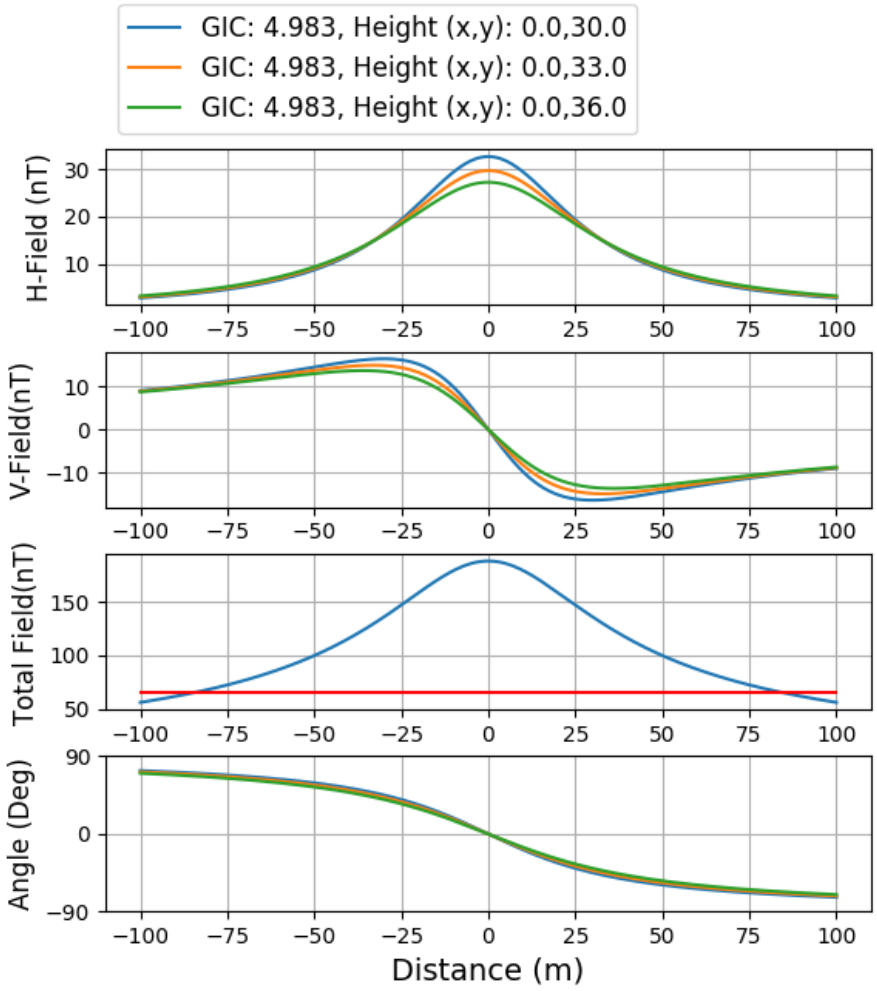

Figure 7-4. Model Test Case 2, 230kV, 300km, Vertical

Figure 7-5 shows the field distributions for a 24m high transmission line with a voltage of 345kV. The increase in voltage level is accompanied by an improvement in the conductivity of the wires in the transmission line, leading to a higher GIC flow, according to previous work in the field. Comparing the increased voltage level of Test Case 3 with the previous Test Cases, the change in configuration is shown to change the simulation of the resultant magnetic fields. The primary change is in overall magnitude of the simulated field, this indicates that while the increasing distance of the transmission line from the detection and measurement system (on the ground) decreases the strength of the observed

magnetic field, it is outpaced by the increase in potential GIC due to system configurations and component selection.

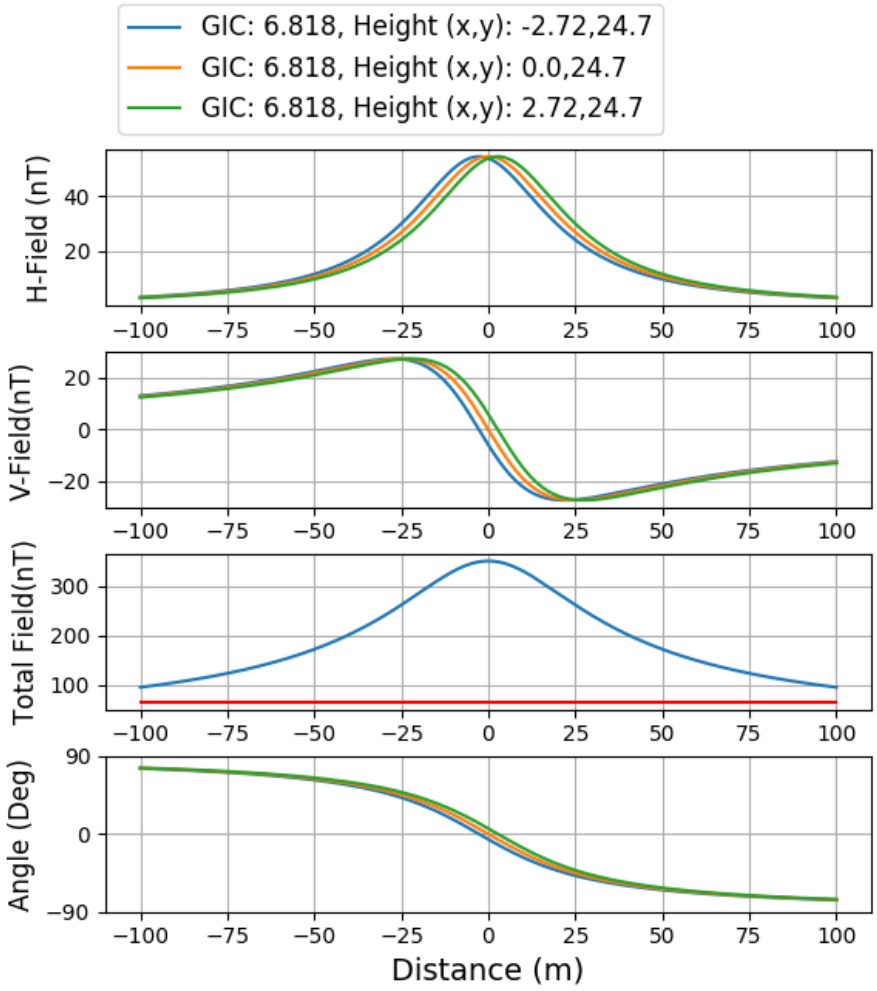

Figure 7-5. Model Test Case 3, 345kV, 300km, Horizontal

The vertical configuration shown in Figure 7-6 shows that the simulation results of the magnetic fields for the vertical configuration at 345kV. The results at this voltage level also show that the total field is significantly higher than the background magnetic fields. In addition, the peak of the magnetic fields can be clearly seen to be inverse order of height from the measurement location as expected. The trend of a higher peak

concentration of the vertical magnetic field component at a distance of ~25m can also be identified.

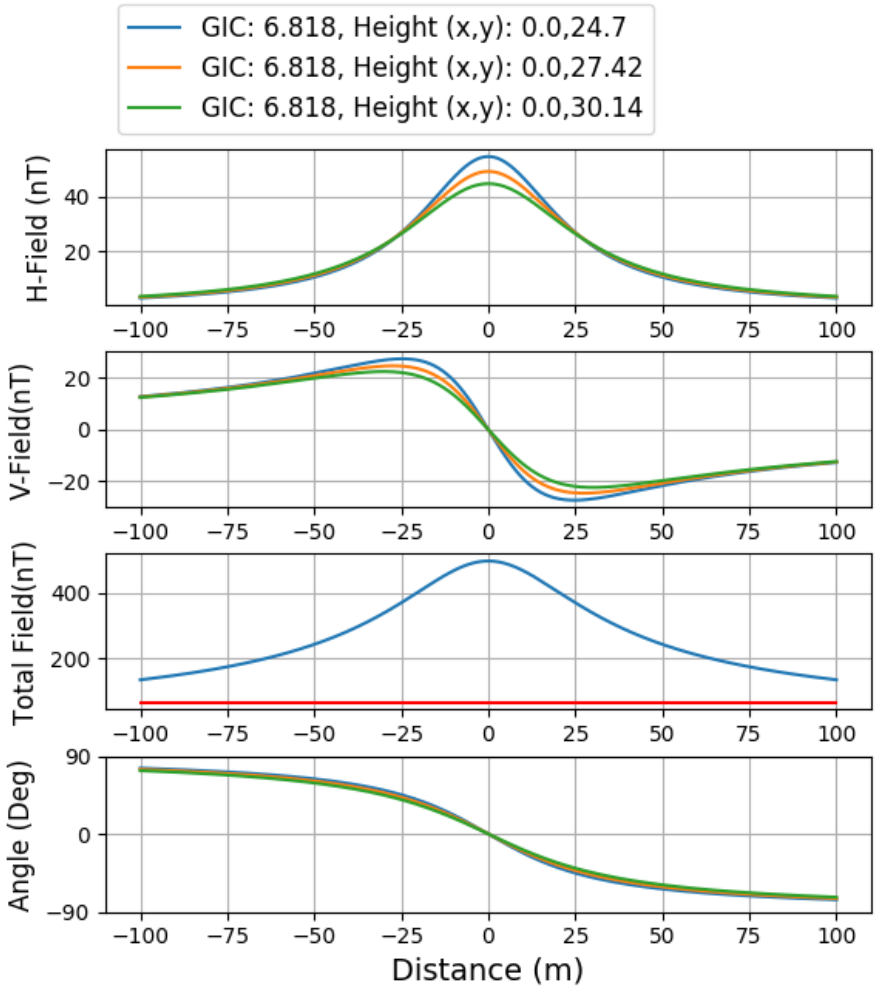

Figure 7-6. Model Test Case 4, 345kV, 300km, Vertical

Figure 7-7 and Figure 7-8 show the simulated fields for a 500kV transmission line in a horizontal and vertical configuration respectively. At the 500kV voltage level the spacing between phases begins to impact the total field observed, resulting in a less accentuated peak value. In addition, the peak of the vertical field is shifted further away from the transmission line centre.

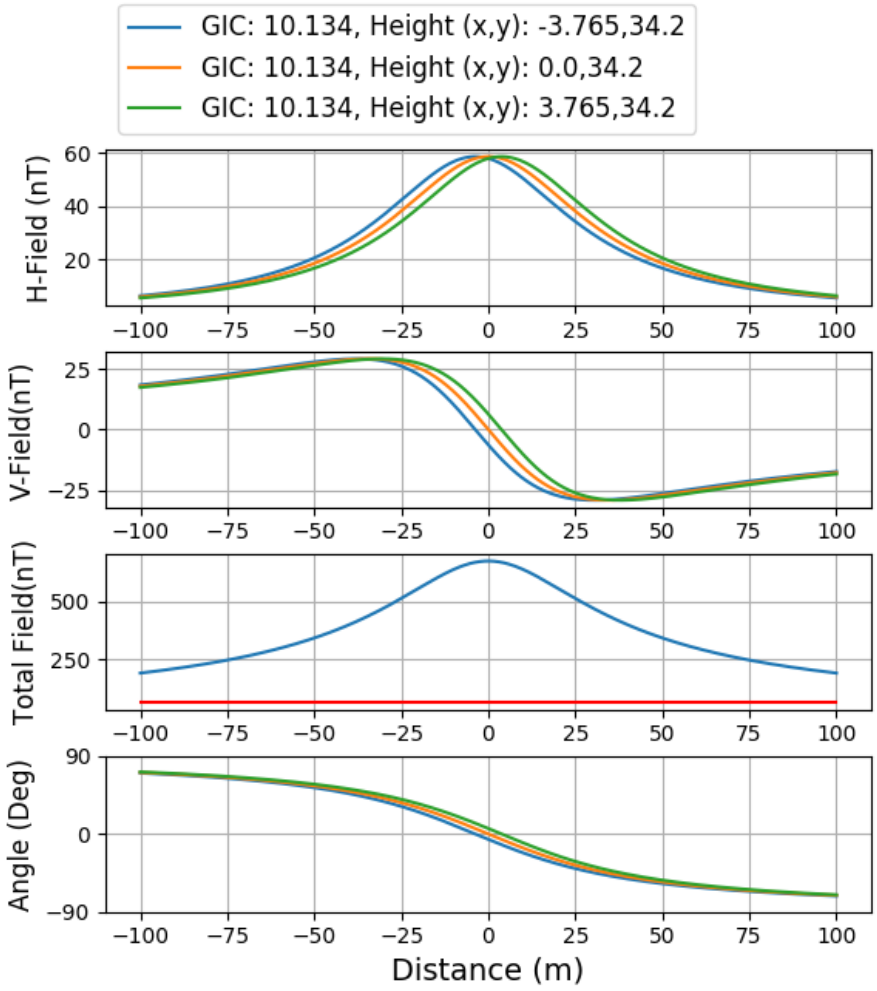

Figure 7-7. Model Test Case 5, 500kV, 300km, Horizontal

The vertical 500kV case shown in Figure 7-8 is similar to the results found in the 345kV case. Common to both cases are the shapes of the horizontal and vertical fields as well as the general change in field angle.

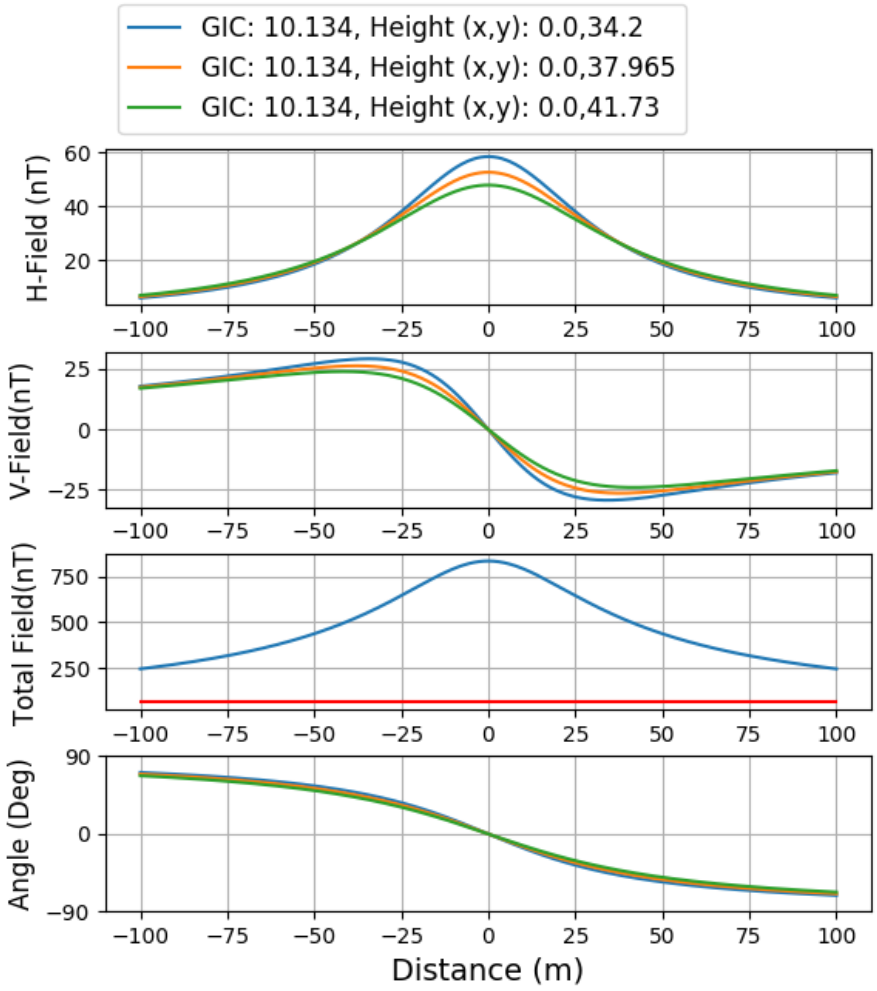

Figure 7-8. Model Test Case 6, 500kV, 300km, Vertical

The final two test cases were simulated for a 735kV transmission line, in both a 3 phase horizontal and three-phase vertical configuration. The results of the simulations are shown in Figure 7-9 and Figure 7-10. This voltage level was considered due to its upper range of a common high voltage system. The results show that the phase spacing further differentiates the magnetic field from each conductor as anticipated. In addition, the greater height of the higher voltage transmission lines does not impact the difference between the simulated field at ground level and the reference Earth magnetic field.

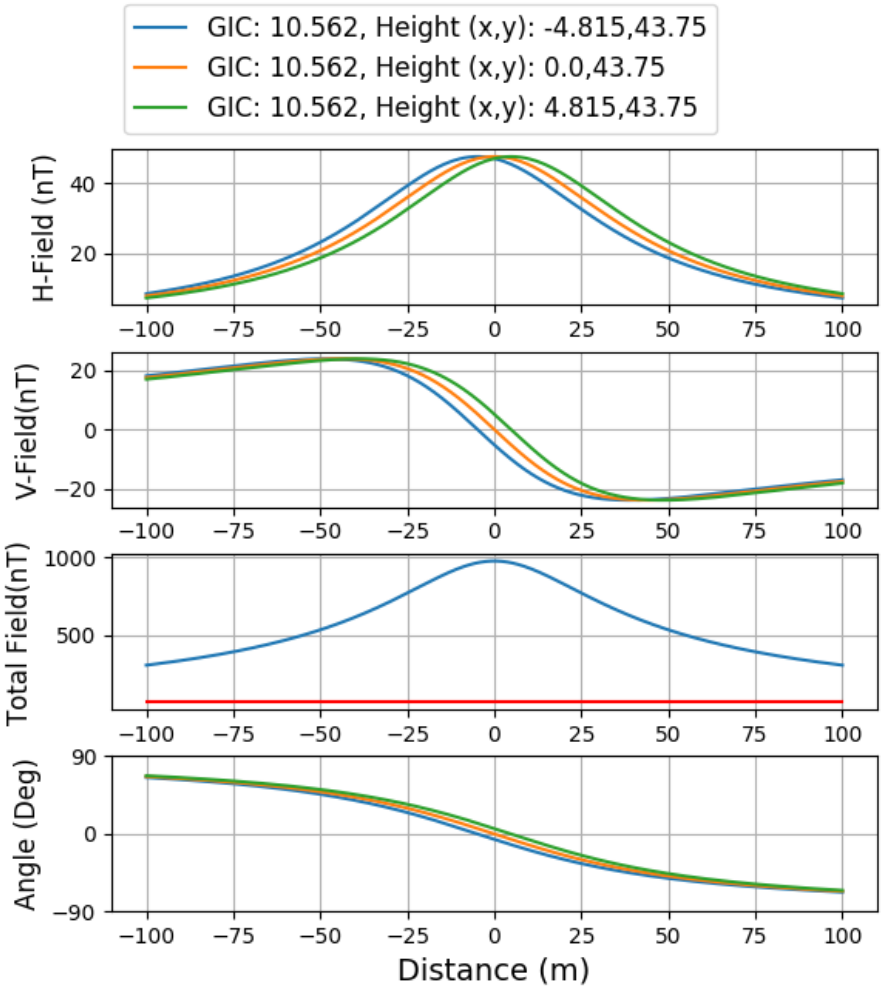

Figure 7-9. Model test Case 7, 735kV, 300km, Horizontal

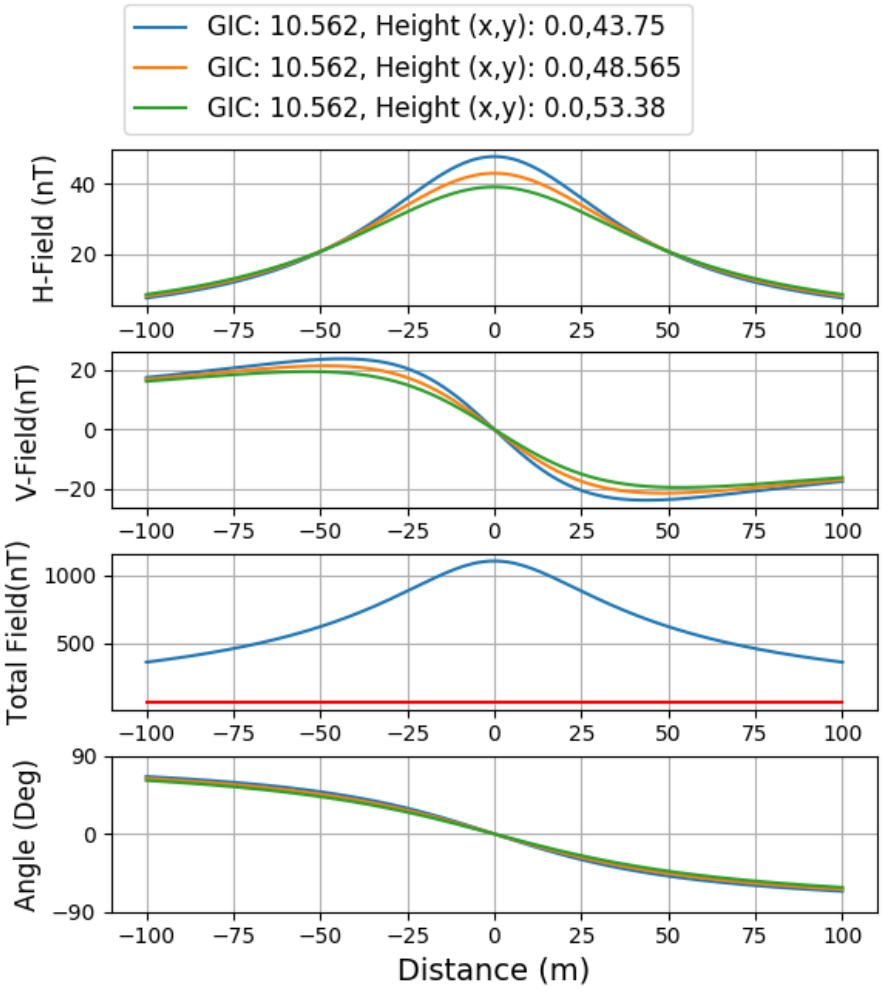

Figure 7-10. Model Test Case 8, 735kV, 300km, Vertical

Overall, eight test cases were used to simulate the distribution of magnetic fields in proximity to a power transmission line. The result of the simulations is the detailed knowledge of expected magnetic fields that can be detected and measured by sensing systems. Consistently, there are expectations that the magnetic fields in real world power systems due to GIC can be measured by the designed GIC measurement platform described in Chapter 6. Predicting the performance of the described system with the new knowledge of the magnetic field characteristics is an important step towards deploying sensing systems.

7.3. Predicting GIC Measurement System Performance

The results of the simulations are used to predict the performance of the GIC detection and measurement system. Figure 7-11 shows the measured data from the GIC sensing platform as presented in Chapter 6 for different scaled heights of the model transmission line ranging from 10cm to 60cm. Each curve generally follows what is expected from fundamental principles, however below 1A of GIC current the measured values intersect with each other due to the sensitivity of the sensors deployed. In addition, the 2A measurement from a distance of 40cm appears out of order with the 50cm measurement curve. This was done to determine the impact of the protective enclosure and if a changing in enclosure significantly changed measurements. This was performed to ensure consistency between all other measurements in the same enclosure configuration.

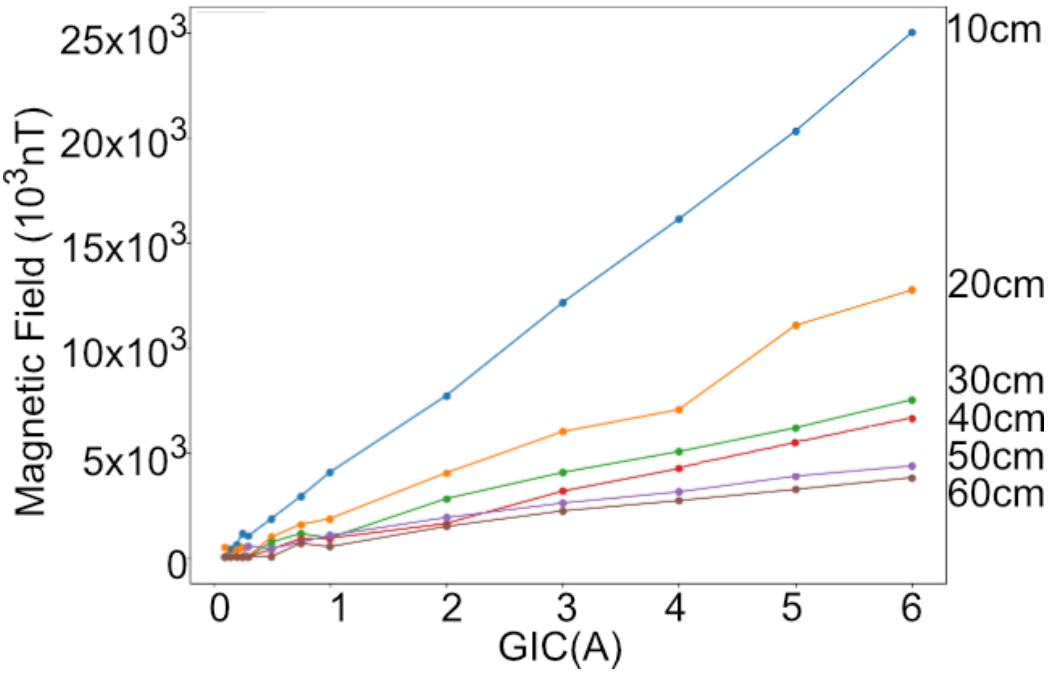

Figure 7-11. Measured Test Bench GIC Values from Sensing Platform

Building on the simulations that were performed in the previous section, new simulations were performed with the values indicated in Figure 7-12. The simulation tool allows for all parameters of a system to be evaluated prior to the deployment of a GIC detection and measurement system. This provided a basis for cross correlating the results from the test bench measurements to the simulation tool.

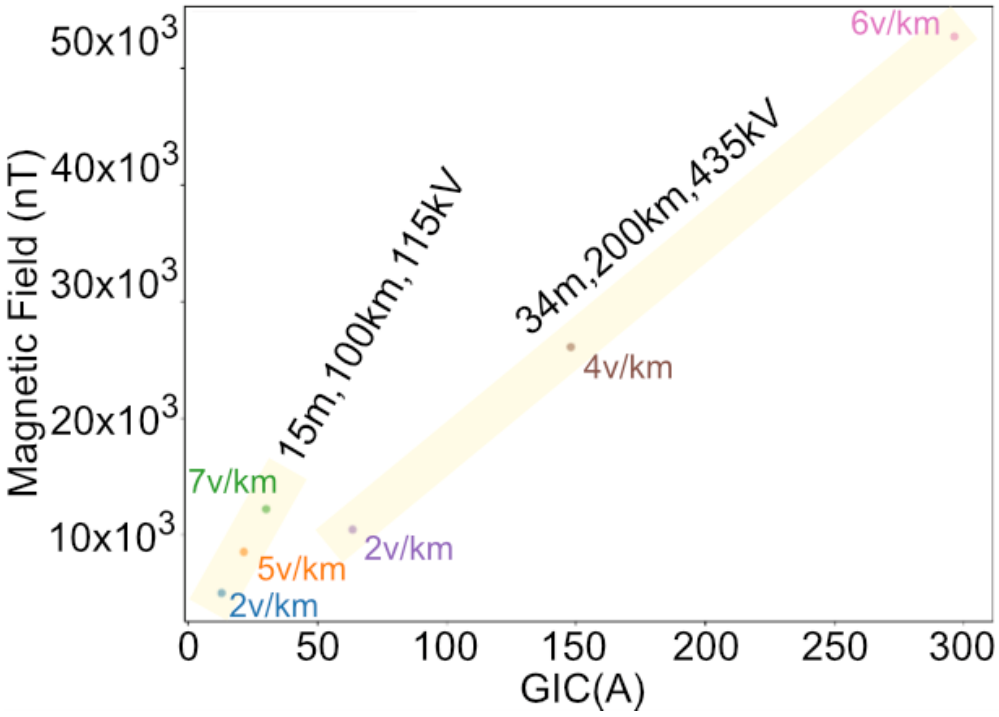

Figure 7-12. Simulated GIC Field Strength for Different Configurations of Transmission Lines

By scaling the modelled field strength down to the test bench size, we can compare the observed measurements in accordance with the configuration of a real-world model of a transmission lines. Scaling the observed magnetic field values obtained from the test bench to correspond to the scaled simulated values results in Figure 7-13 indicating the anticipated performance of the system. This scaling example shows the scaling of GIC

magnitudes down to the test bench physical configuration for a transmission line operating at 115kV, 20.0m tall to the test bench curve at a distance of 0.6m. The difference between the linearly scaled simulated value (red) and the observed values (blue) is the expected accuracy of the GIC detection and measurement system.

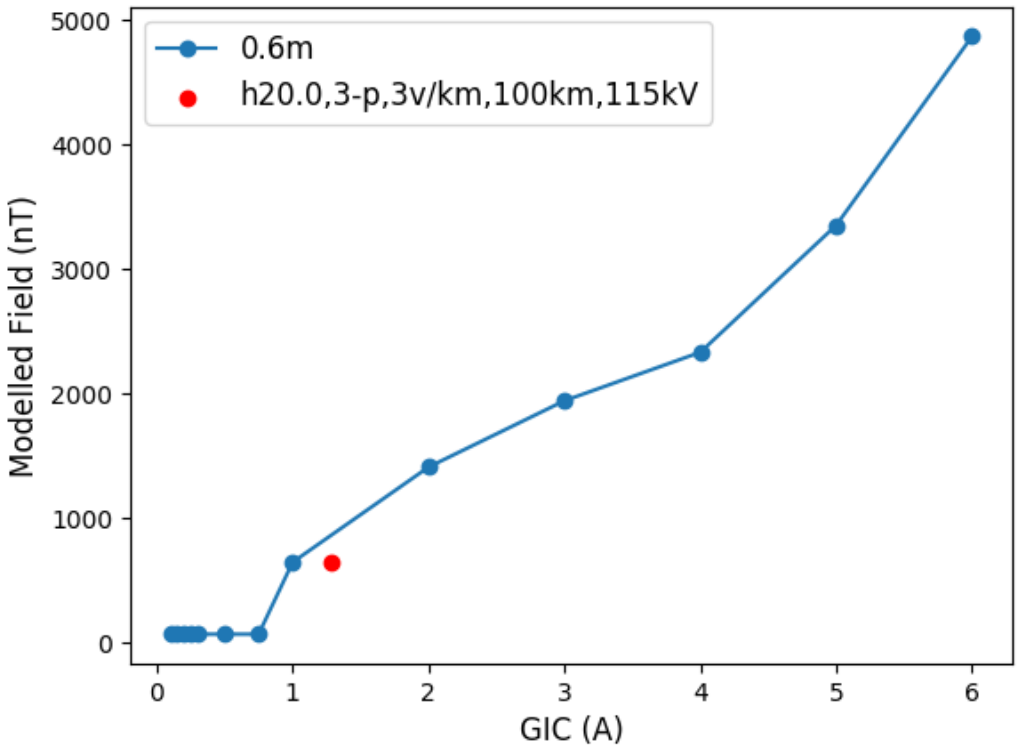

Figure 7-13. Scaled Performance of GIC Sensing Platform Compared to Simulations

The process used in the previous figure was repeated for fifteen characteristic test configurations, and space weather conditions. The resulting accuracy of the developed detection and measurement system, as described in Chapter 6, was calculated to be 92.3% mean with a standard deviation of 4.6%.

.

7.4. Discussion

Comparing the indicated accuracy with the only other work done in the field using a non-contact GIC method as shown in [39], where the accuracy ranges from 60% to 80%, demonstrates the field potential for the developed sensing system. Limitations of a direct contact hall-effect system such as [38], inhibits direct comparisons of accuracy measures.

The field model for GIC distributions addresses technical and deployment challenges in the field of GIC measurement. While AC induction and fields surrounding power transmission lines have been thoroughly studied the measurement systems and data surrounding the phenomena vary greatly. The simulation tools described in this research address challenges in placing non-contact GIC measurement devices underneath power transmission lines and facilitates the selection of magnetometers in addition to guiding requirements for sensors and supporting devices.

Overall the simulation tool provides a model of GIC field distributions in proximity to transmission lines and other long conductors. Evaluating the effectiveness of the sensing platform shows positive results that require further testing in the field to ensure reliability and accuracy can be maintained.

The work presented in this chapter provides the first tool for evaluating the placement and predicted performance of GIC measurement solutions in proximity to power transmission lines. Evaluating the performance of sensing systems prior to deployment allows rapid prototyping and new designs and facilitates innovation and additional development.

Chapter 8. Conclusions and Future Work

8.1. Conclusions

In conclusion, this research has demonstrated a simple GIC detection system that can determine GIC flow through a power transmission line. The scaled test bench described in Chapter 4 can be used to test GIC detection systems using both simulated GIC and previous GIC measurements to accelerate system development. Chapter 5 presented a simplified GIC detection and measurement system that established the use of a simple system that was capable of measuring GIC in an electric transmission line. Chapter 6 continued to develop the work completed by presenting a GIC measurement platform. The combination of Chapter 5 and Chapter 6 shows the development and demonstration of a simple GIC detection system, with results demonstrating that the system can determine GIC flow through a transmission line. Chapter 7 is a transitional chapter in preparation for future work, demonstrating that the simple detection system that has been designed and developed will function in the field based on GIC field modelling.

Outside the scope of this thesis is mitigation of GICs. This was done deliberately to ensure that the research focused on addressing the scientific gaps between simulation and real-world environments. Further analysis and integration of the proposed systems into existing or new mitigation techniques is a promising area for future development, that could benefit from existing industry-academic partnerships and development programs.

The engineering benefits of this research are cross cutting over a wide range of applications. Broadly, the research demonstrates value added to small and medium sized

utilities that are resource constrained. In addition, the scalability and mobility of the test bench and developed sensing systems offer flexibility towards measuring GIC in a range of impacted systems.

Overall, the research has studied some of the key challenges in the field of GIC detection and measurement and developed a system to fill some of the gaps between GIC modelling, simulation tools and real-world data collection. Providing a new system for detecting GIC will allow utilities to better protect their systems from catastrophic space weather events.

While GIC is considered a threat to power system operations the constant hazard has resulted in an increase in robust designs for electric power transmission infrastructure, mitigating potential disruptions from other sources. In addition, the threat to power systems has resulted in increased monitoring capabilities around the Sun resulting in advancing our understanding of heliophysics and magneto-hydrodynamics. Lastly, the existence of GIC and its impacts on pipeline corrosion has resulted in improved monitoring mechanisms for pipeline failure, and more robust communication infrastructure.

8.2. Future Work

The following research areas are proposed as a continuation of the work completed. The first area is to develop the GIC measurement platform into a system that is ready for field deployment. An industry partner would be required prior to developing the system into a pre-commercial device to be deployed for field testing. Field deployment would also require additional study of predictive algorithms to allow for future GIC events to be

identified and improvements in response time implemented. The power requirements for the detection and measurement systems would required further analysis, and could leverage a model as shown in [70] to support real-time operation and extended deployments. Automated deployment and calibration of the GIC measurement platform is another research area that shows promise for remote sensing applications. This work is a natural extension of the work completed on GIC field models for transmission lines.

A second area for future development is the communications systems necessary to deploy a large number of GIC detection systems throughout a power system network. Arrays of the developed system could be deployed to measure the overall health of a power system towards GICs. Increasing operator situational awareness allowing mitigation measures to be more effective and provide an ability to foresee potential grid stability issues before they occur. Future work on this project has the capacity to be expanded into various application areas and finely tuned through subject matter expertise

A third area for further research is in an alternate application of the designed and implemented system. Arrays of the GIC measurement platform can also be deployed as an intrusion detection system by leveraging the magnetic field produced by moving metal objects. Capabilities of the magnetometers and a pattern classification system could be used to determine when an intruder is in close proximity to a transmission line. Similar concepts can be applied to monitoring pipelines and valve stations. The soft magnetization of the ferrous metals in vehicles can be detected and used to differentiate between types intrusions. The real-time performance of the platform would need to be improved to provide relevant and timely results for an intrusion detection system. A project leveraging the GIC measurement platform and developed systems is currently in

its preliminary scoping stages in order to develop an intrusion detection system. Additional research will build knowledge and subject matter expertise in order to address increasing threat due to GIC and improve the resilience of critical energy infrastructure.

References

[1] C. Cid *et al*., "A Carrington like geomagnetic storm in the 21st century," *J. Space Weather and Space Climate*, vol. 5, no. 16, pp. 1-6, Jun. 2015.

[2] J. R. Aguero *et al*., "Modernizing the Grid: Challenges and Opportunities for a Sustainable Future," *IEEE Power and Energy Mag.*, vol. 15, no. 3, pp. 74-83, Apr. 2017.

[3] C. Bataille, "Modelling a low carbon future consistent with the Paris Agreement Goals," Nov. 27, 2017. Accessed: Dec. 12, 2017. [Online]. Available: https://www.cleanenergybc.org/wp-content/uploads/2017/12/Chris-Bataille.pdf

[4] K. Clement-Nyns, E. Haesen and J. Driesen, "The Impact of Charging Plug-In Hybrid Electric Vehicles on a Residential Distribution Grid," in *IEEE Trans. on Power Systems*, vol. 25, no. 1, pp. 371-380, Dec. 2010.

[5] D. Boteler, "On the Interaction of Power Transformers and Geomagnetically Induced Currents," in *IEEE Trans. on Power Delivery*, vol. 31, no. 5, pp. 2188-2195, Oct. 2016.

[6] N. Mohan, J. G. Kappenman and V. D. Albertson, "Harmonics and Switching Transients in the Presence of Geomagnetically-Induced Currents," in *IEEE Trans. on Power Apparatus and Systems*, vol. 100, no. 2, pp. 585-593, Feb. 1981.

[7] B. Bozoki and *et al.*, "The Effects of GIC on protective relaying," in *IEEE Trans. on Power Delivery*, vol. 11, no. 2, pp. 725 - 739, Apr. 1996.

[8] V. D Albertson *et al*., "Solar-induced currents in power systems cause and effects," in *IEEE Trans. on Power Apparatus and Systems*, vol. 92, no. 2, pp. 471-477, Mar. 1973.

[9] L. M. Winter *et al*., "Spectral scaling technique to determine extreme Carrington-level geomagnetically induced currents effects," *J. Space Weather*, vol. 15, no. 5, pp. 713-725, May 2017.

[10] NERC, "1989-Quebec Disturbance," Nov. 1989. Accessed: Jan. 4, 2016. [Online] Available: https://www.nerc.com/files/1989-Quebec-Disturbance.pdf

[11] M. Adibi (Jul. 2015). Impact of Power System Blackouts. Presented at the IEEE Power Engineering Society General Meeting, Denver, CO. Accessed: Sept. 15, 2016. [Online]. Available: http://sites.ieee.org/pes-cascading/files/2015/11/2015_08_Mike-Adibi-Slides-2015-PES-GM-Panel-on-Cascading.pdf

[12] D. Boteler, "Methodology for simulation of GIC in power systems," *J. Space Weather and Space Climate*, vol. 4, no. A21, pp.1-11, Jul. 2014.

[13] DRDC, "Simulation Lab for CSSP Testing and Evaluation," Accessed: Dec. 22, 2016. [Online]. Available: http://www.science.gc.ca/eic/site/063.nsf/eng/h_4AFF4ABA.html

[14] D. Boteler, A. J. C. Lackey, L. Marti and S. Shelemy, "Equivalent Circuits for modelling geomagnetically induced currents from neighbouring networks," *IEEE Power and Energy Society General Meeting*, Vancouver, BC, Canada, Jul. 2013, pp. 1-5.

[15] R. Pirjola, D. Boteler and K. Zheng, "Effects of System Characteristics on GIC," *IEEE Trans. on Power Delivery*, vol. 29, no. 2, pp. 890-898 Apr. 2014.

[16] D. Boteler and L. Tricktchenko, "Modeling GIC Using Geomagnetic Indices and Data," in *IEEE Trans. on Plasma Science*, vol. 32, no. 4, pp. 1459-1467, Oct. 2004.

[17] A. J. C. Lackey and R. Goubran, "Low-cost magnetometer sensing system for detecting geomagnetically induced currents in transmission lines," in *Proc. IEEE Sensors Applications Symposium*, Glassboro, NJ, USA, Mar. 2017, pp. 1-6

[18] A. J. C. Lackey, R. Goubran and F. Kwamena, "Geomagnetically Induced Current Measurement Using an Integrated Magnetometer Platform," in *Proc. IEEE Sensors Applications Symposium*, Seoul, South Korea, Mar. 2018, pp. 1-6

[19] R. Rifaat, "Power System Protective Relays: Principles and Practices," Accessed: Nov., 2016. [Online]. Available: http://sites.ieee.org/sas-pesias/files/2016/12/PowerSystemProtectiveRelays_PrinciplesAndPractices.pdf

[20] U.S. DOE and EPRI, "Joint Electromagnetic Pulse Resilience Strategy," Jul. 2016, Accessed: Aug. 2017. [Online]. Available: https://www.energy.gov/sites/prod/files/2016/07/f33/DOE_EMPStrategy_July2016_0.pdf

[21] M. J. Owens, M. Lockwood and L. A. Barnard, "Coronal mass ejections are not coherent magnetohydrodynamic structures," *J. Scientific Reports*, vol. 7, no. 1, pp. 1-6, Jun. 2017.

[22] NASA, "Human Research - Space Weather," Accessed: Oct. 16, 2017. [Online]. Available: https://www.nasa.gov/feature/nasa-protects-its-superheroes-from-space-weather

[23] QRZ, "Solar Storm Forecast Cycle," Accessed: Apr. 15, 2018. [Online]. Available: http://qrznow.com/a-peek-into-the-new-cycle-solar-storm-forecast-04-12-2018/

[24] NOAA, "Solar Cycle Progression," Accessed: Jun. 18, 2017. [Online]. Available: https://www.swpc.noaa.gov/products/solar-cycle-progression

[25] E. Saiz, G. Antonio, C. Cid, J. Palacios and Y. Cerrato, "Searching for Carrington-like events and their signatures and triggers," *J. Space Weather and Space Climate*, vol. 6, no. A6, pp. 1-12, Jan. 2016.

[26] M. A Clilverd *et al*., "Long- lasting geomagnetically induced currents and harmonic distortion observed in New Zealand during the 7–8 September 2017 disturbed period," *J. Space Weather*, vol. 16, no. 6, pp. 704-717, May. 2018.

[27] R. Pirjola, "GIC in electric power transmission networks at different latitudes," in *Proc. Asia-Pacific International Symposium on Electromagnetic Compatibility*, Beijing, China, Apr. 2010, pp.699-702

[28] D. H. Boteler, Q. Bui-Van and J. Lemay, "Directional sensitivity to geomagnetically induced currents of the Hydro-Quebec 735 kV power system," in *IEEE Trans. on Power Delivery*, vol. 9, no. 4, pp. 1963-1971, Oct. 1994.

[29] K. Zheng et al., "Effects of System Characteristics on Geomagnetically Induced Currents," in *IEEE Trans. on Power Delivery*, vol. 29, no. 2, pp. 890-898, Apr. 2014.

[30] C. M. Ngwira, A. Pulkkinen, F. D. Wilder and G. Crowley, "Extended study of extreme geoelectric field event scenarios for geomagnetically induced current applications," *J. Space Weather*, vol. 11, no. 3, pp. 121-131, Mar. 2013.

[31] D. Feng, Z. Wang and P. Jarman, "Evaluation of Power Transformers' Effective Hot-Spot Factors by Thermal Modeling of Scrapped Units," in *IEEE Trans. on Power Delivery*, vol. 29, no. 5, pp. 2077-2085, Aug. 2014.

[32] Natural Resources Canada, "Geomagnetic Effects on Power Systems," Accessed: Jul. 30, 2018. [Online]. Available: http://www.spaceweather.gc.ca/tech/se-pow-en.php?wbdisable=true.

[33] José Ramírez-Niño *et al*., "Core saturation effects of geomagnetic induced currents in power transformers," *J. Applied Research and Technology*, vol. 14, no. 2, pp. 87-92, Apr. 2016.

[34] S. Gao and M. Barnes, "Making VSC-HVDC control robust to geomagnetically induced current," *IEEE Power and Energy Society General Meeting*, Boston, MA, USA, July 17-21, 2016, pp. 1-5.

[35] D. C. Ferguson, S. P. Worden and D. E. Hastings, "The Space Weather Threat to Situational Awareness, Communications, and Positioning Systems," in *IEEE Trans. on Plasma Science*, vol. 43, no. 9, pp. 3086-3098, Sep. 2015.

[36] J. G. Kappenman *et al*., "GIC mitigation: a neutral blocking/bypass device to prevent the flow of GIC in power systems," in *IEEE Trans. on Power Delivery*, vol. 6, no. 3, pp. 1271-1281, Jul. 1991.

[37] P. H. Yang *et al*., "A multi-objective reactive power optimization strategy for mitigating voltage fluctuation in power network caused by geomagnetic storm," *J. Advances in Mechanical Engineering*, vol. 9, no. 9, pp. 1-11, Sep. 2017.

[38] NERC, "Geomagnetic Disturbance Planning Guide," Jul., 2013. Accessed: May 2016. [Online]. Available:http://www.nerc.com/comm/PC/Geomagnetic%20Disturbance%20Task%20Force%20GMDTF%202013/GMD%20Planning%20Guide_approved.pdf

[39] E. Matandirotya *et al*., "Differential magnetometer method applied to measurement of geomagnetically induced currents in Southern African power networks," *J. Space Weather*, vol. 14, no. 3, pp. 221-232, Mar. 2016.

[40] K. Narendra, "Wide Area Real Time GIC Monitoring using TESLA Phasor Measurement Unit (PMU)," ERLPhase, Accessed: Aug., 2016. [Online]. Available: http://www.erlphase.com/downloads/papers/ Wide_Area_Real_Time_GIC_Monitoring_using_TESLA_PMU.pdf

[41] A. Rezaei-Zare and A. H. Etemadi, "Optimal Placement of GIC Blocking Devices Considering Equipment Thermal Limits and Power System Operation Constraints," in *IEEE Trans. on Power Delivery*, vol. 33, no. 1, pp. 200-208, Jun. 2018.

[42] E. Matandirotya, "Measurement and modelling of geomagnetically induced currents (GIC) in power lines," Ph.D. dissertation, Dept. Elect. Eng., CPUT, Cape Town, South Africa, 2016.

[43] B. Dong, W. Zezhong, D. H. Boteler, and R. Pirjola, "Review of earth conductivity structure modelling for calculating geo-electric fields," *IEEE Power Engineering Society General Meeting*, Vancouver, BC, Jul. 2013, pp. 1-5

[44] Y. F. Ni, Z. D. Wang and P. Jarman, "GIC simulation study for part of UK transmission system by ATP/EMTP," *IEEE Power & Energy Society General Meeting*, Chicago, IL, 2017, pp. 1-5.

[45] Merriam-Webster, *Dictionary,* Springfield, MA: Encyclopedia Britannica, 2016. pp. 450 and pp. 665.

[46] L. Mihet-Popa, Y. Zong, S. You and V. Groza, "Simulation platform developed to study and identify critical cases in a future smart grid," *in Proc. 2016 IEEE Electrical Power and Energy Conference (EPEC)*, Ottawa, Ontario, Oct. 2016, pp. 1-8.

[47] T. Gonen, "Overhead Transmission Lines," in *Electric Power Transmission System Engineering*, 2nd ed., Taylor and Francis Group, Boca Raton, FL, USA: CRC Press, 2009, pp. 123-188.

[48] *Guide for Safety in AC Substation Grounding*, IEEE Standard 80-2013, 2015.

[49] B. Hembroff, M. Ohlen and P. Werelius, "A Guide to Transformer Winding Resistance Measurements," Megger, Eldarvagen, Sweden, Accessed: Oct. 5, 2017 [Online]. Available: http://www.avo.co.nz/images/stories/TechnicalPapers/pdf/Megger_Transformer_Winding.pdf

[50] A. Viljanen, A. Pulkkinen, O. Amm, R. Pirjola and T. Korja, "Fast computation of the geoelectric field using the method of elementary current systems and planar Earth models," *Annales Geophysicae*, vol. 22, no. 1, pp. 101-113, Jan. 2004.

[51] B. Dong, Z. Wang, R. Pirjola, C. Liu and L. Liu, "An Approach to Model Earth Conductivity Structures with Lateral Changes for Calculating Induced Currents and Geoelectric Fields during Geomagnetic Disturbances," *J. Mathematical Problems in Engineering*, vol. 2015, no. 761964, pp. 1-10, Mar. 2015.

[52] C.-M. Liu, L.-G. Liu, R. Pirjola and Z.-Z. Wang, "Calculation of geomagnetically induced currents in mid-to low-latitude power grids based on the plane wave method," *J. Space Weather*, vol. 7, no. 4, pp. 1-9, Apr. 2009.

[53] R. Bailey, T. Halbedl, I. Schattauer, G. Achleitner and R. Leonhardt, "Validating GIC Models With Measurements in Austria: Evaluation of Accuracy and

Sensitivity to Input Parameters," *J. Space Weather*, vol. 16, no. 7, pp. 887-902, Jul. 2018.

[54] D.J. Kweon, K.S. Koo, J.W. Woo and J.S. Kwak, "A Study on the Hot Spot Temperature in 154kV Power Transformers," *J. Electrical Engineering and Technology,* vol. 7 no. 3, pp. 312-319, Jul. 2012

[55] *IEEE Recommended Practice for Protection and Coordination of Industrial and Commercial Power Systems,* IEEE Standard 242-2001, 2001

[56] W. McKinney, "Data Structures for Statistical Computing in Python," Accessed: Jun. 2017. [Online]. Available: https://conference.scipy.org/scipy2010/slides/wes_mckinney_data_structure_statistical_computing.pdf

[57] Keithley, "Series 2390 Programmable DC Electronic Loads," Accessed: Jul. 2016. [Online]. Available: https://www.tek.com/sites/default/files/media/media/resources/2380-DataSheet.pdf

[58] Marathon Motors, "K235A, 56C17D2115, 1/3 Hp, 115/208-230, 1 PH., 56C FR., 1800 Rpm," Accessed: Jul. 2016. [Online]. Available: https://www.marathon-motors.com/K235A-56C17D2115-1-3-Hp-115-208-230-1-PH-56C-FR-1800-Rpm-K235A.htm

[59] BK Precision, "Programmable Triple Output DC Power Supplies," Accessed: Jul. 2016. [Online]. Available: https://bkpmedia.s3.amazonaws.com/downloads/datasheets/en-us/9130B_Series_datasheet.pdf

[60] GW Instek, "APS-7000 Series Data Sheet," Accessed: Jul. 2016. [Online]. Available: http://farnell.com//datasheets/2344134.pdf

[61] Todd Systems, "Power Transformers," Accessed: Jun. 2016. [Online]. Available: http://www.toddsystems.com/

[62] S. Shelemy, "Geomagnetically Induced Currents and Manitoba Hydro," Manitoba Hydro, Mar. 2012. Accessed: Aug. 2017. [Online]. Available: http://sites.ieee.org/winnipeg/files/2012/03/2012_03_27_pes1.pdf

[63] STMicroelectronics, "LSM303 Ultra-compact high-performance eCompass module: 3D accelerometer and 3D magnetometer," 2013. Accessed: Mar. 2016, [Online]. Available: https://www.st.com/resource/en/datasheet/lsm303dlhc.pdf

[64] Natural Resources Canada, "Magnetic Plotting Service," NRCan, 2018. Accessed: Sep. 2015. [Online]. Available: http://www.geomag.nrcan.gc.ca/plot-tracee/mp-en.php?plot_type=magnetic

[65] Melixis, "MLX90393 - Micropower Triaxis® Magnetometer," Accessed: Dec. 2016. [Online]. Available: https://www.datasheetspdf.com/pdf/1093408/Melexis/MLX90393/17

[66] NXP Freescale Semiconductor, "MAG3110 - Xtrinsic MAG3110 Three-Axis Digital Magnetometer," Accessed: Feb. 2013, Rev 9.2. [Online]. Available: https://www.nxp.com/docs/en/data-sheet/MAG3110.pdf

[67] STMicroElectronics, "LSM9DS - iNEMO inertial module," Accessed: March 2016, Rev 3. [Online]. Available: https://www.st.com/en/mems-and-sensors/inemo-inertial-modules.html?querycriteria=productId=SC1448

[68] H. Can, F. N. Ecevit, P. Svec, P. Svec and U. Topal, "The Sensing Characteristics of Ring-Core Fluxgate Sensors at Temperature Interval of −50 °C to +85 °C," in *IEEE Trans. on Magnetics*, vol. 54, no. 7, pp. 1-6, May 2018.

[69] E. Matandirotya, P.J. Cilliers, and R.B. van Zyl, "Differential Magnetometer Method for Measurement of GIC in a power line: Technical aspects," *J. Electrical Engineering*, vol. 66, no. 7, pp. 50-53, Sep. 2015.

[70] *Design Criteria of Overhead Transmission Lines*, IEC Standard No. 60826, IEC, 2017.

[71] D. H. Boteler, R. Pirjola, C. Blais, and A. Foss , "Development of a GIC Simulator," in *Proc. of IEEE PES General Meeting/ Conf. and Exp.*, National Harbor, MD, 2014, pp. 1-5.

Appendix A – Simulation Tool Implementation

The following code is the Python implementation of the simulation tool presented in Chapter 7.

```
#libraries to be loaded
import matplotlib.pyplot as plt
import numpy as np
import scipy.constants
import scipy as sc
import persistent_storage as ps
import pandas as pd

#initialize storage containers
storex=ps.store()
storey=ps.store()
storet=ps.store()

#main GIC simulation class
class gic_profile():
    def
__init__(self,RSA,RSB,line_resistance,electric_field,dista
nce):
"""Instantiates with Default Values for Simulation
RSA and RSB: are the resistance to ground of substation A
and B (in ohms)
line_resistance is an array of resistances for the
transmission line (in ohm meters)
electric_field is the typical field values analytically
generated (in v/km?)
distance is the distance away from the transmission line
to simulated (in meters)"""
        self.RSA = RSA#1.817
        self.RSB = RSB#1.817
        self.line_resistance =
numpy.asarray([line_resistance])
        self.electric_field =
numpy.asarray([electric_field])

        #initialize number of points to simulate
        self.sim_points = 1000
        self.distance = distance
        #distance from the line to simulate
        self.sim_distance = numpy.linspace(self.distance,-
self.distance,self.sim_points)
```

```
    def get_distance(self):
        #to access the overall distance from the line for
each simulation
        return self.sim_distance

    def calc_curscale(self,line_current):
        #declaration of constants
        mag_c=scipy.constants.mu_0
        pi_c=scipy.constants.pi
        current = line_current

        #calculation for the scaling factor
        result_scale = mag_c*current/2*pi_c
        #return the scaling factor
        return result_scale

    def calculate_x(self,scale,x_calc,x_pos,y_pos):
        """Function used to determine the strength of the
horizontal component of the magnetic field"""
        result = []
        #elementwise addition of the x_pos, field
calculations
        #x_calc is a numpy array
        x_calc = x_calc - x_pos
        #calculates the magnetic field at each position
        for x_distance in x_calc:
             result.append(scale*(y_pos/(numpy.square(y_p
             os)+numpy.square(x_distance))))
        storex.sum_Data(result)
        return numpy.asarray(result)

    def calculate_z(self,scale,x_calc,x_pos,y_pos):
        """Function used to determine the strength of the
vertical component of the magnetic field"""
        result = []
        x_calc = x_calc - x_pos
        for x_distance in x_calc:
            #calculates the resultant field
            result.append(((-
1)*scale)*(x_distance/(numpy.square(y_pos)+numpy.square(x_
distance))))
        return numpy.asarray(result)

    def calculate_total(self,x_field,z_field):
        """Returns the total magnetic field strength and
the direction of the field"""
```

```
        #calculates the total field due to both horizontal
and vertical components
        #need to check calculation
        total_mag = numpy.sqrt(numpy.square(x_field) +
numpy.square(z_field))
        total_angle =
numpy.arctan(z_field/x_field)*180/numpy.pi
        storet.sum_Data(total_mag)
        return total_mag,total_angle

    def reference_FieldStrength(self,vector,reference):
        #returns an array of length distance and with all
reference values
        return numpy.full(len(vector),reference)

    def calc_typicalGIC(self, line_length):
        """Calculation of the Typical GIC in different
transmission lines"""
        #potentially write a function to calculate the
below based on temperatures
        line_resistance = self.line_resistance
        electric_field = self.electric_field
        RSA = self.RSA
        RSB = self.RSB

        #empty array/list
        calcGIC = numpy.asarray([])

        #EL is the electric field
        #L is the length of the line
        #r is the resistance of the line
        #RSA is the resistance of the first substation
        #RSB is the resistance of the second substation
        #calculating the typical GIC for each different
cases
        for r in line_resistance:
            for L in line_length:
                for EL in electric_field:
                    #calculation from KZ paper
                    gic_inline = (EL*L)/(r*L*(RSA+RSB))
                    print(gic_inline)
                    #adds the calculated gic to the array
of gic values

calcGIC=numpy.append(calcGIC,gic_inline)
        return calcGIC
```

```
    def
plot_fields(self,x,y,subplot_location,label,showflag,ref_F
ield):
        plt.legend(loc='upper right', shadow=True,
fontsize='small')
        str1 = 'GIC: '+ str(round(label[0],3)) +', Height
(x,y): '+ str(label[1])
        #label[1][0] and label [1][0] access the x and y
components of the label factor ( x, y position)

        if subplot_location==1:
            plt.subplot (411)
            plt.plot(x,y,label=str1)
            plt.title("Magnetic Field Distributions")
            plt.ylabel("Horizontal (nT)")

        if subplot_location==2:
            plt.subplot(412)
            plt.plot(x,y,label=str1)
            plt.ylabel("Vertical (nT)")

        if subplot_location==3:
            plt.subplot(413)
            plt.plot(x,y)
            plt.plot(x,ref_Field,label="Reference",
color='r')
            plt.ylabel("Overall Magnitude (nT)")

        if subplot_location==4:
            plt.subplot(414)
            plt.plot(x,y)
            plt.yticks([-90,0,90])
            plt.grid(True)
            plt.ylabel("Overall Angle (Deg)")
            plt.xlabel("Distance (m)")

        if showflag==True:
            plt.tight_layout()
            plt.show()
            plt.clf()
            print("Plot Cleared")

def simulate(position,line_length,voltage):
    """Simulates the Magnetic Field Strengths around a
Transmission Conductor
```

```
    distance_from_line = range of simulation for the
calculated magnetic field distribution
    vert_pos = transmission line heights (meters)
    line_length = desired calculated for particular line
lengths (km)"""
    #distance from line to simulate

    temp_distance = 400
    temp_efield = [3]
    temp_distance = 50
   #select the electric fields that user desires to
simulate array or single value (may significantly impact
runtime)
    #temp_efield = [8,16.31864]
    #temp_efield =
[1,2,3,4,5,6,7,8,9,10,11,12,13,14,15,16,17,18,19,20]

   #select field model that user desires to run
    #analytic field values calculated from 1000ohm m
    self.electric_field =
numpy.asarray([136.0827,91.85587,46.29100,40.06939,27.6026
2,18.44662])

    #analytic field values calculated from 5 layer model
(ohm m)
   self.electric_field
=numpy.asarray([43.76735,40.32327,26.04161,26.16634,20.748
19,16.31864])

   #select substation resistance as required
    temp_rsa =1.817
    temp_rsb =1.817

    #component for transmission substation resistance and
the line resistance is accurate
    if voltage==230:
        temp_gic_obj =
gic_profile(temp_rsa,temp_rsb,[0.064],temp_efield,temp_dis
tance)
    elif voltage==345:
        temp_gic_obj =
gic_profile(temp_rsa,temp_rsb,[0.037],temp_efield,temp_dis
tance)
    elif voltage==500:
        temp_gic_obj =
gic_profile(temp_rsa,temp_rsb,[0.013],temp_efield,temp_dis
tance)
```

```
    elif voltage==735:
        temp_gic_obj =
gic_profile(temp_rsa,temp_rsb,[0.011],temp_efield,temp_dis
tance)
    else:
        #for worst case GIC
        #create new calculation object
        #instantiaties with values for the desired system
        temp_gic_obj =
gic_profile(temp_rsa,temp_rsb,[0.064],temp_efield,temp_dis
tance)

    #creates a vector to calculate magnetic field
distribution at each point
    desired_distance = temp_gic_obj.get_distance()

    #calculate the typical gic for the line length
indicated
    set_gic = temp_gic_obj.calc_typicalGIC(line_length)

    #performes calculations for all the returned gic
values desired
    for current in set_gic:
        #calculates the current scaling factor for each
typical GIC calculated
        new_scale = temp_gic_obj.calc_curscale(current)
        for coord in position:
            # simulates for each height of the
transmission line
            t_dat_x =
temp_gic_obj.calculate_x(new_scale,desired_distance,coord[
0],coord[1])
            t_dat_z =
temp_gic_obj.calculate_z(new_scale,desired_distance,coord[
0],coord[1])

            calc_temp = temp_gic_obj.calculate_x()
            #returns both magnitude and angle
            t_total =
temp_gic_obj.calculate_total(t_dat_x,t_dat_z)

            storet.save_Data()
            g_total =
temp_gic_obj.calculate_grandTotal(t_total)

            #plots each set of vectors
```

```
temp_gic_obj.plot_fields(desired_distance,t_dat_x,1,[curre
nt,coord],False,ref_field)

temp_gic_obj.plot_fields(desired_distance,t_dat_z,2,[curre
nt,coord],False,ref_field)

temp_gic_obj.plot_fields(desired_distance,t_total[1],4,[cu
rrent,coord],False,ref_field)

    #initiates display
   temp_gic_obj.plot_fields(0,0,0,[0,[0,0]],True,ref_fiel
d)

#simulate example (coordinates of TL in x,y pairs and
transmission line length)
def test_cases(number):

    ll = 700 # line length for particular case (km)
    ll = [1] # line length for particular case (km)

    if number==1:
        #base test case
        #0 off set, 2 meters clearance, 100km long, 100kv
        #results in calling default case
        simulate([[0.0,20.0]],[ll],100)
    elif number==2:
        #230kv case 1
        #min spacing, horizontal phase spacing
        h = 25.0
        sp = 4.37
        simulate([[-sp,h],[0.0,h],[sp,h]],[ll],230)
    elif number==3:
        #230kv case 2
        #min spacing, vertical spacing for phases
        h = 3.0*10
        sp = 3.0

simulate([[0.0,h],[0.0,h+sp],[0.0,h+2*sp]],[ll],230)
    elif number==4:
        #next case
        #Transmission Line 345kV (Double Conductor,
r=0.037ohm/km)
        #2470, 2720
        h = 2.470*10
        sp = 2.720
        simulate([[-sp,h],[0.0,h],[sp,h]],[ll],345)
```

```
    elif number==5:
        #next case
        #Transmission Line 345kV (Double Conductor,
r=0.037ohm/km)
        h = 2.470*10
        sp = 2.720

simulate([[0.0,h],[0.0,h+sp],[0.0,h+2*sp]],[ll],345)
    elif number==6:
        #Transmission Line 500kV (Triple Conductor,
r=0.013ohm/km)
        #3420, 3765
        h = 3.420*10
        sp = 3.765
        simulate([[-sp,h],[0.0,h],[sp,h]],[ll],500)
    elif number==7:
        #Transmission Line 500kV (Quad Conductor,
r=0.013ohm/km)
        #3420,3765
        h = 3.420*10
        sp = 3.765

simulate([[0.0,h],[0.0,h+sp],[0.0,h+2*sp]],[ll],500)
    elif number==8:
        #Transmission Line 735kV (Quad Conductor, r =
0.011ohm/km)
        #horizontal config
        #4375,4815
        h = 4.375*10
        sp = 4.815
        simulate([[-sp,h],[0.0,h],[sp,h]],[ll],735)
    elif number==9:
        #735 vertical config
        h = 4.375*10
        sp = 4.815

simulate([[0.0,h],[0.0,h+sp],[0.0,h+2*sp]],[ll],735)
    elif number==10:
        #GIC mag testing
        h = 4*10
        sp = 3.0
        simulate([[0.0,h]],[ll],230)
    else:
        print("Case Not Found")
        print("Please Manually Enter Parameters")
        print("Feature not yet implemented")
```

```
  # run select test cases or select desired values to
  simulate
  number= 4
  test_cases(number)
```

Below is the Python implementation of the "persistant_storage" library required for running simulations.

```
    import numpy as np
    import time
    #used to store magnetic field data
    class store():
        def __init__(self):
            self.counter =0
            self.data = np.zeros(1000)
        def store_Data(self, data):
            pass
        def get_Data(self):
            print("Retrieving Data")
            return self.data
        def sum_Data(self,new_data):
            #updates self.data
            self.data=np.asarray([x + y for x, y in
zip(self.data, new_data)])
        def save_Data(self):
            self.counter+=1
            maxi = np.amax(self.data)

np.savetxt("simresults_"+str(self.counter)+".csv",maxi,deli
miter=',')
            print("Results Saved")
```